THE ROLE OF SPHINGOLIPID METABOLISM IN SICKLE BONE DISEASE AND BONE STEM CELLS

A Dissertation

Presented to

The Academic Faculty

by

Jada Monique Selma

In Partial Fulfillment

of the Requirements for the Degree

Doctor of Philosophy in the

School of Wallace H. Coulter Department of Biomedical Engineering

Georgia Institute of Technology and Emory University

May 2019

THE ROLE OF SPHINGOLIPID METABOLISM IN SICKLE BONE DISEASE AND BONE STEM CELLS

Approved by:

Dr. Edward Botchwey, Advisor
School of Biomedical Engineering
Georgia Institute of Technology

Dr. Manu Platt
School of Biomedical Engineering
Georgia Institute of Technology

Dr. Wilbur Lam
School of Biomedical Engineering
Georgia Institute of Technology

Dr. Frederik Vannberg
School of Biological Sciences
Georgia Institute of Technology

Dr. Luke Mortensen
School of Chemical, Materials, and Biomedical Engineering
University of Georgia

Date Approved: March 19, 2019

To my loving Selma, Smith, Mitchell, Jackson, and Farrish family

ACKNOWLEDGEMENTS

Like many things in life, there is no way I could have accomplished earning a PhD without the support of countless people. I would like to first thank God for keeping me under his grace and protection as I traveled through this challenging but rewarding PhD journey.

My graduate career has been shaped by many talented professionals. Firstly, I'd like to thank my advisor, Dr. Edward Botchwey, for constantly encouraging me through the PhD process. There were many times where the inevitable failure that is couched in scientific research spurred me to want to quit. Dr. Botchwey's guidance and reassurance helped me to build perseverance in the face of obstacles. Additionally, Dr. Botchwey's tutelage has expanded my scientific intellect and has taught me to tackle quandaries from a multitude of angles. I would also like to thank Dr. Manu Platt for his immense collaboration on this work. Additionally, Dr. Platt's outreach and diversity efforts have empowered me as fellow black scientist. Furthermore, I give immense gratitude to my committee members, Dr. Manu Platt, Dr. Wilbur Lam, Dr. Fredrik Vannberg, and Dr. Luke Mortensen for their instrumental expertise in the areas of sickle cell disease, bone remodeling, MSC biology and migration, cathepsin activity, and microparticle signaling. My thesis has greatly benefited from all of your helpful insight. I would also like to thank Dr. Lakeisha Williams, a professor of my alma mater Mississippi State University, who inspired me as a black woman to attain a PhD in biomedical engineering. Lastly, I would like to thank Dr. Radhakrishnan Srinivasan, my undergraduate academic advisor, who recommended me for the Amgen Scholars program that set me on the path to pursue a PhD.

I would like to thank the members of the Botchwey laboratory, both past and present, for their infinite support. Dr. Anthony Awojoodu, Dr. Claire Olingy, Tiffany Wang, Dr. Jack Krieger, Dr. Cheryl San Emeterio, and Dr. Caitlin Sok, you all have shaped me as a scientist and made going into lab that much more enjoyable. I would like to especially thank Nathan Chiappa for your invaluable expertise in sphingolipid metabolism in sickle cell disease but mostly for your friendship and support. I would like to especially thank Dr. Molly Ogle for your years of service to the Botchwey lab and your invaluable feedback and instruction. I am also grateful to the new perspectives and insights that were brought to my work from the newest member of the Botchwey lab: Julian Rose, Imani Lewis, Claire McClain, Lauren Hymel, S'Dravious (Dre) DeVeaux, Thomas Turner, and Elana Cooper. Lastly, I would like to thank my undergraduate and high school mentees. Thanks to Abhiramgopal (Ram) Akella for your hours of researching sickle bone disease and tedious data entry. Thank you to my Project ENGAGEs student Ciara Dean, who is a mature, self-assured young woman. I am grateful for our many philosophical discussions that have encouraged me to become more entuned with my emotions and aspirations. The both of you have helped me to become a more effective leader and mentor.

I also like to extend gratitude to the Platt laboratory. I consider myself an adopted member of the Platt lab, and I am forever indebted to Dr. Akia Parks, Simone Douglas, Chris Rivera, and Andrew Shockey for your friendship and scientific contributions. I would like to extend a special acknowledgment to Dr. Hannah Song. My graduate school experience was forever changed when you joined the Platt and Botchwey labs. I am a

better scientist, writer, and engineer due to your instruction and guidance. Thank you for your countless hours of sickle mice genotyping and sacrificing, flow cytometry analysis, manuscript editing, abating my internal doubts, and most of all for your friendship and counsel.

Lastly, but certainly not least, I would like to thank my family and friends for their love and emotional, financial, and spiritual support through this demanding journey. I cannot possibly name each individual person, but I am forever in your debt for the numerous pep talks, prayers, outings, and venting sessions. Thank you to my loving parents, Charles and Ethel Selma, for their undying encouragement and sacrifices that have allowed me to pursue my personal and academic aspirations. I am grateful to my father, Charles Selma, for continually compelling me to strive beyond average pursuits. I, and many other black students, am eternally indebted to my mother, Ethel Selma, for her being a pioneer in integrating the public-school system in the 1960's South. I would not have even been able to pursue a PhD at Georgia Tech were it not for your tremendous bravery. Thank you to my older sister, JaNee Michelle-Selma Farrish, for paving the way for me to become an engineer. It is your profound example that inspired me to pursue a scientific career. I would like to thank my late maternal great-grandmother, Ethel O. Smith, for driving JaNee and I towards knowledge and education through our many reading sessions. Thank you to my maternal grandmother, Nelsie Mitchell, for your kind spirt and continuous praise that has guided me through doubtful days. Although I never had the pleasure of meeting her, I would also like to thank my paternal grandmother, the late Juanita Selma, for raising her son to become a caring father. Finally, I would like to

thank my uncle, Edwin Mitchell, for treating me like a daughter and motivating me to have a fighting spirt no matter what adversity life springs my way. My PhD is our PhD.

TABLE OF CONTENTS

LIST OF TABLES

LIST OF FIGURES

LIST OF SYMBOLS AND ABBREVIATIONS

AA	Normal hemoglobin
AS	Normal/Sickle hemoglobin (sickle trait)
BM	Bone marrow
BMD	Bone mineral tissue density
cat	Cathepsin
Cer	Ceramide
C1P	Ceramide 1-phosphate
CXCR4	Chemokine receptor 4
Conn. Den.	Connective density
Cort. Th.	Cortical thickness
EPCs	Endothelial progenitor cells
FBS	Fetal bovine serum
GlcCer	Glucosylceramide
HSPC	Hematopoietic stem and progenitor cell
H&E	Hematoxylin and eosin
HPLC-MSMS	High throughput liquid chromatography- tandem mass spectrometry
IP	Intraperitoneal
kDa	Kilodalton
LSK	Lineage-Sca1+C-kit+
MSC	Mesenchymal stem cell
MicroCT	Micro-computed tomography
mg/kg	Milligram per kilogram
MP	Microparticle
ON	Osteonecrosis
PBMC	Peripheral blood mononuclear cell
PB	Peripheral blood
PBS	Phosphate buffered saline
PCA	Principal component analysis
RANKL	Receptor activator of nuclear factor kappa-B ligand
RBC	Red blood cell
SBD	Sickle bone disease
SCD	Sickle cell disease
Sa	Sphinganine
SaP	Sphinganine 1-phosphate
SM	Sphingomyelin
SMase	Sphingomyelinase
So	Sphingosine
S1P	Sphingosine 1-phosphate
S1PR	Sphingosine 1-phosphate receptor
SK	Sphingosine kinase
SS	Sickle hemoglobin
SMI	Structural model index
Tb.Th.	Trabecular thickness

Tb.Sp.	Trabecular spacing
TRAP	Tartrate-resistant acid phosphatase

SUMMARY

Sickle cell disease (SCD) is the most common inherited blood disorder in the United States. SCD affects approximately 100,000 people domestically and an additional 300,000 babies born globally every year. A collection of pathologies, including osteonecrosis (ON), osteoporosis, and osteopenia, known as sickle bone disease (SBD) are among the most common complications of SCD, which progresses from adolescence and occurs in 50% of individuals by age 35. Transgenic sickle mouse model studies have shown that increased osteoclast activity and reduced mesenchymal stem cell (MSC) differentiation into osteoblasts contributes broadly to pathological bone remodeling in SCD, but underlying cellular and molecular mechanisms are poorly understood. Sphingosine 1-phosphate (S1P), a type of sphingolipid, directs a wide array of cellular processes involved in bone homeostasis including directing MSCs towards an osteogenic lineage and modulating their migration. S1P also regulates osteoclastogenesis and is linked to the activity of cathepsin K (cat K), a protease secreted by osteoclasts to resorb bone. We have previously shown that dysregulated sphingolipid metabolism in SCD leads to increased S1P in sickle patients' blood, plasma, and erythrocytes. Monocytes isolated from people with SCD are primed for inflammation and cat K proteolytic activity induction when binding to endothelial cells. Cat K-induced bone resorption mechanisms are implicated in bone dysfunction without SCD but have not been mechanistically linked to SCD osteopathologies.

The objective of this research is to investigate the relationship between sphingolipid metabolism and cathepsin activation in SCD. It is also the aim of this work to utilize sphingolipid signaling as a potential therapy for SBD. It is hypothesized that

dysregulated sphingolipid metabolism leads to bone loss in SCD that is propagated by increased cathepsin activity and that bone loss can be mitigated by cathepsin inhibition. This study utilizes a transgenic mouse model to characterize the sickle bone phenotype and to test the effect of a cathepsin inhibitor on bone morphology. This research further utilizes a S1P analog in wild-type mice to investigate if mobilizing MSCs out of the bone marrow can aid in bone repair. Elucidation of how dysregulated sphingolipid metabolism contributes to increased proteolytic activity in SCD that leads to increased bone resorption will better inform clinical therapeutic strategies to prevent detrimental bone loss in sickle cell patients.

CHAPTER 1 INTRODUCTION AND SPECIFIC AIMS

1.1 Introduction

Sickle cell disease (SCD) is a genetic disorder affecting nearly 100,000 Americans and millions worldwide [1]. In states of deoxygenation, the homozygous sickle mutation in β-globin (SS) causes polymerization of hemoglobin molecules into rigid fibers within erythrocytes, or red blood cells (RBCs), deforming them into a "sickle" shape. This membrane distortion impedes RBC passage through narrow blood vessels, leading to obstructed blood flow to tissues and organs known as vaso-occlusion. Vaso-occlusion can also be localized in the bone [2, 3]. Increased erythropoiesis and consequent marrow expansion in the long bones increase the frequency of bone infarcts in sickle patients. Pathological bone remodeling begins in adolescence [2, 4], progresses with increasing age, and presents in 50% of individuals by age 35 [5, 6]. To prevent the progression of bone and joint damage, bed rest and avoiding activities such as running or stair climbing are recommended, but these restrictions drastically reduce quality of life [7]. Surgical treatments, such as a total hip replacement (which can occur as early as age 18), have an elevated risk of inducing complications [8, 9]. Although progress has been made in elucidating both acute and chronic dysfunction in several organ systems, the mechanisms and preventive therapeutic treatments for pathological bone remodeling in SCD, or sickle bone disease (SBD), have not been widely investigated.

Dysregulation of sphingolipid metabolism may serve as a feed-forward mechanism that exacerbates SCD-associated pathologies. Sphingolipids are a structurally diverse class of membrane lipids that serve distinct functions in cell signaling. We have shown that due to the dynamic shape distortion of sickled RBCs, the activity of acid

sphingomyelinase (SMase), an enzyme that acts on the sphingolipid sphingomyelin, is increased in the blood, plasma, and erythrocytes of people living with SCD [10]. Moreover, this increase in sphingomyelin hydrolysis causes the increased production and of release of RBC-derived microparticles (MPs) in SCD. Once phagocytosed by osteoclastic precursors, sickled MPs (SS MPs) induce the secretion of osteoclastogenic, proinflammatory cytokines [10]. A connection between dysregulation of sphingolipid metabolism and bone pathology in SCD is bolstered by reports of increased plasma MPs in SS patients with osteonecrosis (ON) of the femoral head (OFNH) compared to SS patients without OFNH [11].

Moreover, we have found that sphingosine 1-phosphate (S1P), a bioactive sphingolipid, is elevated in human SS blood, plasma, and RBCs [10]. Zhang et al. demonstrates that increased production of S1P contributes to erythrocyte sickling [12]. S1P regulates various cellular functions important to bone homeostasis such as mesenchymal stem cell (MSC) differentiation into osteoblasts and osteoclastogenesis [13-15]. Additionally, S1P production is linked to the expression of cathepsin K (cat K) in osteoclasts [16]. Cat K is the key bone resorptive enzyme secreted by osteoclasts. Monocytes isolated from people with SCD are primed for inflammation and cat K proteolytic activity induction when binding to endothelial cells [17]. Cat K-induced bone resorption mechanisms are implicated in bone dysfunction but have not been mechanistically linked to SCD osteopathologies. Lastly, mobilization of MSCs [13, 18, 19] and hematopoietic stem cells (HSCs) from the bone marrow (BM) and into circulation are guided along the S1P gradient via signaling through 5 G-coupled receptors

(S1PR1-S1PR5) [20-22], and it is speculated that poor bone formation in SCD could be due to poor circulation of stem and progenitor cells to the site of bone infarcts [23].

1.2 Research Objectives and Specific Aims

The objective of this work is to investigate whether the disruption of sphingolipid metabolism in SCD induces hyper-proteolytic, bone resorptive activity through cat K. We also aim to utilize sphingolipid signaling in order to improve bone repair. The **central hypothesis** of this thesis is that dysregulated sphingolipid metabolism leads to bone loss in SCD that is propagated by increased cathepsin activity and that bone loss can be mitigated by cathepsin inhibition. The central hypothesis will be addressed with the following three specific aims:

Aim 1. To characterize the transgenic sickle Townes mouse model for bone pathologies. The objective of this aim is to characterize bone pathology in female and male mice to determine the effect of SCD on skeletal development. The hypothesis of this aim is that SS mice show significant delays in skeletal maturation, and adult bones have significantly altered bone morphology and biomechanical properties compared AA and AS mice. We further hypothesize that bone pathology in SCD is sex dependent. Skeletal maturity will be assessed by examining the proximal femur epiphyseal fusion of 3-and-5month old mice via micro-computed tomography (microCT). Analysis of the amount of calcified bone present will be determined with Mimics Materialise software. The cortical and trabecular bone morphology will be characterized at 3 and 5 months of age in male and female mice through microCT imaging. We will generate a multivariate data set with the 23 bone parameters from microCT software, using principal component

analysis to characterize which parameters most vary in sickle mice. This aim will elucidate how bone microarchitecture in the sickle cell mouse model varies over several months and how SBD affects each sex.

Aim 2. To characterize link between sphingolipid metabolism and cathepsin-mediated proteolysis to the bone loss in SCD. The objective of this aim is to investigate the nexus of sphingolipid metabolism, cathepsin proteolytic activity, and pathological bone remodeling in SS mice. Dysregulated sphingolipid metabolism in SCD causes an increase in the production of proinflammatory MPs. We believe the transport of MP-derived signaling molecules to osteoclast precursors induces hyper-proteolytic, bone resorptive activity through the cat K pathway. We hypothesize that E-64, a cysteine cathepsin inhibitor, will decrease the proteolytic activity increased in SCD and will result in diminished bone loss. To this end, we will characterize sphingolipid expression in the blood of sickle mice through high throughput liquid chromatography- tandem mass spectrometry (HPLC-MS/MS). In order to investigate the effect of sphingolipid dysregulation on bone marrow progenitors that regulate bone homeostasis, lipidomic analysis on MSCs and flow cytometry characterization of osteoclast progenitors (OPCs) will be performed. Sphingolipidomic analysis via HPLC-MS/MS will be performed on circulating, erythrocyte-derived SS MPs. Moreover, the potential of proinflammatory, erythrocyte-derived SS MPs to induce cathepsin activity in monocytes will be evaluated through enzyme zymography for cat K and western blotting. Due to the bone loss present in SCD, we expect sickle animals will have increased cat K activity that can be mitigated over two months with daily injections of E-64. Cortical and trabecular bone morphology

in mouse femurs will be assessed with microCT imaging. Four point bending mechanical testing will be performed to determine the effect of E-64 treatment on the mechanical properties of the bones. We expect sickle animals receiving E-64 to have increased bone and mechanical strength. This aim will elucidate the relationship between sphingolipid metabolism and bone loss in SCD as well as determine if cathepsins are a viable target to treat SBD.

Aim 3. To evaluate the role of S1P signaling in MSC migration and subsequent bone healing. The objective of this aim is to determine if pharmacological inhibition of S1P receptor 3 (S1PR3), which has been shown to play a role in stem cell mobilization, can be used to mobilize MSCs to modulate bone repair. We hypothesize that VPC01091, a S1P1 agonist and S1PR3 antagonist, will mobilize endogenous MSCs out of the BM and into circulation, which will result in accelerated bone healing. In this aim, S1PR3 knockout mouse model will be used to determine if there is an increase in the MSC population in the PB, as detected by flow cytometry. We will treat wildtype mice intraperitoneally with VPC01091 and assess via flow cytometry if MSCs are present within the PB following 1.5, 3, and 24 hours after treatment. We will utilize an ectopic bone and critical size cranial defect model to evaluate VPC01091's effect on new bone formation over the course of 6 and 8 weeks, respectively. Bone growth will be assessed by microCT imaging and histology. Characterization of cells recruited to the bone defect site will be assessed by flow cytometry. This aim examines the potential of pharmacological inhibition of S1PR3 to mobilize endogenous MSCs as a therapeutic strategy for bone fractures as well as chronic bone metabolic diseases such as SBD.

CHAPTER 2 LITERATURE REVIEW

2.1 Sickle Cell Disease

Sickle cell disease (SCD) is a genetic blood disorder caused by the substitution of valine for glutamic acid in the β subunit of the gene encoding for hemoglobin and affects approximately 100,000 Americans and millions worldwide [24]. While the annual prevalence of SCD in African Americans is estimated to be 1 in every 360 births, the global prevalence is estimated to be an astounding 400,000 annual births by the year 2050. Moreover, approximately 1 in every 67 infants born in the United States are genetic carriers [25]. In states of hypoxia in blood vessels, hydrophobic valine is subjected to the aqueous environment of erythrocyte cytoplasm [26]. This contact causes for sickle hemoglobin (HbS) to alter into rigid, rod-shaped fibers that disfigure the normal shape of red blood cells (RBCs) into a "sickle" conformation [27]. Loss of the bi-concave shape of erythrocytes limits deformation that is required to traverse the vasculature and leads to their entrapment in small vessels such as the capillaries, thus obstructing blood flow [26]. This blockage produces one of the hallmarks of SCD: the vaso-occlusive, or pain, crisis. Vaso-occlusion can lead to several pathologies including chronic pain and inflammation, stroke, cardiovascular disease, organ failure, and eventually death [28, 29].

SCD pathophysiology has been shown to affect both sexes differently. Men typically endure an increased frequency of pain crises following the age of 15, compared to women with SCD [30]. This difference could be attributed to multiple factors such as decreased nitric oxide availability in men that leads to increased infarction or that females with SCD express higher levels of fetal hemoglobin (HbF), which unlike HbS, does not polymerize in states of deoxygenation [30, 31]. In fact, male patients with SCD are only

expected to live up to the age to 42, while the life expectancy of female patients is 48 years old [32]. With the variability of SCD symptoms being sex-dependent, it is imperative to study SCD complications separately in men and women.

2.1.1 Treatment for Sickle Cell Disease

Even though the discovery for the mutation of SCD is a century old, there is currently only a minimal number of FDA-approved drugs for treatment. One such drug, hydroxyurea, aims to increase the production of HbF, which does not polymerize in states of hypoxia, in order to decrease vaso-occluison [33]. Endari, or L-glutamine, is the first drug approved for pediatric sickle patients and lowers SS RBC stiffness and sickling by reducing their oxidative stress [34]. The gold standard of care is blood transfusions, which are utilized to amplify the number of non-sickle erythrocytes in sickle cell patients and thus decrease the number of vaso-occulsions caused by RBC sickling. Due to iron overload, however, this treatment causes cardiovascular and hepatic damage, increased inflammation, and osteoporosis [35, 36]. Furthermore, transfusions and pain management cause costly hospitalizations for patients, leading to annual health care costs of more than $1.1 billion dollars in the United States [37]. While gene editing techniques such as engineered zinc finger nucleases have been studied to rectify the sickle-cell-anemia-causing mutation for the substitution of the amino acid of glutamic acid to valine in the β globin sub-unit of hemoglobin, bone marrow (BM) transplants are the only current remedy for SCD [38]. With SCD affecting mainly African Americans in the United States, (who only make up 13% of the population) finding a full-match donor is very challenging. Furthermore, BM transplants come with the potentially fatal risk of graft-vs host disease, in which the immune cells from the donated tissue attack the recipient's

tissues/cells [39]. Finally, the pain that sickle cell patients suffer from and treatments for their various resulting underlying disorders, such has sickle bone disease (SBD), have not been properly addressed.

2.2 Sickle Bone Disease

Many hospitalizations of sickle cell patients are often due to vaso-occlusive crises. As sickled erythrocytes become unable to travel through narrow blood vessels, irremediable injury occurs to subsequent tissues and organs [26]. Being a highly vascularized connective tissue, bone is not immune from this damage, and often pain crises occur in the bone and joints of people with SCD. The prevalence of bone loss increases from 3% in adolescents to 50% in sickle cell patients over 35 as vaso-occlusive crises increase in frequency with age [4]. Bone and joint disorders including osteopenia, osteoporosis, osteonecrosis (ON), known collectively as sickle bone disease (SBD), are among the most common complications of SCD [40]. SBD can impact various parts of the skeleton with 30% of cases being present in the tibia/fibula, 25% in the femur, and 21% of cases affecting the radius, ulna, and humerus [41]. Osteopenia, a precursor to osteoporosis, is characterized by loss of bone mineral density. In the case of osteoporosis, people with SCD experience approximately 6-21% reduction in bone mineral density in all bone regions due to BM hyperplasia, but it is quite frequently associated with vertebral collapse [42]. ON, which is the death of bone tissue, results from vaso-occlusions that most commonly occur in the head of long bones. Nearly 41% of adults and 27% of children with SCD have been found to have ON, particularly in the femoral or humeral head [2]. Without treatment, ON can produce constricted joint spaces, bone spurs, and eventual collapse of the femoral head within 5 years of onset [7, 43].

Diagnosing and treating SBD remains difficult and insufficient. During the initial phase of vaso-occlusive crises, standard radiographs are unable to detect BM infarcts [43]. Other methods such as radioisotope bone scanning and MRI can detect infarcts in the acute phase; however, these methodologies are unreliable for developing accurate diagnoses. For instance, a BM infarct can be erroneously attributed to ON when a patient actually has osteomyelitis, or infection of the bone [41, 44]. Furthermore, dual-energy X-ray absorptiometry (DXA) is the standard clinical metric to evaluate bone mineral density and assess the onset of osteoporosis. However, this metric's results can be muddied with signal gleaned from surrounding muscle or other soft tissue [45]. Surgical treatments of SBD for distinct bone lesions, such as core decompression of the femoral head (early stage) or hip replacement (advanced stage) are performed at an average age of 26 in one study with 40% of the patients in their teenage years [8]. Those undergoing surgeries also have an elevated risk of inducing complications such as infection, congestive heart failure, and acute chest syndrome [8, 9]. As an alternative to delay or prevent surgical intervention, bed rest and avoiding activities such as running or stair climbing are recommended to prevent the progression of joint damage, but these methods drastically affect the quality of patient life [7]. Clearly, there is a need to investigate new therapeutic paradigms to develop more effective SBD treatments.

2.3 Sphingolipid Metabolism

2.3.1 Sphingolipid Metabolism Overview

Sphingolipids are a structurally diverse class of membrane lipids that are composed of an 18-carbon amino-alcohol backbone, sphingosine (So), and are synthesized in the endoplasmic reticulum [46]. So and sphinganine

(Sa)/dihydrosphingosine, referred to as long-chain base sphingolipids, are the basic building blocks of sphingolipids in mammalian cells. The "sphingoid" backbone can be modified to produce a wide variety of sphingolipids with distinct functions in cell signaling and structural adaptations of biological membranes [47]. N-acylation of sphingosine by ceramide synthases (CerS) generates ceramide (Cer), a complex sphingolipid, whereas phosphorylation of the C1-hydroxyl group of So by sphingosine kinase (SK) produces sphingosine 1-phosphate (S1P) [48] (Figure 2.1). The fatty acyl structure of complex sphingolipids represents a major building block of Cer and other complex sphingolipids such as sphingomyelin (SM) and ceramide 1-phosphate (C1P), and a considerable number of variations exist in the structure of mammalian cell membranes. Among the complex sphingolipids, small differences in acyl chain length or unsaturation can be functionally consequential. For example, the production of different Cer species in cell membranes impacts membrane morphology and fluidity [49, 50]. As the hub of the sphingolipid metabolic network, Cer can serve as the precursor of more complex sphingolipids, such as glucosylceramides (GlcCers) and SMs. Owing to the smaller head group of Cer compared to SM, the hydrolysis of SM by acid sphingomyelinase (SMase) to produce Cer results in decreased membrane rigidity and the efflux of membrane lipids through the shedding of cell-derived microparticles (MPs) that can serve as messengers to neighboring cells [51].

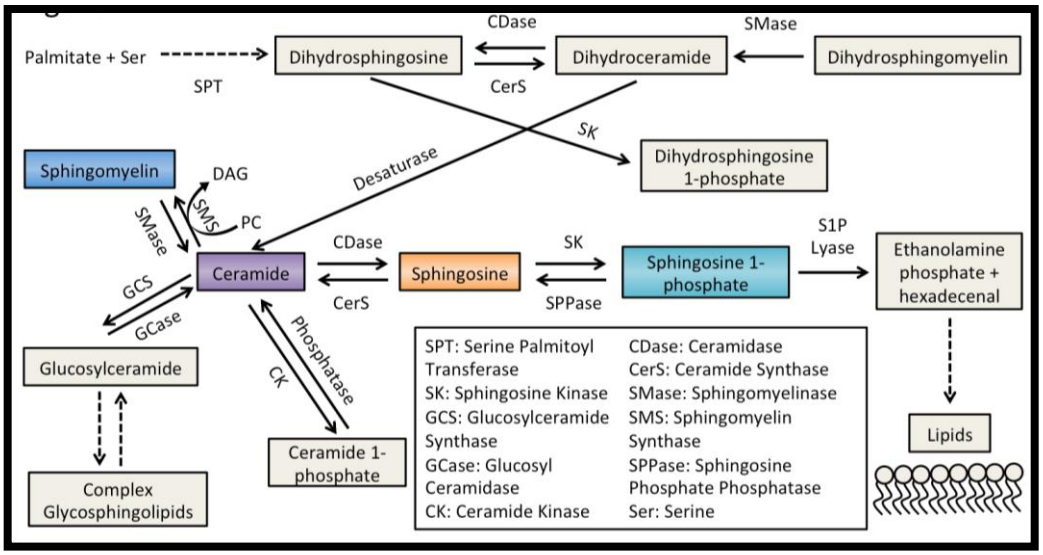

Figure 2.1. Sphingolipid metabolism. Sphingolipids are synthesized *de novo* via the reaction between serine and palmitoyl CoA, which is facilitated by serine palmitoyl transferase. Due to the activity of several enzymes, sphingolipids are produced by many reversible and irreversible reactions. The enzyme SMase catalyzes the hydrolysis of sphingomyelin to create ceramide, the central hub of the sphingolipid metabolism network. Ceramide is further metabolized to yield sphingosine and sphingosine 1-phosphate (Adapted from [10]).

2.3.2 Sphingolipid Metabolism Involvement in Sickle Cell Pathology

Dysregulation of sphingolipid metabolism may serve as a feed-forward mechanism that exacerbates SCD-associated pathologies. Acid SMase secretion can be prompted by RBC death and prolonged inflammation, both processes which are hallmarks of SCD [52, 53]. Consequentially, erythrocytes obtained from donors homozygous for sickle (SS) hemoglobin have an elevated activity of acid SMase; this elevated activity also exacerbates SCD inflammation through the production of RBC-derived MPs, which in turn induce increased pro-inflammatory cytokine secretion and adhesion of myeloid cells [10]. Consequentially, MPs have been implicated in many processes in SCD including coagulation [54] and vaso-occlusions [55]. Membrane curvature and associated increases in mechanical bending stresses in erythrocytes

activates SMase, reducing sphingomyelin and increasing ceramide [56]. This discovery further supports Awojoodu et al.'s previous findings that Cer is elevated in SS erythrocytes and that the activity of acid SMase is highest in the densest or irreversibly sickled fraction of SS erythrocytes [10]. Production of Cer has a direct effect on a wide range of cellular processes, and Cer is the direct precursor of So, which can be phosphorylated by either isoform of SK (SK1 or SK2) to produce S1P [46]. SK1 - mediated increase of S1P has been shown to contribute to erythrocyte sickling [12]. Furthermore, S1P is elevated in SS blood, plasma, and RBCs [10]. By activating S1P receptor 1 (S1PR1), S1P has been found to increase local and systemic inflammation that causes tissue damage and kidney failure [57]. With sphingolipids playing such a pervasive role in SCD, there is a strong motivative to investigate the role of S1P in sickle bone pathology.

2.4 Sphingosine 1-Phosphate (S1P)

2.4.1 S1P Overview

S1P is a bioactive sphingolipid that regulates various cellular functions such as migration, cell-cell adhesion, survival, and proliferation. These processes are controlled extracellularly through 5 G-protein coupled receptors (S1PR1-5) as well as can be initiated intracellularly by metabolized S1P [58-61]. This lipid intermediate also regulates cellular processes important to bone homeostasis such as mesenchymal stem cell (MSC) differentiation and osteoclast progenitor (OPC) circulation [14, 62].

2.4.2 S1P's Role in Bone Homeostasis

S1P is an osteoanabolic lipid. Marycz et al. recently showed how in vitro incubation of MSCs with S1P enhanced mineralized matrix formation during osteoblastic differentiation [63]. Moreover, S1P has been shown to promote osteogenic differentiation

but inhibit the adipogenic differentiation of multipotent stem cells [64]. This is further verified in an in vivo study where pharmacological or genetic inhibition of S1P lyase, an enzyme that degrades S1P, increases bone development and strength while simultaneously inhibiting adipogenesis [65]. This process is conducted through S1PR2 signaling, whereby expression of genes that are involved in osteoblastogenesis such as Sparc (osteonectin) and Col1a (collagen type 1-α) are upregulated while genes involved in adipocyte formation such as PPAR-γ are downregulated in primary murine osteoblasts treated with S1P. Additionally, S1PR2 activation downregulates the differentiation of osteoclasts by increasing the production of osteoprotegerin [65]. Osteoprotegrin binds to receptor activator of nuclear factor κ- B ligand (RANKL) to prevent it binding to the RANK receptor on OPCs that propagates osteoclast differentiation. Consequentially, S1PR2 knockout mice are obese and have low bone mass. Furthermore, Higashi et al. found that S1P upregulates runt-related transcription factor 2 (RUNX2) expression through S1PR2 signaling and leads to bone formation in vivo [14]. RUNX2 is a transcription factor that is responsible for pushing MSCs towards an osteogenic lineage [66]. Consequently, it has been shown that decreased expression of S1PR2 on MSCs decreases their differentiation into osteoblasts and is correlated to an increase in pluripotency factors including Nanog, Sox-9, and Oct-4 [13]. However, there is evidence that S1P can conduct bone formation through its S1PR3 receptor as well. FTY720 is an analog of S1P that binds to all 5 receptors, except for S1PR2. S1PR3 knockout mice suffer from osteopenia and reduced bone formation, but not increased bone resorption. Keller et al. found that FTY720 treatment increased bone formation in wild-type but not in S1PR3 knockout mice [67]. Furthermore, VPC23019, a S1PR1 and S1PR3 antagonist, inhibits the increased alkaline phosphatase production and mineralization seen in osteoblasts treated with S1P [16]. In a rat model of post-menopausal osteoporosis, FTY720 treatment of isolated MSCs increased osteogenic differentiation in comparison to sham and control groups [68]. Interestingly, one study in post-menopausal Korean

women found a correlation of high S1P levels in the blood to increased expression of the bone resorption marker C terminal telopeptide of type 1 collagen (CTX) and decreased bone mineral density [69]. However, this negative association was only found for some femoral locations such as the femoral shaft and not at the femoral neck or lumbar spine. Additionally, this was not a longitudinal study in which S1P plasma levels could be correlated with changes in bone mineral density over time. Still, Lee et al. makes the claim that higher circulating S1P can lead to bone resorption in women [69]. Weske et al. argues that increased S1P levels are more so indicative of the body's response to diminishing bone quality to increase bone formation; in a German population study in which men and women data were reported together, S1P levels were not correlated to CTX and were positively correlated with the bone formation marker procollagen type 1-N-terminal propeptide (PINP) [65]. With these varying results and S1P being increased in SCD, it is imperative to fully characterize the sickle bone phenotype.

S1P also plays a role in the other side of bone homeostasis: bone resorption. Osteoclasts secrete S1P to act on themselves intracellularly as well as to aid in osteoclast-osteoblast crosstalk. RANKL is secreted by osteoblasts and binds to RANK on OPCs to promote osteoclastogenesis. This pathway increases SK1 and S1P production in osteoclasts. However, once SK1 activity reaches a certain threshold, intracellular S1P attenuates further osteoclastogenesis and thus serves in a negative feedback loop [15]. However, osteoclast-secreted S1P can also bind to osteoblasts to promote further RANKL production and increase osteoclast differentiation [15, 16]. Additionally, S1P secretion by osteoclasts is further increased when cathepsin K (cat K), a protease that osteoclast secret to resorb bone, is inhibited [16]. Furthermore, S1P directs the migration of OPCs between the BM and blood. S1PR1 on OPCs directs them towards a higher S1P gradient. With RBCs being a S1P reservoir, S1P levels are higher within the peripheral

blood (PB) than in the BM. In a process deemed chemorepulsion by Ishii et al., S1PR2 on OPCs directs their chemotaxis towards lower S1P levels within the BM [70]. With S1P being increased in the blood of SCD patients [10], it is of interest of to investigate if the migration of OPCs is dysregulated in SCD.

2.4.3 S1P Signaling Utilization for Mobilizing MSCs

Stem and progenitor cells mobilized from the BM play a critical role in healing injured tissues. In fact, the production, mobilization, and recruitment of these cells are critical phases of tissue regeneration after traumatic injury [71-74]. Previous studies demonstrated that upon long bone fractures and other ischemic injuries, progenitor cells are mobilized and promote bone generation via vasculogenesis and osteoblastic differentiation [75-80]. Since endogenous stem and progenitor cells have been known to contribute to tissue repair, increasing their mobilization and recruitment at the defect site through pharmacological intervention has been studied to enhance healing. Systemic delivery of G-CSF or AMD3100, two potent stem cell mobilizing agents, has been shown to increase bone healing in fractures and calvarial defects, respectively [75, 76]. Recently, Fu et al. utilized G-CSF in rabbits to mobilize MSCs into the blood to be harvested and cultured to treat ON [81]. Deng et al. mobilized MSCs with G-CSF into the PB and found that they can aid in repair of injured cerebral tissue [82]. However, in certain populations, such as cancer patients undergoing chemotherapy or sickle cell patients, G-CSF has proven to be an ineffective or even life-threatening drug [83-85]. Furthermore, MSCs express the chemokine receptor 4 (CXCR4), which supports stem cells staying in the BM. AMD3100, being a CXCR4 antagonist, is thus capable of interrupting this linkage and mobilizing MSCs into circulation [86, 87]. Antagonism of the stromal cell-

derived factor-1 (SDF-1) receptor, CXCR4, by the small molecule AMD3100 is sufficient to cause rapid egress of hematopoietic stem and progenitor cells (HSPCs) into the blood; however, AMD3100 may impair the cells' ability to return to the niche since CXCR4 is necessary for homing and hematopoietic reconstitution [88] [89, 90]. Toupadakis et al. showed that twice daily AMD3100 injections for 42 days negatively impacted bone healing in a mouse femur fracture model [91]. Consequently, Granero-Molto et al. and Osturu et al. demonstrated that the CXCR4/SDF-1 pathway is necessary for MSCs to home to the bone and then differentiate into osteoblasts [92, 93]. Prolonged antagonism of CXCR4 impedes re-engraftment potential of MSCs into bone. Clearly there is a need to find another pathway to induce MSC mobilization.

S1P chemoattracts hematopoietic stem cells (HSCs) and other progenitor cells and guides their egress from BM into the PB [21, 22]. S1PR1 and S1PR3 in particular, have been shown to have significant effects on stem cell mobilization and chemotaxis. SEW2871, an S1PR1 agonist, enhances the motility and mobilization of OPCs in vivo and regulates bone homeostasis [62]. S1PR3 activation on human endothelial progenitor cells (EPCs) resulted in phosphorylation of CXCR4 and enhanced SDF-1 mediated chemotaxis and homing to ischemic tissues [61]. Kimura et al. also showed that S1PR3 activation with a small molecule analogue of S1P, FTY720, resulted in enhanced CXCR4 function in HSCs in vitro and in vivo as well as enhanced homing and proliferation [94]. Additionally, Awojoodu et al. showed that BM-derived cells are recruited via S1PR3 to inflamed tissues and induce a reduction in proinflammatory cytokine secretion and microvascular remodeling [95]. According to Ogle et al., the use of VPC010191, a S1PR1 agonist and S1PR3 antagonist, is capable of mobilizing HSPCs into circulation;

HSPCs cells pre-treated with VPC01091 had greater BM engraftment capacity in comparison to pre-treated AMD3100 cells [96]. Interestingly, Kong et al. demonstrated that the migration induced by S1P of human MSCs is conducted through S1PR1 and S1PR3 [18]. There is a need to further investigate the role that S1P signaling plays in MSC retention in the BM niche and subsequent migration.

2.5 Cathepsins

2.5.1 Cathepsin Overview

A class of proteases known as cathepsins degrade intracellular and extracellular proteins [97, 98]. Cathepsins break peptide bonds optimally in acidic environments, such as in the lysosome of cells [97, 98]. These enzymes are also secreted and active in extracellular spaces such as the cytosol or within the cellular membrane [99]. There are several classes of cathepsins that can be differentiated from one another based on the type of amino acid located in their active site. Serine cathepsins include A and G; aspartic cathepsins include D and E [98, 100]. The most prevalent class, cysteine cathepsins, include K, B, C, W, S, V, X, H, F, L, and O [99]. Cysteine cathepsins have been shown to play a role in several aliments such as cancer [101], cardiovascular disease [102], atherosclerosis [103], rheumatoid arthritis [104], and osteoporosis [105, 106]. In the context of SCD, activated monocytes in people with SCD increase the activity of cathepsins K and V in endothelial cells, leading to pathological remodeling of the vasculature [17]. Additionally, cysteine cathepsins B and L are activated by acid SMase, an enzyme that enhances inflammation in SCD. [10, 107]. Inactive cathepsins or procathepsins become active through the removal of the N-terminal propeptide either by other mature cathepsins or proteases, such as in the aforementioned example of acid

SMase, or by self-proteolysis to unveil the active site [108]. Cystatin C, an endogenous inhibitor of cathepsins, is present in extracellular fluids such as blood and is elevated in sickle cell patients, especially those in crises [109, 110].

2.5.2 Cathepsins' Role in Bone Remodeling

2.5.2.1 Cathepsin K

Osteoclasts are cells that resorb bone through the secretion of cathepsin K (cat K). In order to resorb bone, osteoclasts form a resorptive lacunae or pit between their ruffled border and the bone surface by attaching to the extracellular matrix proteins via $\alpha v\beta_3$ integrins [111, 112]. Cat K is transported from lysosomes and/or cytoplasmic vesicles and released into the resorption pit to degrade bone matrix [111, 112]. With bone's organic matrix being 90% type I collagen, it is no surprise that cat K is the most effective mammalian collagenase [113]. This vigorous proteolytic activity can be attributed to cat K's ability over other proteases to cleave the collagen triple helix as well as the cross-linked telopeptide sequences [99, 113]. Additionally, cat K is adept in degrading other proteins that compose the remaining 10% of bone matrix including fibronectin, biglycan, osteocalcin, bone sialoprotein, osteonectin, and osteopontin [114]. Cat K expression as well as osteoclastogenesis and osteoclast activation is regulated through RANKL binding to the RANK receptor on osteoclasts; this reaction induces the phosphorylation of transcription factor $NFAT_{c1}$ (nuclear factor of activated T-cells, $cytoplasmic_1$) and thus ensues the activation of the cat K gene (CTSK) promoter. Other modulators of cat K secretion include TNF-α, transcription factor Mitf, and INF-γ [115].

2.5.2.2 Cathepsin K Inhibition

Cat K inhibition has been used as a therapeutic strategy to combat overactive osteoclasts in such orthopedic maladies such as osteoporosis and osteoarthritis. Despite successes in preclinical and primate models, many cat K inhibitors have failed clinical

trials [116]. For example, balicatib, a reversible cat K inhibitor, was found to increase cortical thickness (Cort.Th.) and decrease bone turnover in ovariectomized cynomolgus monkeys [117]. However, due to the accumulation of balicatib in lysosomes, off target effects occurred in the form of cat S inhibition as well as the accumulation of collagen deposits in the skin that lead to dermal lesions patients in a discontinued Phase II clinical trial [116, 118, 119]. Odanacatib, a selective cat k inhibitor, increased the femoral neck bone mineral density and improved the biomechanical strength of bone in ovariectomized rhesus macaque monkeys [120]. Moreover, odanacatib was found to increase the bone mineral density by at least 4% in the hip and femoral neck of post-menopausal women in Phase II clinical trials [121]. Conversely, Phase III trials were discontinued due to the increased risk of patients developing stroke [122]. Likewise, there is clinical evidence that suggests complete cat K inhibition is not such a favorable outcome. Pycnodysostosis is a rare recessive disorder in humans in which mutations in CTSK lead to increased bone mineral density, but also cause brittle bones that are at an increased risk for fracture [117, 123]. Furthermore, although cat K is the most abundant cathepsin in osteoclasts, there is evidence that other cysteine cathepsins contribute to bone resorption. In mice, Hill et al. demonstrated that inhibitors for cat B and cat L inhibit bone resorption [124]. Ishibashi et al. has shown expression of cathepsin B, L, S in human osteoclasts [125]. Furthermore, Park et al. utilized enzyme zymography to establish the presence of activity of cat K, S, L, and V in human macrophages and osteoclasts [126]. These finding can be explained by the fact that cathepsins L, V, and S, similar to cat K, are collagenases [99, 113]. In fact, Everts et al. discovered that the broad cysteine cathepsin inhibitor, E-64, significantly increased the amount of non-digested bone matrix of mouse long bones explants, while the specific cat K inhibitors Z-Gly-Pro-Gln-VS-Ph and Z-Gly-Pro-Leu-CHO had no significant effect on bone resorption [127]. With these results, E-64 can be utilized as a useful tool in discerning if cysteine cathepsins are an effective target for bone disorders, such as SBD.

CHAPTER 3 Extensive Characterization of the Sickle Bone Phenotype

3.1 Introduction

Sickle cell disease (SCD), which affects approximately 100,000 Americans, is a genetic hematological disorder caused by a single mutation in the β-subunit of the gene encoding for hemoglobin [24]. In states of hypoxia, this mutation causes hemoglobin to transform into rod-shaped polymers and consequently distort erythrocytes, or red blood cells (RBCs), into a "sickle" shape. This membrane deformation causes erythrocytes to lose their flexibility and become trapped in small capillaries and arteries [26]. This vaso-occlusion blocks blood supply to downstream tissues and is often associated with acute/chronic pain, frequently in the bone and joints. In addition, the vascular blockages can lead to potentially fatal pathologies such as irreversible organ damage, chronic inflammation, coronary/peripheral artery disease, ischemic and transient ischemic attack (TIA) stroke, and myocardial infarction [28, 29]. Bone and joint disorders including osteonecrosis (ON), osteoporosis, osteopenia, known collectively as sickle bone disease (SBD), are among the most common complications of SCD [40]. Nearly 41% of adults with SCD have ON, particularly in the femoral or humeral head [2]. Joint destruction in the femoral head leads to bone infarctions at the proximal epiphyseal plate [128]. As this region supports the greatest amount of weight-bearing forces, the anterior superior portion of the femoral head is frequently susceptible to collapse [129]. Within the proximal femur or hip, a process known as epiphyseal plate fusion, which occurs at the end of puberty in humans and by 6 months in mice, is essential for the joint to be able to withstand load-bearing forces and to prevent deformation during skeletal development

[130, 131]. During this process, an area known as the physis (depicted in Figure 3.1) that contains proliferating chondrocytes becomes senescent and is resorbed and replaced with ossified bone [130]. Epiphyseal fusion is a marker of skeletal maturity, and premature closure of the epiphysis is speculated to be the cause of growth retardation in children with SCD [132, 133]. Therefore, there is a need to characterize this process in SCD as the process of epiphyseal fusion is crucial to the structural integrity and skeletal development of the femoral head.

Recent studies utilizing a transgenic sickle cell mouse model found that detrimental structural modifications to the microarchitecture of trabecular and cortical bone in SCD progresses over time and worsens with age [45, 134]. The trabecular bone in the microarchitecture of the femoral neck changes with age, including decreased number of trabeculae and a more rod-like structure. These changes cause the femoral neck to be susceptible to fracture, an injury common in SCD patients [135, 136]. These aforementioned sickle mouse studies mainly focused on the knee joint or distal femur and do not characterize the trabecular bone in the hip joint or proximal femur. Therefore, in this work we made the novel characterization of the trabecular bone within the proximal femur in the sickle Townes transgenic mouse model.

Furthermore, previous studies have either focused on one sex when using transgenic mouse models to investigate SBD [45, 134] or reported combined observations and data from both sexes [137]. It has been well established that bone morphometry can vary in humans, depending on sex and age. For instance, aging in men leads to weaker trabecular bone due to reduced trabecular thickness (Tb.Th.), while trabecular bone fragility in older women is due to the loss of trabecular plates [138]. One previous study

suggested that age and sex may play a role in SBD [139]. Furthermore, the standard clinical measurement of bone health, which is bone mineral density, varies in people with SCD due to age and sex [2, 140-142]. Since sex and age both influence bone physiology, this study sought to further characterize the sickle bone phenotype of male and female mice during bone development at three and five months in the Townes SCD mouse model.

In this work we characterized bone development and the sickle bone phenotype through Mimics Materialise and micro-computed tomography (microCT) analysis of femurs from 3 and 5-month-old male and female mice. Homozygous sickle (SS) mice were compared to heterozygous sickle (AS) and homozygous non-sickle (AA) mice in regard to their proximal epiphyseal fusion and bone microarchitecture. We demonstrate for the first time that SCD delays skeletal maturity, SBD implements bone loss in different anatomical areas in male and female mice, and that trabecular morphology is the most important aspect in characterizing the sickle bone phenotype.

3.2 Materials and Methods

3.2.1 Animals

Animal procedures and animal care protocols were performed in accordance and with approval from the Georgia Institute of Technology Animal Care and Use Committee. We utilized the Townes sickle transgenic mouse model (B6; 129-Hbatm1(HBA) Tow Hbbtm2 (HBG1, HBB*) Tow/Hbbtm3 (HBG1, HBB) Tow/J) from Jackson Laboratories [143]. The genotype of the Townes mice was determined through Native polyacrylamide gel electrophoresis (PAGE) of their blood obtained via the tail vein. Femurs from 3 and 5-month

old male and female mice were isolated for microCT, Mimics Materialise, and histology. The bones were stored at -20°C wrapped in gauze until time of evaluation.

3.2.2 MicroCT Analysis

Bone tissue mineral density (BMD) density and cortical and trabecular bone morphology within the femurs of 3-and 5-month-old male and female mice were examined by microCT imaging (μCT 40, Scano Medical, SUI) as previously reported [45, 144]. The mid diaphysis (1mm region at femur mid-point, 66 slices), distal epiphysis (0.32 mm in length distal from the growth plate, 25 slices), and femoral neck (44 slices extending distally from the proximal physis) were scanned at 12 um isotropic voxel size. Each section of interest is depicted in Figure 3.1. The analysis settings were as follows: 55kVp voltage, 144uA current, and a medium resolution (1024 X 1024-pixel image detection matrix). Cortical and trabecular bone were separated in each region utilizing an auto-contorting program, with additional manual adjustments for proper boundary allocation [145]. Mineralized and soft tissue were distinguished within the mid diaphysis, distal epiphysis, and femoral neck using a Gaussian noise filter of 0.8, support of 1, and thresholding bone at 205-1000 mg hydroxyapatite (HA)/cm^3, 62-1000 mg hydroxyapatite (HA)/cm^3, and 211-1000 mg hydroxyapatite (HA)/cm^3, respectively.

Utilizing direct distance transformation algorithms in Scanco software [144, 146], we measured the cortical bone area (BA), total area (TA), cortical bone area fraction (BA/TA), and cortical thickness (Cort.Th.) for the mid diaphyseal region. For the trabecular bone in the distal epiphyseal and femoral neck regions, we additionally measured trabecular spacing (Tb.Sp.), trabecular thickness (Tb.Th.), trabecular number (Tb.N.), trabecular connectivity density (Conn.Den.), bone volume (BV), total volume

(TV), bone volume fraction (BV/TV), and structure model index (SMI). A blinded investigator assessed all scans.

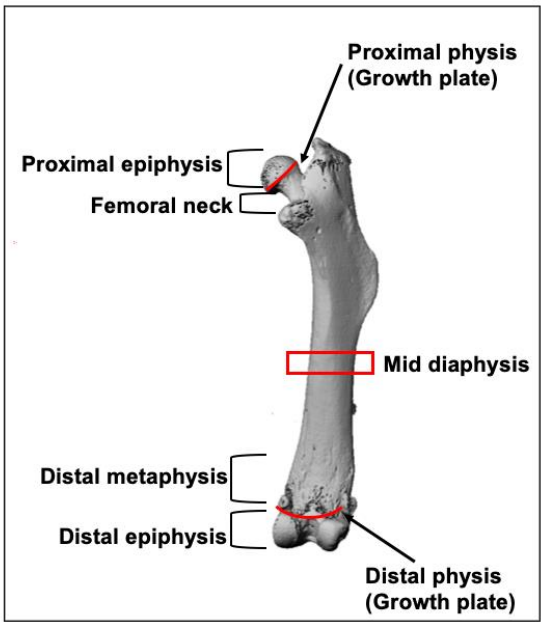

Figure 3.1. Femoral bone schematic. Diagram of microCT image of femoral bone with labeled areas analyzed by microCT.

3.2.3 Mimics Materialise Analysis

MicroCT images from male and female mice 3-and 5-months of age were used to reconstruct the first 5mm of the proximal femur. Mimics Materialise 15.0 (Leuven, Belgium) was used to generate a segmentation mask with a minimum threshold of 3070 Housefield units, a value recommended by the software. For each mask a cuboidal region was manually segmented from the epiphysis in the femoral head and used to reconstruct a 3D model. Porosity (%) was calculated from the reconstructed models using tools in Mimics. Bone volume fraction (%) was then calculated from porosity using the following equation:

$$Bone\ Volume\ Fraction(\%) = 100 - Porosity\ (\%)$$

3.2.4 Histology

Femurs were harvested, fixed in 10% neutral buffered formalin for 24 hours at 4^{o}C, and decalcified using a formic acid decalcifying solution (Immunocal, StatLab, McKinney Tx) for 3 hours at room temperature. The bones were embedded in paraffin and the 5-month-old femoral heads were sectioned for hematoxylin and eosin (H&E) staining. Bone sections were mounted with xylene mounting media (Thermo-Fisher) and visualized under a bright field microscope.

3.2.5 Data Analysis and Statistical Comparisons

By utilizing MATLAB software (Natick, MA), principal component analysis (PCA) was utilized on 23 bone parameters generated with microCT. Principal components (PC) were generated, with the PC1 depicting the greatest percentage of data variance and PC2 (statistically independent from PC1) depicting the next utmost percentage of data variance. The microCT data was prepared in a matrix for each age (3 and 5 months) with bone parameters in rows, and the individual mice in the first column separated by sex and genotype. Correlation coefficients between BV/TV and mouse body weight bone were produced with GraphPad Prism (La Jolla, CA).

Statistical comparisons were performed utilizing GraphPad Prism. The resulting analysis is conveyed as mean ± standard deviation (SD). Two-tailed t-test was used for column analysis. For grouped analyses, one-way ANOVA with Tukey's post-test for multiple comparisons was utilized. For grouped analyses comparing data between genotype and age, two-way ANOVA with Tukey's multiple comparisons test was used. A *p*-value less than 0.05 was considered statistically significant.

3.3 Results

3.3.1 SCD delays epiphyseal plate fusion

Femoral microCT scans of 3- and 5-month-old male and female mice demonstrated a difference in proximal epiphyseal plate fusion among ages and genotype in the male mice, with no discernable differences in female mice. Based on previously reported results, we expected by 5 months to see fusion occur only in the male mice and not the females [130] . By 5 months of age, plate fusion (indicated by the appearance of hardened bone) occurs as anticipated for AA and AS male mice, but not for SS males (Figure 3.2A). As expected, epiphyseal plate fusion did not occur at 3 or 5 months for female mice regardless of genotype (Figure 3.2A). To confirm these observations, we quantified the bone volume fraction (BV/TV), which is the percent of mineralized bone per volume of sample, of the proximal epiphysis through Mimics Materialise. The BV/TV was significantly decreased in SS males (54.86 ± 5.5%) in comparison to AA males (90.53± 8.8%) at 5 months while no differences were observed for females (Figure 3.2B-C).

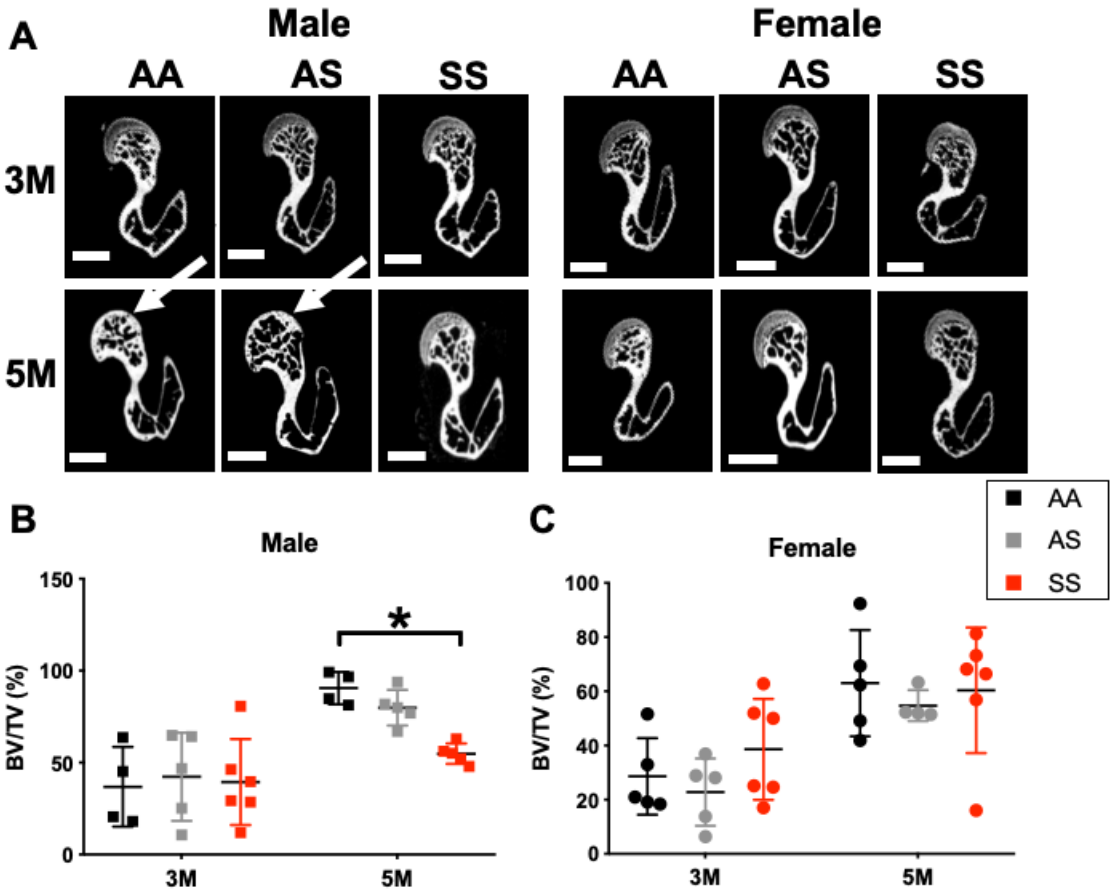

Figure 3.2. Epiphyseal plate fusion in the femoral head is age, sex, and genotype dependent. (A) Proximal femur microCT scans of male and female Townes mice at 3 (top) and 5 (bottom) months. Arrow indicates epiphyseal fusion. Mimics Materialise analysis of bone volume fraction in the proximal epiphysis of the femur in (B) male and (C) female mice at 3 and 5 months (n=4-6 mice per group). AA=black, AS=gray, SS=red. Data expressed as mean ± SD. Statistical significance, * $p < 0.05$, determined by two-way ANOVA with Tukey's post-hoc test, scale bar 1mm.

Based on previous observations made in C57BL6 mice [130], we expectantly observed no epiphyseal fusion in the distal epiphysis of the femurs, with no discernable differences between genotype, sex, or age (Figure 3.3).

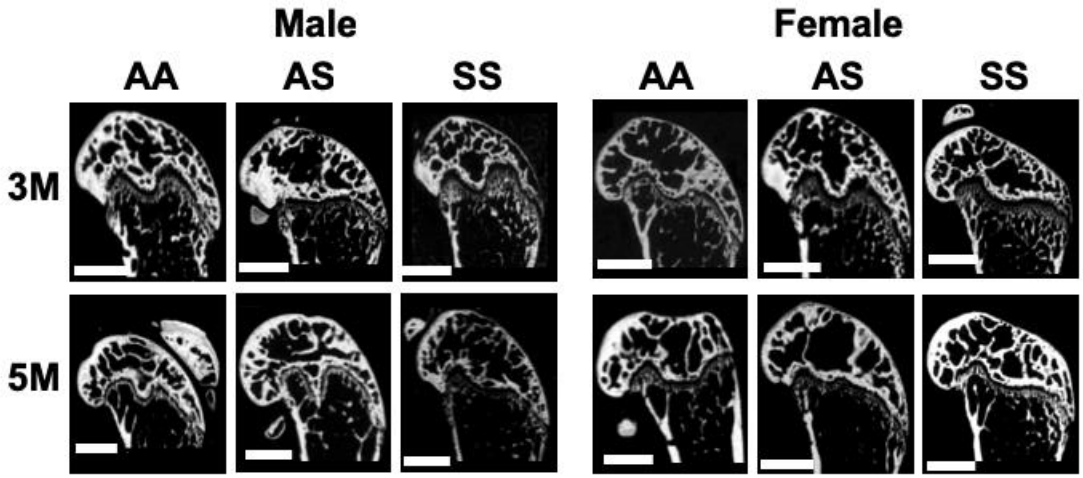

Figure 3.3. Epiphyseal plate fusion does not occur in the distal femur. MicroCT scans of male and female mice at 3 (top) and 5 (bottom) months that display no epiphyseal plate fusion. Scale bar 1mm.

H&E staining of SS male mice indicated that the proximal epiphyses were still in the senescence phase of epiphyseal plate fusion, characterized by the diminished presence of hypertrophic chondrocytes, rather than the state of fusion that is expected by 5 months (Figure 3.4A). For female mice, each genotype's proximal epiphysis remained in the senesce stage as signified by the reduced existence of proliferating chondrocytes (Figure 3.4B).

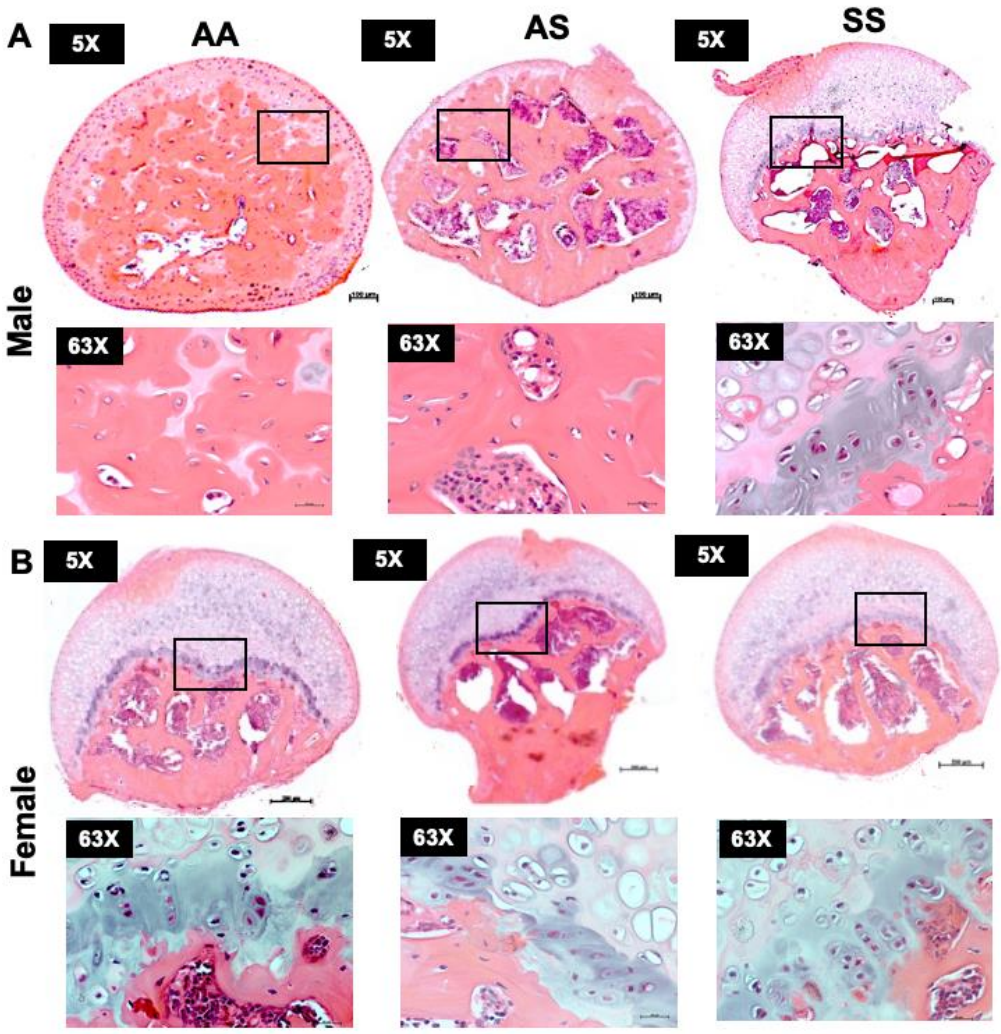

Figure 3.4. Histological staining of proximal epiphysis of the femur. Hematoxylin and eosin staining of (A) male and (B) female 5-month old proximal epiphysis. Complete resorption of the physis and epiphyseal fusion in AA and AS male mice occur by 5 months, while SS males and all three genotypes of female mice remain in the senescence stage, indicated by diminished presence of proliferating chondrocytes. Scale bar 100um for 5X and 20 um for 63X images.

MicroCT analysis of 12-month old SS male mice did show evidence of epiphyseal fusion (Figure 3.5A), further confirmed by their proximal epiphysis BV/TV trending towards being increased in comparison to 3- and 5-month SS males (Figure 3.5B). This data

suggests that SCD does not prevent ossification of bone but delays it. Additionally, we determined that epiphyseal BV/TV is significantly positively correlated to mouse body weight in AA (r= 0.9769, p= 0.0231) and AS (r=0.8793, p=0.0494) mice; however, there was no correlation in SS males (r=0.03971, p=0.9495) (Figure 3.5C). This further suggests a delay in overall growth and skeletal development due to SCD. Interestingly, the BV/TV of female AA (r=0.0074, p=0.9906) and AS (r=0.5185, p=0.4815) mice either had no correlation or were poorly positively correlated to body weight, respectively, while the BV/TV of female SS mice (r= -0.8029, p=0.1018) were negatively correlated to body weight (Figure 3.5D).

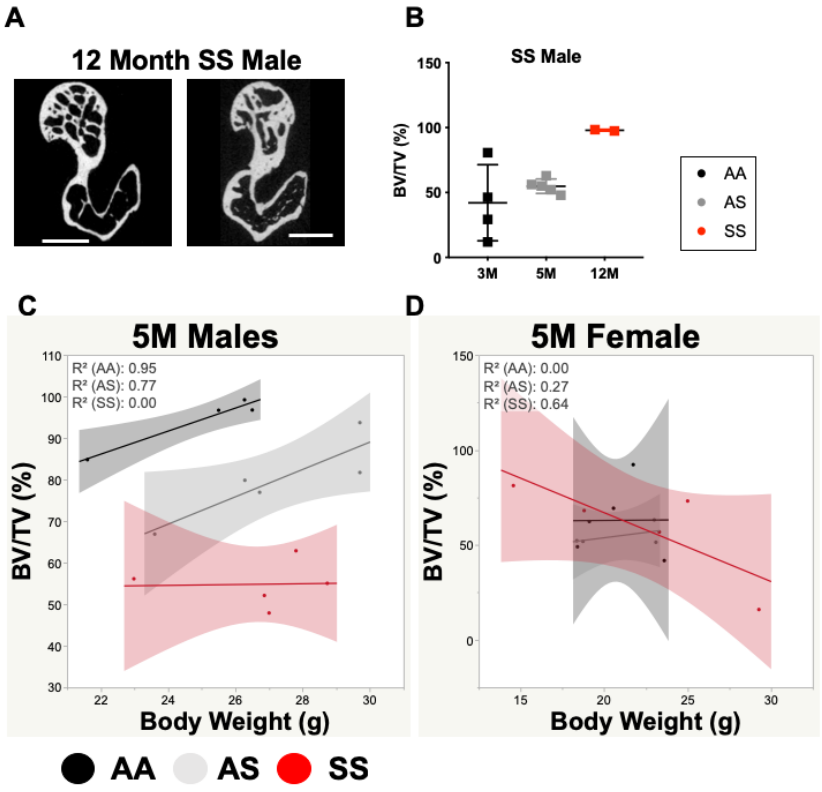

Figure 3.5. SCD delays epiphyseal fusion and skeletal growth. (A) Micro-CT scans of 12-month-old SS male mice that display epiphyseal plate fusion. (B) Mimics Materialise analysis of BV/TV of the proximal epiphysis in SS male mice at 3, 5, and 12 months (n=2-5 mice per group). Correlation plots for 5-month old (C) male and (D) female mice between BV/TV and mouse body weight. AA=black, AS=gray, SS=red (n=4-5 mice per

group). Data expressed as mean ± SD. Statistical significance, * $p < 0.05$, determined by correlation, scale bar 1mm.

3.3.2 Sickle trabecular bone morphology varies with sex

Due to the differences in epiphyseal fusion between genotypes for male mice, we further analyzed the proximal femur and characterized the trabecular bone in the femoral neck via microCT. SCD did not have an effect on male trabecular bone, which can be visually seen in Figure 3.6A, as the overall trabecular structure and thickness is similar across genotypes. Trabecular thickness (Tb.Th.) (48% increase in SS) and BV/TV (65% increase for SS) increase from 3 to 5 months while the structure model index (SMI) (1.173 to -0.63 for SS) decreases from the same time points for male mice of all three genotypes (Figure 3.6B-D). The latter indicates that over time the trabecular bone in the femoral neck in male mice changes to more concave morphology. Interestingly, SCD did have a negative effect in a 15% reduction of Tb.Th. in the femoral neck of SS female mice at 5 months in comparison to AA (Figure 3.6B). Bone mineral tissue density (BMD) was not significantly changed with respect to age or genotype for both sexes (Figure 3.6E).

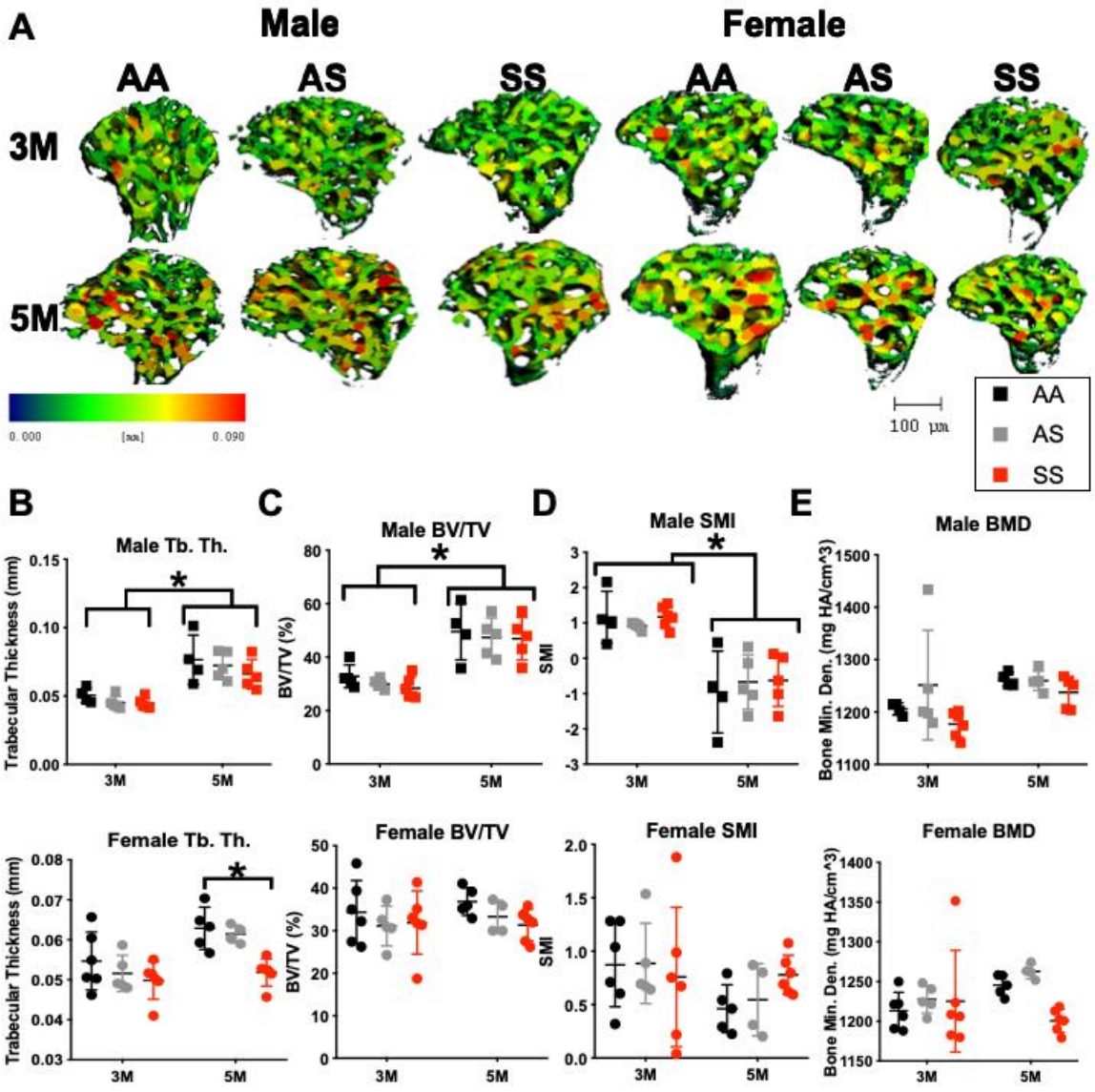

Figure 3.6. Trabecular bone in the femoral neck increases in male mice with age. (A) Representative 3D heat maps of trabecular morphology in the femoral neck region of the proximal femur in AA, AS, and SS 3 (top) and 5 (bottom) -month-old male and female mice. A pseudocolor scale of blue (0 mm) to red (0.09 mm) depicts trabecular thickness. (B-D) Trabecular bone parameters generated by microCT scans for male (top) and female (bottom) including (B) trabecular thickness, (C) bone volume fraction, (D) structure model index and (E) bone tissue mineral density. AA=black, AS=gray, SS=red. Data expressed as mean ± SD. Statistical significance, * $p < 0.05$, determined by two-way ANOVA with Tukey's post-hoc test, n=4-6 mice per group, scale bar 100 µm. Abbreviations: Tb.Th., trabecular thickness; SMI., structure model index; BMD, bone tissue mineral density.

The aforementioned reduction in proximal Tb.Th. in SS females is also present in the distal epiphyseal region, which is depicted in Figure 3.7A. Female SS Tb.Th. is decreased in comparison to AA mice at 3 and 5 months (Figure 3.7B). Of the female mice, only the AA genotype sees an increase (16%) in Tb.Th. from 3 to 5 months (Figure 3.7B). Conversely, male AS and SS Tb. Th. increases 20% and 26% with age, respectively (Figure 3.7B). This suggests that sickle trait and SCD results in reduced trabecular bone growth with age only in female mice. Furthermore, the interconnectivity of the trabecular bone decreases 37% and 18% with respect to age for AS and SS females, respectively (Figure 3.7C). Interestingly, trabecular spacing (Tb.Sp.) is reduced up to 10% in SS females at both time points in comparison to controls, indicating that by 5 months the trabeculae are close together, but do not compose as well as a connected structure (Figure 3.7C-D). The connective density (Conn. Den.) of AS and SS mice decreases 35% and 21% from 3 to 5 months for males as well, respectively (Figure 3.7D). However, no significant differences for Tb. Sp. were found for male mice (Figure 3.7C), suggesting a difference in trabecular morphology between SS males and females. This difference is further demonstrated in the BMD of SS female mice being reduced up to an astounding 79% at 5 months in comparison to AA and AS mice, while the BMD in SS male increases 8% with respect to age (Figure 3.7E).

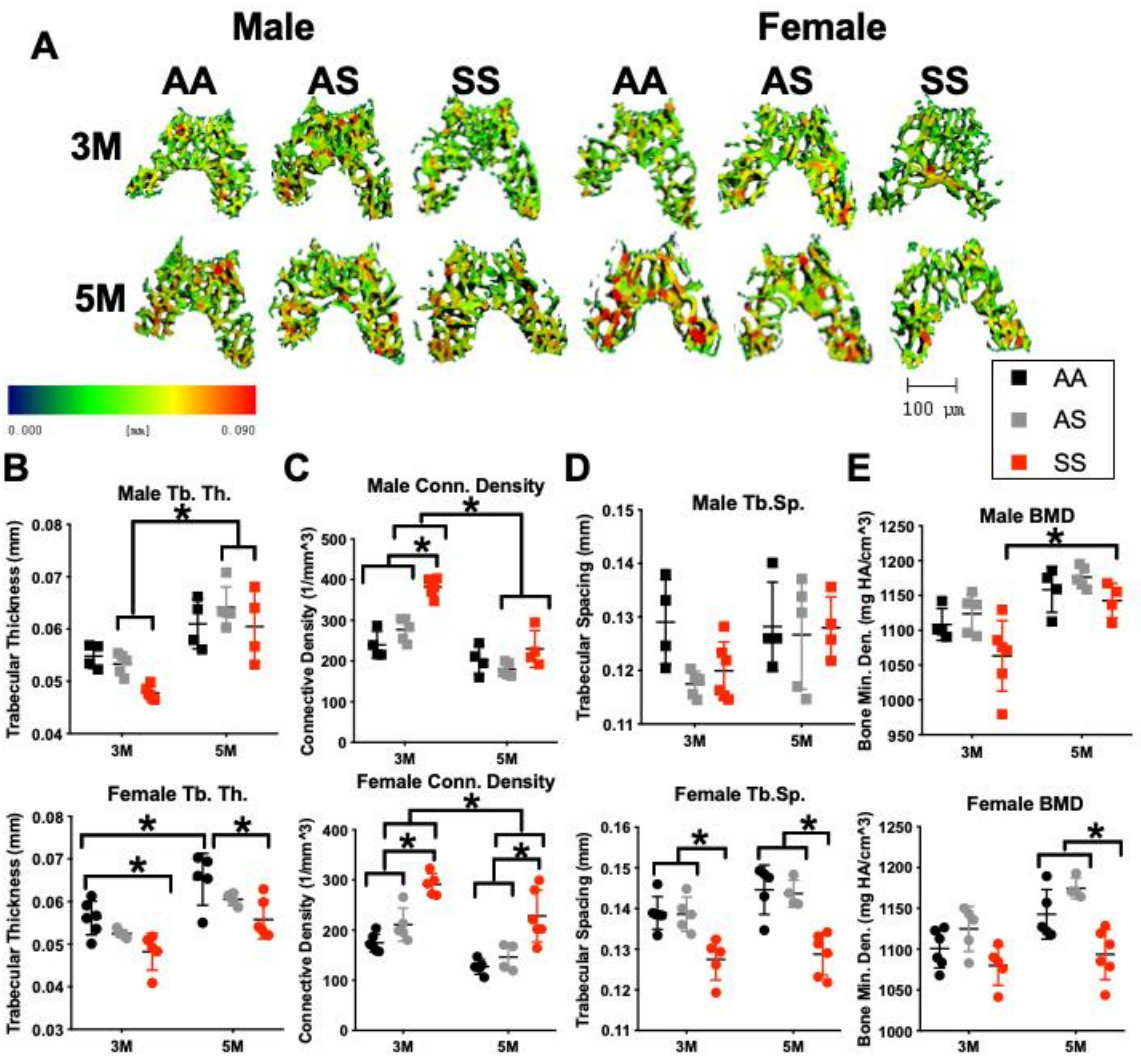

Figure 3.7. Trabecular bone in the distal epiphysis is reduced in 3- and 5-month female SS mice. (A) Representative 3D heat maps of trabecular morphology in the epiphyseal region of the distal femur in AA, AS, and SS 3 (top) and 5 (bottom) -month-old male and female mice. A pseudocolor scale of blue (0 mm) to red (0.09 mm) depicts trabecular thickness. (B-E) Trabecular bone parameters generated by microCT scans for male (top) and female (bottom) including (B) trabecular thickness, (C) connective density (D) trabecular spacing, and (E) bone mineral density. AA=black, AS=gray, SS=red. Data expressed as mean ± SD. Statistical significance, * $p < 0.05$, determined by two-way ANOVA with Tukey's post-hoc test, n=4-6 mice per group, scale bar 100 µm. Abbreviations: Tb. Th., trabecular thickness; Tb. Sp., trabecular spacing; Conn. Density, connective density; BMD, bone mineral density.

3.3.3 Cortical bone is decreased in sickle mice

With cortical thickness (Cort. Th.) being a main contributor to bone strength [147], we also analyzed the cortical bone in the murine femurs within the mid diaphyseal region. SS femurs exhibited up to 27% in reduction of Cort. Th. in comparison to AA and AS genotypes at 3 and 5 months for both sexes (Figure 3.8B), which is visually indicated by more red being present in the 3D renderings of the area (Figure 3.8 A). However, Cort. Th. was found to increase up to 29% from 3 to 5months for all three genotypes for males and 16% for AA females (Figure 3.8B). This suggests that sickle trait and SCD subdues cortical bone growth with age only in female mice. This distinction is further apparent in which again only AA female mice had a significant increase (16%) in BMD with age (Figure 3.8C). Furthermore, BMD was reduced up to 5% in SS male and female mice in comparison to wild-type and/or sickle trait at 3 and 5 months (Figure 3.8C). Mineralized tissue present, or bone area (BA) was also reduced up to 33% in SS male mice at 3 and 5 months in comparison to controls, but only significantly reduced (21%) for female mice at 5 months (Figure 3.8D). Similarly, bone area fraction (BA/TA) decreases up to 25% in SS mice of both sexes in comparison to AA and AS at both 3 and 5 months. Interestingly, SS male mice BA/TA increases 18% from 3 to 5 months, but not to the level of AA or AS (Figure 3.8E).

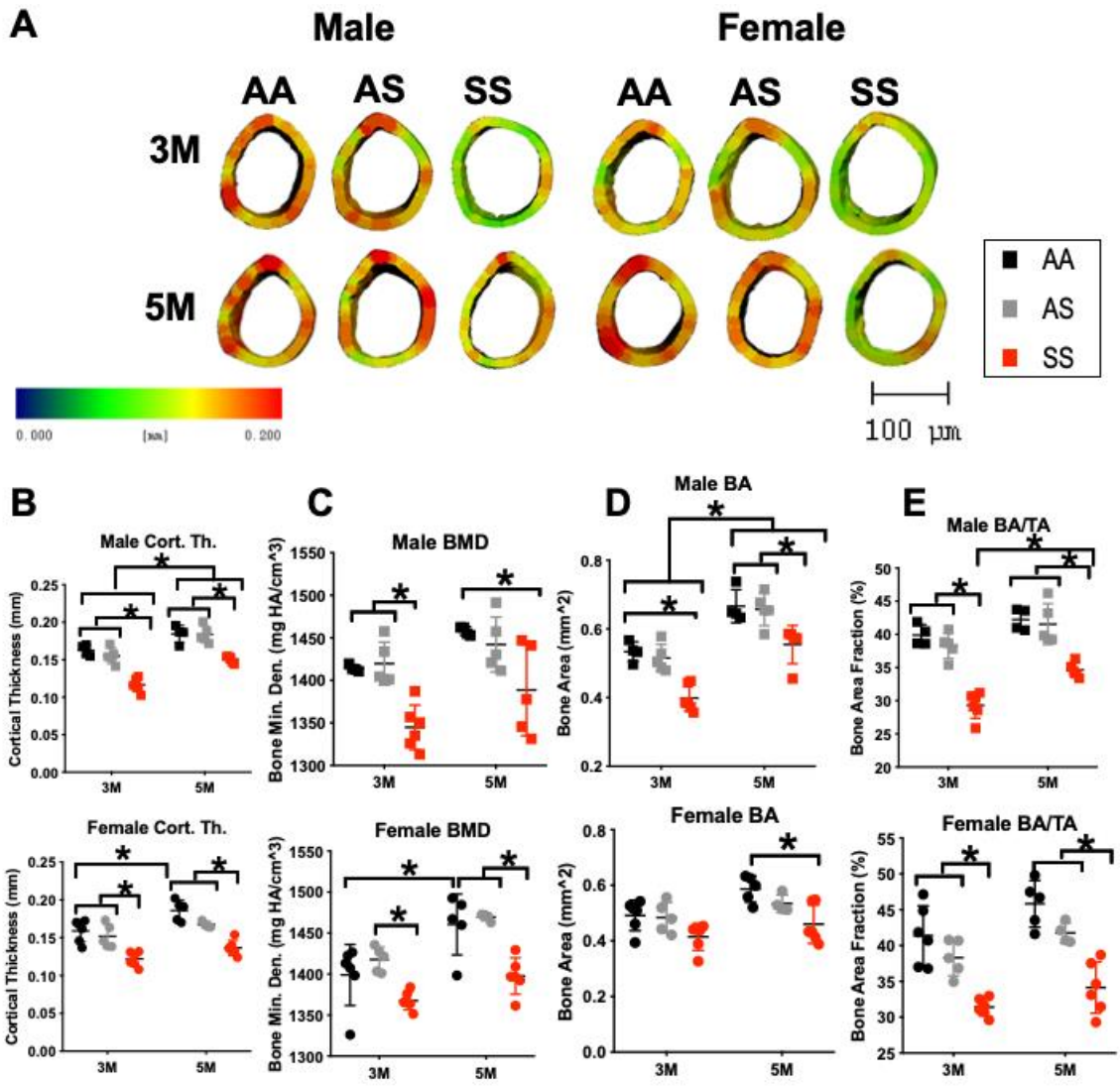

Figure 3.8. Cortical bone deficiency in SS male and female mice persists at 3 and 5 months. (A) Representative 3D heat maps of cortical thickness in the mid diaphyseal region in AA, AS, and SS 3 month (top) and 5 month (bottom) -month-old male and female mice. A pseudocolor scale of blue (0 mm) to red (0.2mm) depicts cortical thickness. (B-E) Cortical bone parameters generated by microCT scans for male (top) and female (bottom) mice including (B) cortical thickness, (C) bone tissue mineral density, (D) bone area, and (E) bone are fraction. AA=black, AS=gray, SS=red. Data expressed as mean ± SD. Statistical significance, * $p < 0.05$, determined by two-way ANOVA with Tukey's post-hoc test, n=4-6 mice per group, scale bar 100 µm. Abbreviations: Cort. Th., cortical thickness; BMD, bone tissue density; BA, bone area; TA, total area.

3.3.4 Principal component analysis of microCT measurements on mouse femurs

Since microCT analysis produces large multivariate datasets, we used unsupervised principal component analysis (PCA) to determine exactly what bone parameters contribute to the variability in the data we observed in Figure 3.6, Figure 3.7, and Figure 3.8. We wanted to also elucidate if age, genotype, or gender matter most in differences in bone morphology in the Townes mouse model. Figure 3.9A-B shows the two-dimensional (2D) principle component (PC) scores of each animal and the microCT parameters that contribute to each animal's placement within the 2D PCA space. The first two PCs account for 62.48% of the variability in the data. There is very little observable clustering in the 2D renderings (Figure 3.9A-B). This indicates a need to further analyze the data with more separation.

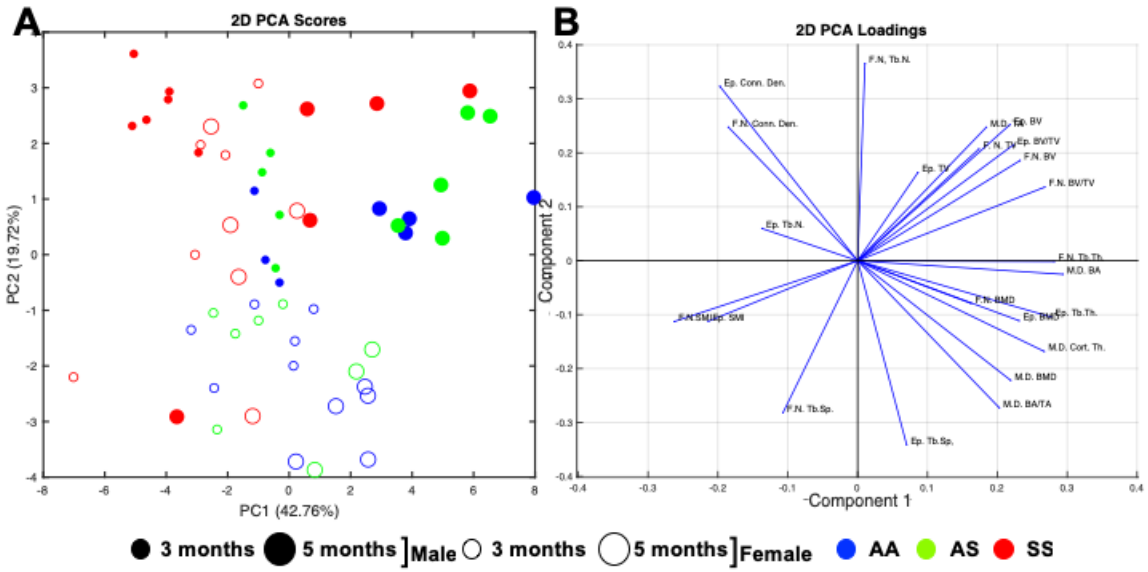

Figure 3.9. Unsupervised PCA of trabecular and cortical bone parameters of male and female mice at 3 and 5 months. (A) 2D scores plot of bone parameters for male and female AA, AS, and SS mice at 3 and 5 months. (B) 2D loadings (weight coefficients) plot of the 23 input variables in the reduced principal component space. Input variables are the following: mid diaphysis cortical bone- bone area, total area, bone area fraction, bone mineral density, cortical thickness; distal epiphysis and femoral neck trabecular

bone- bone volume, total volume, bone volume fraction bone mineral density, trabecular thickness, trabecular spacing, trabecular number, connective density, structure model index. N= 4-6 mice per group. Abbreviations: PCA, principal component analysis; F.N., femoral neck; Ep., Epiphysis; M.D., mid diaphysis.

We repeated PCA on the bone but instead this time we attempted to see if clustering of the data occurred when we separated the data based on age. Contrasting with the earlier PCA, there was clustering of the data based on genotype and gender. Figure 3.10A-B and Figure 3.11A-B show the 2D scores of each animal and the microCT parameters that contribute to each animal's placement within the 2D PCA space. For 3-month-old mice, the first two PCs account for 55.3% of the variability in the data, while they account for 62.69% for the 5-month-old mice. The data generally clustered by genotype, with the SS animals separating from AA and AS animals (Figure 3.10A, Figure 3.11A). This suggests that genotype is the main contributor to differences we observed in the bone in Figure 3.6, Figure 3.7, and Figure 3.8.

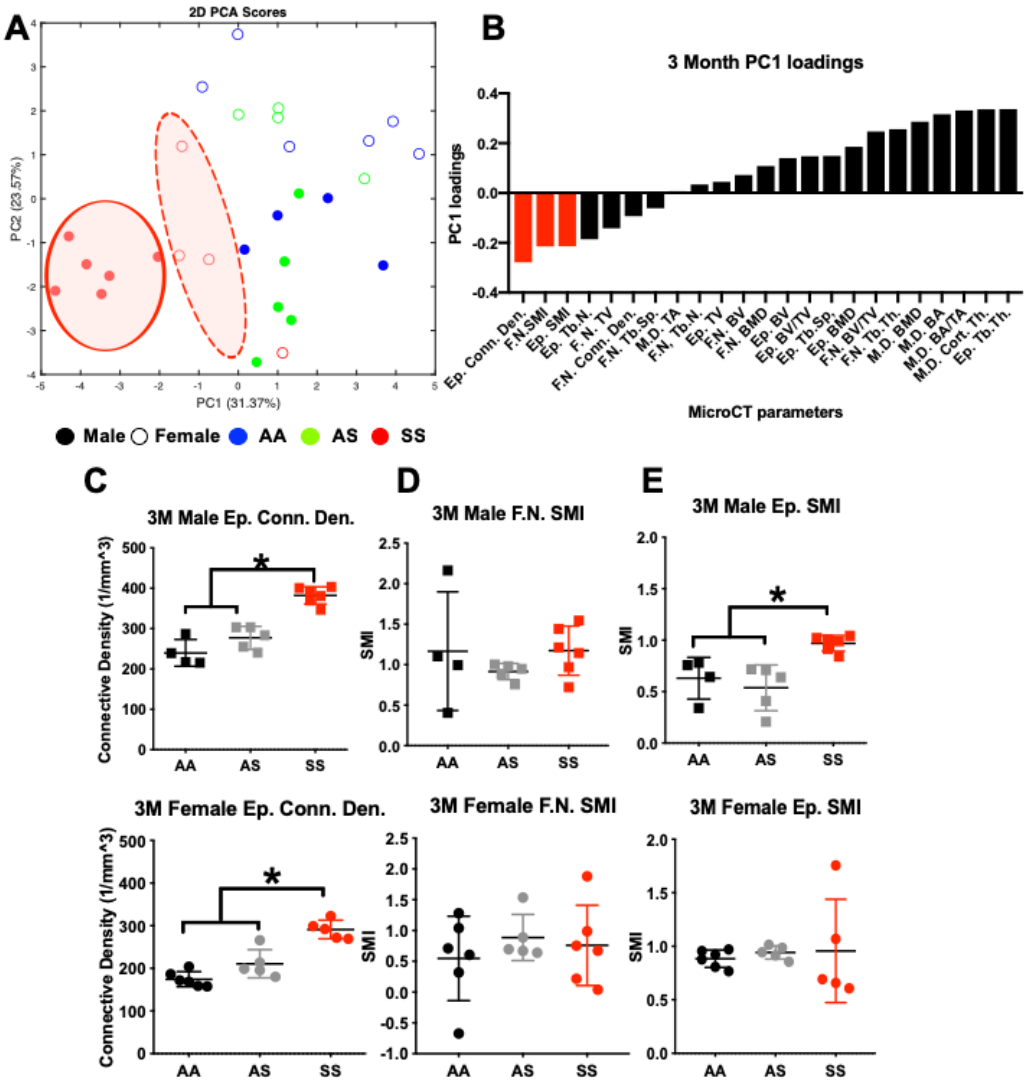

Figure 3.10. Unsupervised PCA of cortical and trabecular bone parameters of male and female mice at 3 months. (A) 2D scores plot of bone parameters for male and female AA, AS, and SS mice at 3 months. (B) 2D loadings (weight coefficients) plot of the 23 input variables in PC1. Top components separating sickle samples are depicted in red. (C-E) Top three parameters in PC1 for 3-month-old males (top) and females (bottom) including (C) distal epiphyseal connective density, (D) femoral neck SMI, and (E) distal epiphyseal SMI. Input variables are the following: mid-diaphysis cortical bone- bone area, total area, bone area fraction, bone mineral density, cortical thickness; distal epiphysis and femoral neck trabecular bone- bone volume, total volume, bone volume fraction bone mineral density, trabecular thickness, trabecular spacing, trabecular number, connective density, structure model index. Statistical significance, * $p < 0.05$, determined by one-way ANOVA with Tukey's post-hoc test, n=4-6 mice per group. Abbreviations: PCA, principal component analysis; F.N., femoral neck; Ep., Epiphysis; M.D., mid diaphysis; Conn. Den., connective density; SMI, structural model index.

When we plot PC1 vs PC2 for 3-month-old mice, we see that the SS male and female animals separated from the AA and AS groups primarily along PC1, with both genders clustering into their own groups (Figure 3.10A). This separation is due to several parameters that are in PC1, including, Conn. Denn. (epiphysis and femoral neck), SMI (epiphysis and femoral neck), epiphysis Tb.N., femoral neck TV, and femoral neck Tb.Sp. (Figure 3.10B). In the loading parameters contributing to negative PC1 scores, we see a similar pattern for significant differences among genotypes in the males and females for epiphysis Conn. Den. (Figure 3.10C) and femoral neck SMI (Figure 3.10D). However, with epiphyseal SMI (Figure 3.10E), SS males have an increased SMI in comparison to wild-type and trait. This difference, however, is not seen in females. This indicates that SS males at 3 months are reaching more rod-like architecture in the distal trabecular bone. This is indicative of accelerated ageing and deterioration in bone structure [148]. In the AA and AS groups, female animals separate from the male animals along PC2, further indicating the need to study the bone in all three genotypes separately by sex (Figure 3.10A). The PC1 vs PC2 plot for 5-month-old mice reveals that the SS animals cluster away from the wild-type and trait groups along both PC1 and PC2. This separation is due to several parameters including, Conn.Den. (epiphysis and femoral neck), and epiphysis SMI (Figure 3.11A-B). For these parameters, SS Conn. Den. in the epiphysis is increased in female mice (Figure 3.11C) but is increased in SS male mice in the femoral neck (Figure 3.11D). This demonstrates that the sickle trabecular bone morphology is different depending on the region and gender, further supporting the results depicted in Figure 3.6 and Figure 3.7. Epiphysis SMI was not significantly different among the genotypes for males and females. It is interesting however that some male AS mice have negative SMI, indicating a concave trabecular morphology (Figure 3.11E). Finally, as seen with three-month animals, AA and AS males separate from their female counterparts along PC2 (Figure 3.10A, Figure 3.11A).

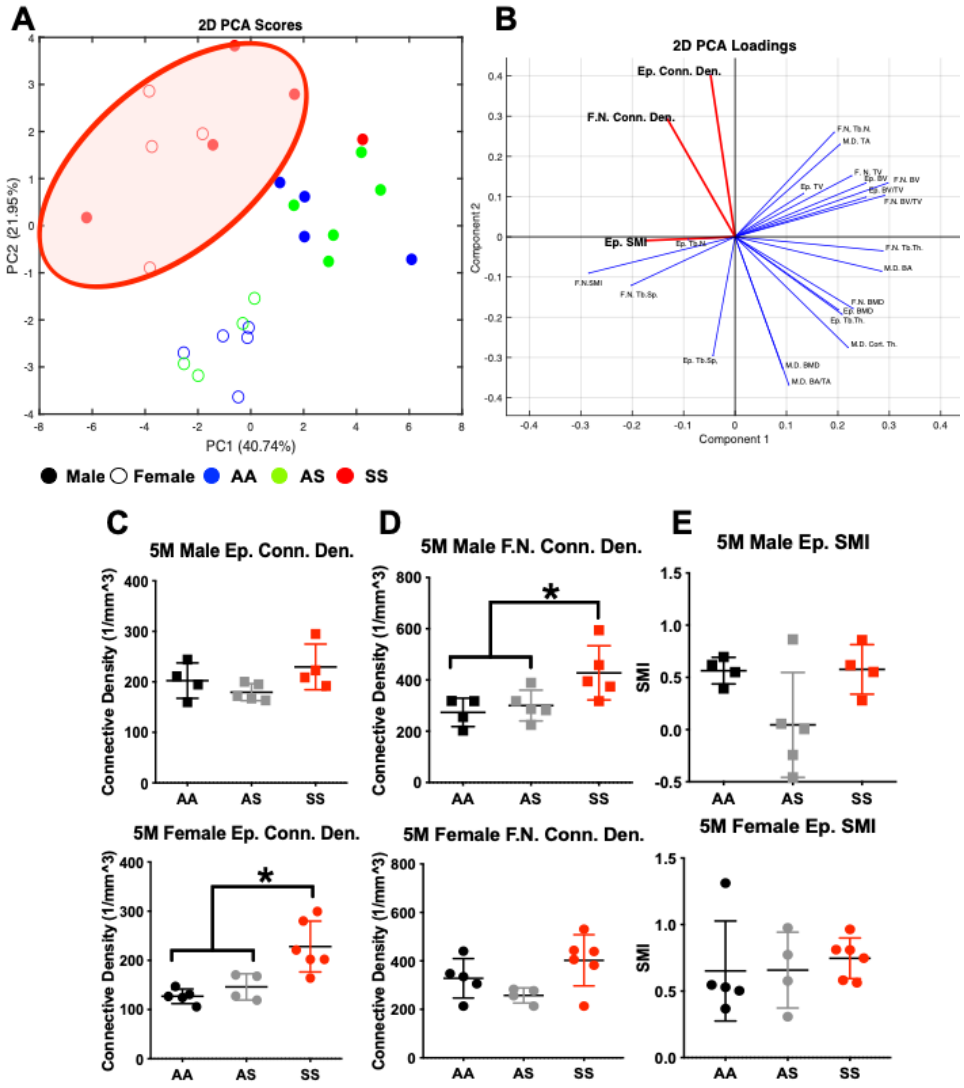

Figure 3.11. Unsupervised PCA of cortical and trabecular bone parameters of male and female mice at 5 months. (A) 2D scores plot of bone parameters for male and female AA, AS, and SS mice at 5 months. (B) 2D loadings (weight coefficients) plot of the 23 input variables in the reduced principal component space. Top components separating sickle samples are depicted in red. (C-E) Top three parameters in PC space for 5-month-old males (top) and females (bottom) including (C) distal epiphyseal connective density, (D) femoral neck connective density, and (E) distal epiphyseal SMI. Input variables are the following: mid-diaphysis cortical bone- bone area, total area, bone area fraction, bone mineral density, cortical thickness; distal epiphysis and femoral neck trabecular bone- bone volume, total volume, bone volume fraction bone mineral density, trabecular thickness, trabecular spacing, trabecular number, connective density, structure model index. Statistical significance, * $p < 0.05$, determined by one-way ANOVA with Tukey's post-hoc test, n=4-6 mice per group. Abbreviations: PCA, principal component analysis; F.N., femoral neck; Ep., Epiphysis; M.D., mid diaphysis; Conn. Den., connective density; SMI, structural model index.

3.4 Discussion

During human development, bones grow in length due to a process called endochondral ossification, where an avascular matrix of cartilage formed by chondrocytes in the physis of the bone is resorbed by osteoclasts and new bone is formed from the deposit of bone matrix by osteoblasts [130]. Once the physis is fully resorbed, epiphyseal fusion occurs, and the bone has reached skeletal maturity. This process is thought to be impaired and potentially occurs too quickly in sickle cell children [132, 133]. Children with SCD often are of reduced stature or height, have abnormal lengths in their femurs resulting in a limp or altered gait, and even see bone abnormalities as early as 19 months [132, 133, 149].

For the first time, we characterized epiphyseal plate fusion in a sickle transgenic mouse model. In a previous study, male C57BL6 mice had undergone epiphyseal fusion in the proximal femur by 4 months, while only approximately 60% of C57BL6 female mice had undergone epiphyseal fusion by 6 months [130]. This is opposite of what has been witnessed in clinical data in which females on average reach skeletal maturity by age 17 and males reach this milestone by age 18.5 [150]. In our study we saw fusion occur in AA and AS mice by 5 months, but not SS males (Figure 3.2A). During longitudinal bone growth, the growth plate is composed of three zones of resting, proliferating, and hypertrophic chondrocytes, with the latter two arranged in columns. Once the growth plate enters the senescence phase of development, the proliferating and resting chondrocytes become disorganized, and the zone of hypertrophy becomes diminished [130, 151]. At 5 months, SS males and all three genotypes in the females appear to be still in the senescence phase of development, indicated by the presence of disorganized chondrocytes that are not flanked by ossified bone (Figure 3.4A-B). The

lack of ossified bone is further apparent in our BV/TV measurements. BV/TV has been shown in previous studies through Archimedes' principle to be directly proportional to bone mineral density [152]. We demonstrate that BV/TV in SS 5-month males is decreased in comparison to AA and AS (Figure 3.2B). By 12 months, we show that fusion does occur in the male mice with even an increased BV/TV in the proximal femur in comparison to SS males at 3 and 5 months (Figure 3.5A-B) We speculate to the reason why this delay in ossification occurs in the sickle environment. In order for fusion to occur in mice, chondrocytes in the physis differentiate and allow hypoxia inducible factor 1 alpha (HIF1-α)-induced production of vascular endothelial growth factor (VEGF) [153]. This allows for blood vessels to enter the epiphysis around 12 weeks, induction of chondrocyte apoptosis, resorption of the physis, and thus complete ossification of the epiphysis through the cartilage being substituted for trabecular bone by 15 weeks [130]. In mice this process is controlled through intricate timing between the expression of VEGF from chondrocytes from the physis (starting at 5 weeks) and the epiphysis (starting at 10 weeks) [130, 154]. We hypothesize that since the skeletal maturation in sickle mice is delayed, this production of VEGF is inhibited or delayed and thus so is the ossification of the epiphysis. Moreover, VEGF is upregulated in the growth plate of humans undergoing puberty, a stage of development that is delayed in children with SCD [155, 156]. Scantiness of other growth factors could also be playing a role in delayed epiphyseal fusion in SCD. Vitamin D in mammals leads to a decrease in chondrocyte proliferation and increase in hypertrophic chondrocyte apoptosis in the growth plate [157, 158] . Consequentially, people with SCD who have suffered several bone injuries also are plagued with vitamin D deficiency [159]. Furthermore, chondrocytes in the physis are

adapted to proliferate and survive hypoxic environments [160]. If the vasculature that crosses into the epiphysis is blocked due to sickled RBC vaso-occlusions, then chondrocytes are allowed to remain in a prolonged hypertrophic state that delays the complete ossification of the epiphysis. In pediatric patients, the BMD is decreased in the proximal femur due to vascular occlusions [2]. Furthermore there is evidence that this type of epiphyseal fusion is impaired in sickle patients in the metacarpals, metatarsals, and phalanges; these long bones in sickle cell patients can undergo premature fusion of the epiphysis and thus result in short fingers [161]. Future studies are needed in which hypoxic conditioning of AA and AS male mice will be performed to see if a similar delay in epiphyseal fusion as we saw in the SS mice occurs. Also, characterization of the vascular development within the proximal femur of all three genotypes to ascertain if blood vessels cross into the epiphysis at the expected time point of 12 weeks is needed.

SCD's effect on delaying bone development is further evident in our correlation plots relating BV/TV of the proximal epiphysis to mouse body weight in 5-month mice. For SS males, there is no correlation, while we see a significant positive correlation for AA and AS males (Figure 3.5C). This shows that SCD hinders overall growth and skeletal development. These findings coincide with clinical data in which adolescent males with SCD were discovered to have lower mean body weight and body mass index in comparison to the non-sickle population [155]. AA females also have no correlation of their body weight to BV/TV, demonstrating that SCD causes for males, who are typically larger in size, to be on the same level of growth as females (Figure 3.5D). Furthermore, SS females' body weight is negatively correlated with BV/TV, demonstrating that as their body weight increases, the BV/TV actually decreases (Figure 3.5C-D). According to

Iwaniec et al., alterations to body weight come before any adjustments are made to the skeletal system that will allow bones to properly handle the modification in the mechanical loads [162]. Our data suggests that even though the sickle mice are growing, there is delayed development in the femurs. This postponed response puts sickle cell patients at an even greater risk for fracture, especially growing children [162] [163].

Another aim of this study was to characterize the sickle bone phenotype over time in female and male mice in comparison with control and sickle-trait mice. Although bone mineral density measured with DXA is the standard clinical metric to evaluate overall bone health, we utilized microCT to measure BMD of cortical and trabecular bone in order to not muddle our results with metrics gleaned from any surrounding muscle or other soft tissue. Furthermore, microCT imaging is capable of detailed assessment of trabecular bone morphology [164]. In the femoral neck, there were no significant differences for trabecular BMD for male or female mice (Figure 3.6E). However, the trabecular BMD in the distal epiphysis for 5-month-old SS females was reduced in comparison to AA and AS (Figure 3.7E). This finding is in accordance with a previous study in female sickle mice as well as in human studies that have found reduced BMD in adult and pediatric patients [42, 134, 142, 165]. However, consideration must be taken in that our results are looking at a specific region in the bone, while the aforementioned studies analyzed the entire femur. Similarly, to Green et al.'s findings, we did not see any reduction in BMD for male mice in comparison to their age matched controls [45] (Figure 3.7E). However, our data makes the novel finding that there are sex differences in how SCD effects the BMD of trabecular bone within the distal femur. Finally, within the mid diaphyseal region, BMD was decreased at 3 and 5 months for males and females in

comparison to AA and/or AS controls (Figure 3.8B). This is again accordance with a Xiao et. al who also saw this reduction in cortical BMD for female mice, but Green et. al did not find differences among their male subjects [45, 134]. This discrepancy could be due to the fact that we utilized AA transgenic Townes mice as our control rather than wild-type C57BL/6 mice as in the Green study [166].

In order to further illustrate the microarchitecture of bone in male and female mice, we looked at additional structural parameters through microCT analysis and discovered further changes in SS bone in comparison to AS and SS that are sex dependent. Male and female SS mice have varying trabecular morphology in the proximal and distal end of the femur (Figure 3.6, Figure 3.7). In the proximal region or femoral neck, SS females have reduced Tb.Th. at 5 months in comparison to age-matched controls, which means there is loss of trabecular bone, whereas male SS animals see an increase in Tb.Th. from 3 to 5 months (Figure 3.6B). This suggest that older female sickle patients may be at greater risk for fracture at the femoral neck. However, for proximal trabecular bone in general, SCD does not decrease the strength of the bone which is apparent in no significant changes to the BMD (Figure 3.6B). In the femoral neck, we surprisingly see more of changes with respect to age in male mice then with respect to genotype. BV/TV and Tb.Th. increase while SMI decreases with age (Figure 3.6B-D). SMI is a parameter that measures the plate-to-rod like structure of the trabeculae [148]. With aging, trabeculae change their shape from more plate like, a SMI score of 0, to more rod-like, a SMI score of 3 [139]. Any scores in between these values are to indicate a structure with a mixture of plates and rods [139]. However, we see in the male mice a decrease in SMI not necessarily due to magnitude but in positivity. A

negative SMI value means that surface of the bone is concave rather than the convex assumption that is made in the parameter measurement [167]. With this in mind, it appears male mice's overall plate-rod ratio is not changing with time, but just the convexity. In the distal epiphysis, SS females also have weaker, less dense trabecular bone as is apparent by the reduction in BMD and Tb.Th. (Figure 3.7B, E). However, the trabecular bone that is present has more connections and less spaced apart in SS females in comparison to controls, which means SBD does affect the overall Tb.N. (Figure 3.7D). However, in SS males there is no decrease in Tb. Th. or BMD (Figure 3.7B, E). This suggests that sickle trait and SCD results in reduced trabecular bone growth with age only in female mice. These differences in trabecular morphology being site and sex dependent coincide with clinical data in which cancellous bone loss seen with age in men and women does not happen uniformly at each section such as the iliac crest or vertebrae[168, 169]. Overall, there is evidence of trabecular bone loss in SS females, but not in SS males indicating that the trabecular bone loss characteristic of SBD is sex dependent.

In the mid diaphyseal region we found the Cort. Th. and BA to be reduced in male and female SS mice (Figure 3.8B, D). These findings are in accordance with previous studies that have characterized the cortical bone in male or female mice at similar ages [45, 134]. The Cort. Th. and BA being decreased in SS animals speaks to the bone not being able to withstand as high of mechanical loads in comparison to AA and AS bones. Reduced Cort. Th. and BA has been attributed to decreased mechanical strength of bone [147, 166]. This puts sickle bone at an increased risk of fracture. Furthermore, we have discovered differences in the cortical as well as the trabecular structure in male and female SS mice (Figure 3.6, Figure 3.7, Figure 3.8). Due to the fact that varying cortical

and trabecular architectures can have an effect on the mechanical properties of bone [170, 171], we aim to do mechanical testing in the future to ascertain if these differences have any effect on the biomechanical loadings that SS male and female femurs can withstand.

From our microCT findings, we wanted to elucidate what mattered the most when characterizing bone loss in SCD: genotype, sex, or age. When plotting all of our groups together in the PC space (AA, AS, SS males and females at 3 and 5 months) we did not see any separation in the data (Figure 3.9A-B). However, the data did cluster into distinct groups once we separated it by age (Figure 3.10, Figure 3.11). This demonstrates how important age is when studying bone development and the need for age-matched controls. At 3 and 5 months, SS males and females mostly separated from AA and AS males and females (Figure 3.10A, Figure 3.11A). This demonstrates that regardless of sex, sickle mice have distinct bone phenotype different from AA and AS mice. Additionally, we wanted to ascertain which of the 23 bone parameters we analyzed lead to the separation of sickle animals from non-sickle. Trabecular parameters of SMI and Conn. Den. are the most important factors in distinguishing the sickle bone phenotype (Figure 3.10, Figure 3.11). This of great interest since trabecular bone architecture takes on 75% of external loads and thus is of great importance in bone resisting fracture [172]. Trabecular bone is known to change from plate-like (score of zero) to rod-like (score of three) architecture, which is indicative of trabecular thinning, due to the bone loss and imbalance in remodeling that occurs as people age [146, 164, 173]. When performing linear regression analysis of trabecular bone microCT parameters, SMI was the best predictor of elastic modulus of human bone [174]. As SMI increased, the elastic modulus decreased,

indicating rod-like trabecular architecture leads to weaker bones. This relationship is further evident in a large-animal model, where SMI was able to predict the ultimate strength of trabecular bone [175]. In our analysis, 3-month-old SS male mice had a significant increase in SMI in comparison to their age matched controls, indicating premature aging and thinning of the bone (Figure 3.10E). However, by five months, this difference in SS SMI is no longer present (Figure 3.11E). Conn. Den. which is normalized by total volume of bone, relays how many links there are between trabeculae that can be severed before the construct can be divided into two [148]. The relation to Conn. Den. and mechanical properties of bone are still up for debate. In the aforementioned previous two studies, Conn. Den. was a poor predictor of elastic modulus and strength [174, 175]. However, Kabel, et al. argues that Conn. Den. is limited in being able to ascertain bone elastic properties, but that it is a better predictor for mechanical strength in bone that has undergone pathologic remodeling, such as in SBD [176]. Alterations to connectivity has been suggested as the cause for the reduction in bone strength related to age [177]. One study found that connectivity loss during bone remodeling is indicative of trabecular fracture and is, therefore, directly linked to a deficiency mechanical stiffness and strength [178]. Bone turnover rate and osteoclast activity have been shown to be increased in SS mice while bone formation has been shown to be decreased [134, 137]. With this increase in bone remodeling, this makes SS mice susceptible to loss in connectivity and thus decreased mechanical strength. In our analysis we actually see increased Conn. Den. in the distal epiphysis for 5-month females (Figure 3.11C), which should mean they have greater mechanical strength than AA or AS. However, Tb. Th. has been correlated to mechanical strength of bone [179], and SS

females have decreased Tb. Th. as well at 5 months (Figure 3.7B). Collectively, this suggests that even though certain trabecular parameters lead to the most variance in the microCT data, one or two of them cannot give a complete picture of what is happening in the sickle trabecular morphology. This further implores us to perform mechanical testing in future studies. Our data, however, still drives home the fact that trabecular morphology is what distinguishes the sickle bone phenotype and should be studied extensively in a complete context utilizing multiple parameters.

In conclusion, we have shown in this work for the first time the novel characterization of SBD within both male and female mice. We found that SCD delays skeletal maturity in male mice. Essentially, this research demonstrates that the Townes sickle transgenic mouse model can be used to study growth retardation that plagues people with SCD. Additionally, we demonstrate that trabecular bone morphology changes in male mice with respect to age as opposed to with respect to genotype as in female mice. Consequentially, we found that trabecular parameters are what distinguishes the sickle bone phenotype from normal and sickle-trait controls. Thus, this study implores the need to study both sexes when studying SBD and to focus upon trabecular bone loss as future therapeutic targets, especially for female SS patients.

CHAPTER 4 Dysregulated Sphingolipid Metabolism Enhances Cathepsin Proteolytic Activity that Promotes Pathological Bone Loss in Sickle Cell Disease

4.1 Introduction

Sickle cell disease (SCD) is the most prevalent inherited blood disorder in the United States. Every year approximately 1 in 360 African Americans are born with this disease, while as many as 1 in 13 are born as genetic carriers [1, 180]. SCD is caused by a missense mutation in the β-globin subunit of the hemoglobin gene that results in red blood cells (RBCs) or erythrocytes to bend into an abnormal "sickle" shape in states of hypoxia. This deformation of the RBC membrane causes RBCs to lose their flexibility and therefore the capability of being able to travel in small vessels such as capillaries. Additionally, sickled RBCs become more "sticky" and adhere to monocytes and the endothelium in vessel walls, forming cell aggregates that lead to blocked blood vessels [26]. This leads to painful complications known collectively as vaso-occlusive crises which can lead to tissue neurosis and eventual organ failure. Due to the intricate microvasculature present within bone, SCD also affects bone health.

A collection of pathologies, including osteonecrosis (ON), osteoporosis, and osteopenia, known as sickle bone disease (SBD), are among the most common complications of SCD and progresses from adolescence, occurring in 50% of individuals by age 35 [4, 45]. To prevent the progression of joint damage, bed rest and avoiding activities such as running or stair climbing are recommended, but these methods drastically affect the quality of patient life [7]. Surgical treatments, such as a total hip replacement (which can occur as early as age 18), have an elevated risk of inducing

complications such as acute chest syndrome, infection, and congestive heart failure for sickle cell patients [8, 9]. With these current inadequate treatment options, there is a great need to find targets for new therapies for SBD.

Sphingosine 1-phosphate (S1P) is a bioactive sphingolipid that has been implicated in many bone processes. S1P acts on cells' extracellular membranes by signaling through 5 G-protein coupled receptors (S1PR1-5), as well as intracellularly to initiate a variety of cellular processes such as differentiation, migration, and apoptosis [58-61]. In the context of bone homeostasis, S1P has an active role in regulating new bone formation as well as resorption. In human mesenchymal stem cells (MSCs) and mouse myoblasts, S1P increased the differentiation of the cells into osteoblasts [181, 182]. Osteoblasts are responsible for the synthesis of new bone, production of bone matrix proteins such as type 1 collagen, and subsequent mineralization of bone. Other studies have shown that this process is propagated through S1PR2, whose activation increases the expression of transcription factor RUNX2 that is needed for osteoblast differentiation [14]. Additionally, S1P, via its receptors S1PR1 and S1PR3, increases the migration of human MSCs in vitro [18]. S1P also directs the differentiation of osteoclasts, cells that resorb bone. By increasing the osteoblast production of receptor activator of nuclear factor κ-B ligand (RANKL), S1P has been shown to increase osteoclastogenesis [15]. This process is further amplified when cathepsin K (cat K), a cysteine protease used by osteoclast to resorb bone, is deleted in osteoclasts as a feedback mechanism to increase osteoclast differentiation [16]. S1PR1 and S1PR2 has also been shown to direct the migration of osteoclast progenitors (OPCs) in and out of the bone marrow (BM) niche [70]. Studies in sickle murine models have discovered that there is an unbalance in bone homeostasis that contributes to the bone loss in SBD. Increased

osteoclast activity and reduced MSC terminal differentiation into osteoblasts contributes to bone loss and impartment in SCD mice [134, 137]. With this information in mind we set out to further characterize the role of S1P in the BM niche of SCD. We hypothesized that SS MSCs dysregulated sphingolipid metabolism and increased osteoclast progenitors in SCD mice could contribute to the imbalanced bone formation and resorption in SCD.

Previously, our work and others have shown that sphingolipid metabolism is dysregulated in SCD. We found that S1P, as well as its precursor sphingosine (So), are elevated in the blood, plasma, and in RBCs of human sickle donors. Additionally, we found an increase in sphingosine kinase 2 (SK2), one isoform of the enzyme that phosphorylates So to produce S1P [10]. Zhang et al. discovered that inhibiting SK1, another isoform of SK, leads to decreased RBC sickling and diminished tissue necrosis [12]. We also have shown an increase in acid sphingomyelinase (SMase) activity in sickle (SS) RBCs. Acid SMase alters the biconcave shape of RBCs and induces the production of lipid-raft-rich microparticles (MPs) [183]. We found that proinflammatory RBC-derived MP production is increased in SS human donors. Additionally, we discovered that these MPs when engulfed by monocytes, lead to an increase in the production of proinflammatory, osteoclastogenic cytokines IL-6 and TNF-α [10, 184]. Additionally, MPs have been utilized as biomarkers for ON in sickle patients [11]. As stated earlier, osteoclasts utilize cat K to resorb bone. Keegan et al. has shown that cat K activation is increased in SCD and disrupts vascular integrity [17]. Carbonare et al. has also shown an increase in cat K expression in SS mice in sickle crisis [137]. With our knowledge of sphingolipid metabolism being dysregulated in SCD and the S1P link to cat K expression in osteoclasts, we sought out to investigate cathepsins' potential role in

pathological bone remodeling in SBD. We hypothesized that there is a link between sphingolipids and cathepsins that can elucidate viable targets for SBD.

In this study we demonstrate a mechanism for SBD of dysregulated sphingolipid metabolism and increased osteoclast cathepsin activity. Through lipidomics and flow cytometry, we infer that increased S1P in the blood contributes to the imbalance in bone formation and resorption in SCD. Furthermore, we utilize enzyme zymography to establish that SS MPs increase cathepsin activity of immune cells as well as SS osteoclasts have elevated cat K activity, which leads to increased bone degradation. Utilizing the cysteine cathepsin inhibitor E-64, we are able to demonstrate for the first time that cathepsins are a viable target to treat SBD. This work exhibits the novel mechanistic link between sphingolipid metabolism and cathepsin activation in SCD that contributes to the progression of SBD.

4.2 Materials and Methods

4.2.1 Animals

Animal procedures and animal care protocols were performed in accordance and with approval from the Georgia Institute of Technology or the University of Virginia Animal Care and Use Committee. We utilized wild-type C57BL/6 and Berkley SCD Tg mice, solely expressing human sickle hemoglobin (HbS) [185], for blood lipidomic studies. Berkley and C57BL/6 mice underwent hypoxic conditioning for 24 hours in a polypropylene hypoxia chamber (Coy Laboratory Products) at 8% oxygen that was maintained with nitrogen gas. We used Townes transgenic sickle mice that were non-carriers (AA), heterozygous (AS), or homozygous (SS) for the sickle mutation from Jackson Laboratories (C57BL/6 and 129 background) [143] for all other studies. The

genotype of the Townes mice was determined through Native polyacrylamide gel electrophoresis (PAGE) of their blood obtained via the tail vein. One-month old mice were injected with sterile saline or 9mg/kg of the drug E-64 via intraperitoneal (IP) injection daily for 2 months. Femurs from 3-month old male and female mice were isolated for microCT analysis, four-point bending mechanical testing, and histological analysis. The bones were stored at -20°C until time of evaluation.

4.2.2 MSC In Vitro Culture[1]

MSCs from 4-6-week-old Townes mice of all three genotypes (AA, AS, SS) were isolated according to a previous protocol [186]. Briefly, bone marrow (BM) cells were flushed from murine long bones and collected in α-MEM media supplemented with 10% heat-inactivated fetal bovine serum (FBS), 1% penicillin-streptomycin (Gibco), 2.2mg/ml sodium bicarbonate, and plated in a 100-mm petri dish. Five days later, the cells were passaged into a tissue culture flask at $1.5x10^6$ cells/cm^2 seeding density. The media was changed every 3-4 days and cells were passaged at 60-80% confluence.

4.2.3 Whole Blood, RBC-Derived MPs, and MSC Lipidomic Analysis

Whole blood for lipidomic analysis was harvested by cardiac puncture from Berkley and C57BL/6 mice immediately before and after hypoxic conditioning. RBCs

---

[1] Adapted from: J.M. Selma, A. Das, A.O. Awojoodu, T. Wang, A.P. Kaushik, Q. Cui, H. Song, M.E. Ogle, C.E. Olingy, E.G. Pendleton, K.F. Tehrani, L.J. Mortensen, E.A. Botchwey, Novel Lipid Signaling Mediators for Mesenchymal Stem Cell Mobilization during Bone Repair, Cell Mol Bioeng 11(4) (2018) 241-253. Reprinted with permission from Springer Nature

isolated from human AA and SS donors were isolated from whole blood through density fractioning with Ficoll-paque (GE Healthcare). RBC-derived MPs were isolated from the RBC fraction through ultracentrifugation. Passage 1 MSCs isolated from Townes AA, AS, and SS mice, RBCs from Berkley and C57BL/6 mice, and human AA and SS RBC MPs were used for sphingolipidomic analysis based on a previously published method [187]. Two classes of sphingolipids were quantified: sphingoid bases which include sphingosine, sphinganine, sphingosine-1-phosphate, and sphingaine-1-phosphate and complex sphingolipids which include sphingomyelins, ceramides, and glucosylceramides (Table 4.1). Different acyl chain lengths were measured for each complex sphingolipid (Table 4.1). Separate extraction methods were utilized to quantify long chain bases and complex sphingolipids. Sphingoid bases were separated using reverse phase liquid chromatography, and complex sphingolipids were separated using normal phase liquid chromatography. For absolute quantification, 25 pmol/sample of an internal standard (Avanti Polar Lipids) was added to each sample, and each sample was normalized to its total protein content determined via a BCA assay. Calibration curves were generated with the internal standard lipid cocktail at 0.5-1000 pmol per 50uL injection to allow quantitation. Sphingolipids were quantified through high-performance liquid chromatography-tandem mass spectrometry (HPLC-MS/MS) using a Micromass Quattro LC triple quadrupole tandem mass spectrometer (Waters).

Table 4.1. List of sphingolipids characterized in RBCs, MPs, or MSCs by HPLC-MS/MS.

Lipid Class	Sphingolipid	Associated Enzymes	Acyl Chains	Sample
Complex	Ceramide (Cer)	SMase, SMS, CDase, CerS, Phosphatase, Ceramide Kinase (CK), Glucosidase (GCase), Glucosylceramide Synthase (GCS)	16,17, 18:1, 18:2, 20, 20:1, 20:2,22, 22:1, 23, 23:1, 24, 24:1	MPs
	Ceramide 1-phosphate (C1P)	Phosphatase, CK	16, 16:1,18, 18:1, 18:2, 18:3,20, 20:2, 20:3, 20:4, 22, 22:2, 22:4, 24, 24:2, 24:4	MPs
	Dihydroceramide (DCer)	SMase, Ceramidase (CDase), Ceramide Synthase (CerS), Desaturase. SMase, SMS	16,17, 18, 20, 22, 24,24:1	MPs
	Glucosylceramide (GlcCer)	GCase, GCS	16, 18, 20, 21:1, 21:2, 22, 22:1, 23, 23:1, 23:2, 23:3, 24, 24:1	MPs
	Sphingomyelin (SM)	SMS, SMase	13, 13:1,14, 14:1, 15,15:1,16,16:1,17, 17:1, 18, 18:1, 19, 19:1, 20, 20:1, 21, 21:1, 22, 22:1, 22:2, 23, 23:1, 24, 24:1, 24:2, 25, 25:1, 26, 26:1, 26:2	MPs
	Lysosphingomyelin (LSM)	Deacylase	18:0, 18:1, 20:1, 20:2	MPs
Long Chain Base	Sphinganine (Sa)	CDase, CerS, Serine Palmitoyl Transferase (SPT), Lipid Phosphate Phosphatase (LPP)	NA	MPs
	Sphinganine 1-phosphate (SaP)	Sphingosine Kinase (SK), Sphingosine 1-phopshate Phosphatase (SPP), LPP	NA	MPs
	Sphingosine (So)	CDase, CerS, SK, SPP, LPP	NA	MPs, RBCs, MSCs
	Sphingosine 1-phosphate (S1P)	SK, SPP, S1P lyase. LPP	NA	MPs, RBCs, MSCs

4.2.4 Characterization of MSCs and OPCs

BM was harvested from both femurs and tibias of Townes mice euthanized by CO_2 inhalation. BM-derived cells were isolated in phosphate buffered saline (PBS) supplemented with 3% FBS to characterize MSCs and OPCs via FACS analysis. Flow cytometry immunophenotyping was performed according to standard procedures and was analyzed on a BD FACSAria II or Fusion cytometer. Fluorophore conjugated monoclonal antibodies to stem cell antigen-1 (Sca1), CD45, CD34, CD90, CD29, and CD44 were used to identify MSCs while antibodies for CD11b, CD3, CD45R/B220, CD117, and CD115 were used for OPCs as previously described [188]. Live cells were determined by utilizing the live/dead stain of Zombie Violet (Biolegend).

4.2.5 Microparticle Isolation and THP-1/PBMC incubation

Primary RBCs and peripheral blood mono-nuclear cells (PBMCs) from human AA and SS donors were isolated from whole blood through density fractioning with Ficoll-paque (GE Healthcare). RBC-derived MPs were collected from the RBC fraction diluted 10-fold in PBS. The RBC-PBS solution underwent ultracentrifugation at 37,000xg for 1 hour at 4ºC. The supernatant was removed, and MPs were resuspended in PBS for cellular treatment or lipidomic analysis. Contamination of RBCs was removed from the PBMC fraction using RBC lysis buffer (0.835 ammonium chloride, 0.1% potassium bicarbonate, and 0.0037% EDTA). THP-1cells, human monocytes, were cultured in RPMI-1640 medium (Sigma-Aldrich) augmented with 10% FBS, 1% penicillin-streptomycin, and 0.05 mM β-mercaptoethanol. THP-1 monocytes, AA PBMCs, and SS PBMCs (2×10^5 cells per/well) were treated with 1×10^6 SS MPs for 24

hours in a 24 well plate. After three washes with PBS, cells were isolated and prepped for enzyme zymography.

4.2.6 Osteoclast Differentiation

BM-derived cells isolated from Townes mice were collected in 24-well plates in Dulbecco's modified eagle medium (DMEM) supplemented with 10% heat-inactivated FBS, 1% L-glutamine, 1% sodium pyruvate (Gibco), 5% heat-inactivated horse serum, 1% penicillin-streptomycin (Gibco), 1% MEM-essential amino acids (Gibco), 50uM β–mercaptoethanol, and 10ng/mL of macrophage colony stimulating factor (M-CSF) for 24 hours. After 1 day, the media was changed, and the control wells were supplemented with 10ng/mL M-CSF while the experimental wells were supplemented with 30ng/mL M-CSF and 100ng/mL RANKL. The media was changed every other day for 21 days. Osteoclast differentiation was verified via a tartrate-resistant acid phosphatase (TRAP) and nuclear staining kit (Takara Bio, Kusatsu Japan).

4.2.7 THP-1/PBMC and Osteoclast Cathepsin Zymography

Protein from AA and SS osteoclast samples as well as THP-1/PBMC samples that were treated with MPs was collected in lysis buffer (20 nM Tris-HCl (pH 7.5), 5 mM EGTA, 150 mM NaCl, 20 mM β-glycerol-phosphate, 10 mM NaF, 1 mM sodium orthovanadate, 1% Triton X-100, 0.1% Tween-20) supplemented with 0.1 mM leupeptin and then resuspended in 5X reducing loading dye for zymography. For osteoclast samples, RAW 264.7 cells (mouse macrophages) were loaded along the samples to serve as a positive control. Enzyme zymography was completed utilizing a previously described protocol [189, 190]. Briefly, equal volumes of each sample were loaded into 12.5% SDS-PAGE gels embedded with a 0.2% gelatin substrate at 4°C. To ensure that

cathepsins can bend into their active structures, gels were washed in renaturing buffer following electrophoresis. In order for the cathepsins to degrade the gelatin substrate, the gels were coated in sodium phosphate buffers (pH6) supplemented with 2mM dithiothreitol and 1mM EDTA for 18hrs at 37°C. Each gel was stained with Coomassie Blue, destained, and imaged with an ImageQuant LAS 4000 (GE Healthcare, Little Chalfont, UK). Proteolytic activity was visualized as white bands in the gels and quantified through densitometry by utilizing ImageJ. Specific cathepsins were distinguished by molecular weight. To further characterize proteolytic activity, gels were incubated with either 10μM E-64 or 1μM cat K inhibitor (1-(N-benzyloxycarbonyl-leucyl)-5-(N-Boc-phenylalanyl- leucyl) carbohydrazide [Z-L-NHNHCONHNH-LF-Boc], EMD Biosciences) for 18hrs at 37°C. For MP gels, cathepsin bands were normalized to the non-MP-treated control groups run in each gel. For osteoclast gels, cathepsin bands were normalized to the maximum intensity for each gel.

4.2.8 Cathepsin K Western Blot

AA and SS osteoclast samples were resuspended in 5X reducing loading dye for SDS-PAGE and Western blotting. Human recombinant cat K was loaded along the samples to serve as a positive control. To ensure equal amounts of protein from each sample were loaded into the 12.5% polyacrylamide Western blot gels, a BCA assay was performed. Following separation of the samples by molecular weight, the protein from each gel was put onto nitrocellulose membranes. Cat K was detected by blocking membranes with Odyssey blocking buffer, staining the membranes with primary rabbit anti-mouse cat K polyclonal antibody (Proteintech Rosemont, IL) overnight, and finally staining with anti-rabbit secondary antibody (LI-COR, Lincoln, NE). The membranes

were imaged with a LI-COR Odyssey CLx (LI-COR, Lincoln, NE) machine.

4.2.9 Histology

Femurs were harvested, fixed in 10% neutral buffered formalin for 24 hours at 4^{o}C, and decalcified using a formic acid decalcifying solution (Immunocal, StatLab, McKinney Tx) for 3 hours at room temperature. The bones were embedded in paraffin and the 3-month-old distal ends were sectioned for and stained with TRAP and a hematoxylin counterstain. Bone sections were mounted with xylene mounting media (Thermo-Fisher) and visualized under a bright field microscope for positive staining.

4.2.10 MicroCT Analysis

Bone tissue mineral density (BMD) density and cortical and trabecular bone morphology within the femurs of 3-month and 5-month-old male and female mice were examined by microCT imaging (μCT 40, Scano Medical, SUI) as previously reported [45, 144]. The mid diaphysis (1mm region at femur mid-point, 66 slices), distal epiphysis (0.32 mm in length distal from the growth plate (or physis), 25 slices), and distal metaphysis (50 slices extending proximally towards the mid diaphysis from the starting point of 0.05mm above the growth plate) and were scanned at 12 μm isotropic voxel size. Each section of interest is depicted in Figure 3.1. The analysis settings were as follows: 55kVp voltage, 144μA current, and a medium resolution (1024 X 1024-pixel image detection matrix). Cortical and trabecular bone were separated in each region utilizing an auto-contorting program, with additional manual adjustments for proper boundary allocation [145]. Mineralized and soft tissue were distinguished within the mid diaphysis, distal epiphysis, and distal metaphysis using a Gaussian noise filter of 0.8, support of 1,

and thresholding bone at 205-1000 mg hydroxyapatite (HA)/cm^3, 162-1000 mg hydroxyapatite (HA)/cm^3, and 155-1000 mg hydroxyapatite (HA)/cm^3, respectively.

Utilizing direct distance transformation algorithms in Scanco software [144, 146], we measured the cortical bone area (BA), total area (TA), cortical bone area fraction (BA/TA), and cortical thickness (Cort. Th.) for the mid diaphysis region. Additionally, the maximum moment of inertia around the medial-lateral axis (I_{Max}) was measured for four-point bending analysis of the mid diaphysis region. For the trabecular bone in the distal epiphysis and distal metaphysis, we additionally measured trabecular spacing (Tb.Sp.), trabecular thickness (Tb.Th.), trabecular number (Tb.N.), trabecular connectivity density (Conn.Den.), bone volume (BV), total volume (TV), bone volume fraction (BV/TV), and structure model index (SMI). All scans were assessed by a blinded investigator.

4.2.11 Mechanical Testing

Utilizing force and deflection data gathered from a MTS 858 Mini Bionix system (Eden Prairie, MN), the mechanical properties of stiffness, ultimate stress, and maximum force were determined for femurs via four-point bending as previously reported [45, 144]. A load was administered to the mid diaphyseal region of freshly-thawed femurs at a rate of 0.04 mm/s until failure. The femurs were tested posterior-side up, with the mid diaphyseal region at approximately 3.1 mm between two support pins with a radius of curvature 0.5mm. The stiffness was determined as the slope of the linear potion of the force-deflection curve. The maximum moment of inertia about the medial-lateral axis, I_{Max} was determined via microCT to calculate the ultimate stress.

4.2.12 Bone Marrow Transfer Studies

Tibias and femurs were harvested from 2-month old AA and SS mice. The BM was collected by flushing the long bones with sterile saline by utilizing a 25-gauge needle and 10mL syringe. One week before bone marrow transfer (BMT), host mice were treated with 0.5 mg/ml Baytril (enrofloxacin) in their drinking water. Following lethal irradiation dose of 5 Gy with an X-ray irradiator (RS-2000), 2-month-old host C57/BL6 and Cat K knockout (CatK-/-) mice received BM (~ 3 X 10^6 cells) from either AA or SS mice resuspended in 100µL of sterile saline through jugular vein injection. Following BMT, host mice were treated with 0.5 mg/ml Baytril in their drinking water for 7 days. Host mice were sacrificed at 6-months, 4 months post BMT, and microCT analysis was performed on the excised femurs.

4.2.13 Data Analysis and Statistical Comparisons

Principal component analysis (PCA) and volcano analysis was utilized on 89 variables (sphingolipids) with MATLAB software (Natick, MA). Principal components (PC) were generated, with PC1 depicting the greatest percentage of data variance and PC2 (statistically independent from PC1) depicting the next utmost percentage of data variance. The MP data was prepared in a matrix with lipid species in rows and the 12 MP samples in the first column separated by genotype. Linear regression analysis with confidence intervals as well as correlation coefficients between bone parameters and mechanical properties were produced with JMP (version 14).

Statistical comparisons were performed utilizing GraphPad Prism 8 (La Jolla, CA). The resulting analysis is conveyed as mean ± standard deviation (SD). Two-tailed t-test was used for column analysis. For grouped analyses, one-way ANOVA with Tukey's

post-test for multiple comparisons was utilized. For grouped analyses comparing data between control and E-64 treatment, two-way ANOVA with Tukey's multiple comparisons test was used. A *p*-value less than 0.05 was considered statistically significant.

4.3 Results

4.3.1 The sickle bone marrow niche is dysregulated

Due to our previous findings of increased So and S1P in the blood of sickle patients, we wanted to investigate if a similar dysregulation in sphingolipid metabolism was present in a sickle transgenic mouse model. In Berkley and wildtype mice, we implemented hypoxic conditioning for 24 hours to induce sickle crisis. We found So to be decreased after hypoxia in SS mice (0.32 ± 0.06 pmol/mg protein) in comparison to wild type (0.532 ± 0.04 pmol/mg protein) and SS (0.477 ± 0.17 pmol/mg protein) mice before hypoxia (Figure 4.1A). Conversely, we found S1P to be increased in the blood of SS mice before (2.32 ± 0.19 pmol/mg protein vs 2.86 ± 0.34 pmol/mg) and after hypoxia (2.89 ± 0.27 pmol/mg protein vs 3.408 ± 0.59 pmol/mg protein) in comparison to their timepoint-matched controls (Figure 4.1B). These results indicate that the phosphorylation of So to create S1P increases in sickle mice in hypoxic conditions. Since mouse sickle (SS) MSCs have previously shown lower osteogenic potential [134, 137] and that S1P and other sphingolipids play a role in bone development, we performed lipidomic analysis on MSCs from all three genotypes. MSCs were harvested from the BM and characterized through flow cytometry for known surface markers (CD29 (97.9%), CD90 (98.2%), CD44 (98.1%), Sca1 (96.4%)) and for the absence of hematopoietic cell markers (CD45 (0.99%), CD34 (0.14%)) (Figure 4.1C). The long-chain-base

sphingolipid So was two orders of magnitude higher in SS MSCs in comparison to AA and AS (Figure 4.1D), while its phosphorylated successor, S1P, was not significantly increased (Figure 4.1E).

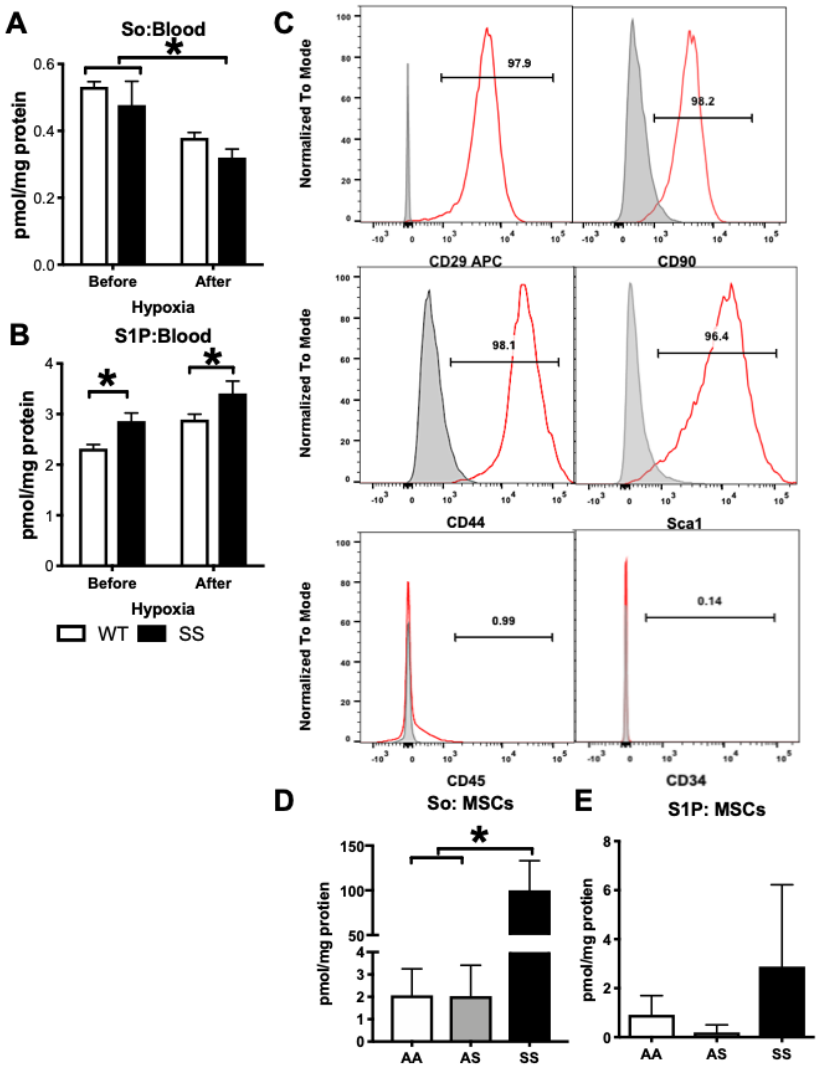

Figure 4.1. Sphingolipid metabolism is dysregulated in the blood and bone marrow in SCD. Sphingolipid profile of blood from wild-type and SS mice before and after hypoxic conditioning including (A) sphingosine and (B) S1P (n= 6 mice per group). (C) Characterization via flow cytometry of MSCs isolated from Townes' mouse model for MSC surface markers CD29, CD90, CD44, Sca1 and for the absence of hematopoietic cell markers CD45 and CD34. Unstained cells= gray, Single-stained cells=red. Sphingolipid profile of MSCs including the lipids (D) sphingosine and (E) S1P (n=3-5 mice per group). Data expressed as mean ± SD. Statistical significance, * $p < 0.05$, determined by two way or one-way ANOVA with Tukey's post-hoc test. Abbreviations: So, sphingosine; S1P, sphingosine-1 phosphate; MSCs, mesenchymal stem cells.

The other type of cell involved in bone homeostasis is osteoclasts, which can be produced from OPCs. OPCs circulate in the blood stream, migrate into the BM cavity, and eventually attach to the bone surface and mature into bone-resorbing osteoclasts [70]. Thus, we investigated whether there could be increased numbers of OPCs in the BM in SCD. Through flow cytometry gating for CD11b-, CD3-, CD45R/B220-, and CD117+/CD115+ cells (Figure 4.2A), we determined that the percentage of OPCs are increased in the BM of SS mice (0.11± 0.05%) compared to AA mice (0.02 ± 0.02%) (Figure 4.2B). This data gives an explanation as to why other studies have found increased osteoclast activity on the bone surface of sickle mice [137].

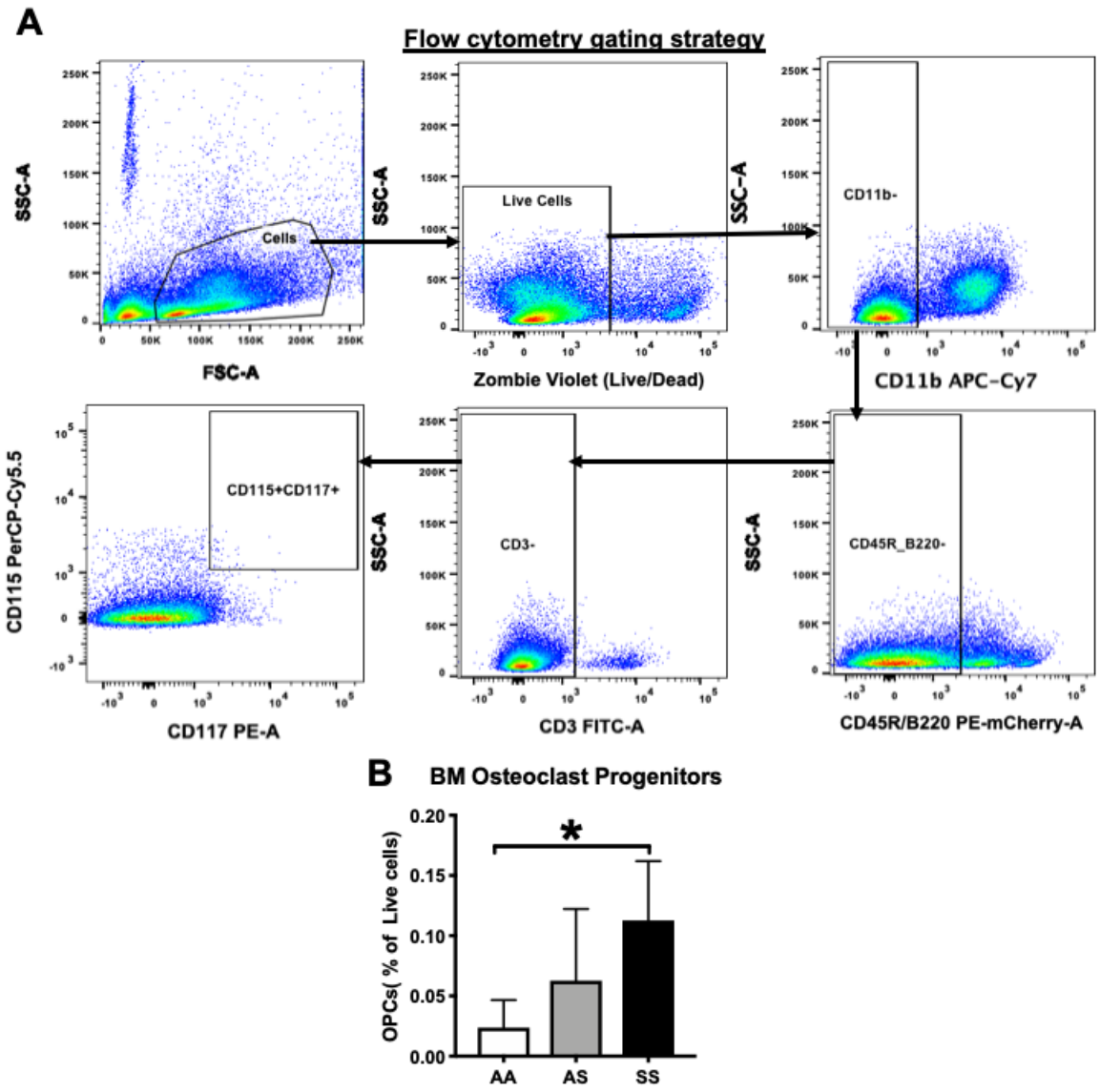

Figure 4.2. Bone marrow osteoclast progenitors are increased in SCD. (A) Flow cytometry identification of OPCs in the BM by gating for cells, live cells, CD11b-, CD45R/B220-, CD3-, and finally CD117+/CD115+ cells. (B) Quantification of OPC percentage of live cells in the BM of AA, AS, and SS mice (n=5-8 mice per group). Data expressed as mean ± SD. Statistical significance, * $p < 0.05$, determined by one-way ANOVA with Tukey's post-hoc test. Abbreviations: BM, bone marrow.

4.3.2 Sickle RBC-derived MPs have a distinct sphingolipid profile

Previously, we have shown that So and S1P are increased in SS RBC-derived MPs [10]. With S1P's vast role in bone homeostasis, we wanted to investigate if these sphingolipids solely aid in distinguishing SS MPs from non-sickle (AA) MPs. We performed HPLC-MS to quantify 89 complex and long-chain base sphingolipids. Through volcano analysis, we determined that four complex sphingolipids were significantly altered in SS MPs. Glucosylceramide (GlcCer) 22:0 (5.40 pmol/mg vs 18.90 pmo1/mg) and GlcCer 24:0 (4.74 pmol/mg protein vs 25.64 pmol/mg protein) were significantly upregulated in SS MPs, while ceramide 1-phosphate (C1P) 18:2 (984.6 pmol/mg protein vs 423.1 pmol/mg protein) and C1P 24:4 (52.94 pmol/mg protein vs 62.76 pmol/protein) were significantly downregulated in SS MPs relative to AA MPs (Figure 4.3A). All of the aforementioned lipids' expression except for C1P 24:4 were significantly altered in SS MPs relative to AA via t-test analysis (Figure 4.3B). To further analyze our multivariate dataset, we utilized unsupervised principal component analysis (PCA) to determine exactly what sphingolipids contribute to the variability between AA and SS MPs. As depicted in Figure 4.3C, principal component 2 (PC2) separated our AA and SS MP datasets. Unsurprisingly, GlcCer 22:0 and 24:0 aided heavily in the separation, while C1P 18:2 and C1P 24:4 had the least effect on this separation. These lipids can be visualized in red in the PCA loadings graph in Figure 4.3D. Furthermore, each ceramide (Cer) species, depicted in gray in Figure 4.3D, was found to be weighted heavily in the PC2 loadings, and thus distinguishes SS MPs from AA MPs (Figure 4.3D). In looking at each individual Cer species, we found Cer 16:0

(903.3 pmol/mg protein vs 2809 pmol/mg protein) and Cer 24:1(2656 pmol/mg protein vs 4689 pmol/mg) to be elevated in SS MPs (Figure 4.3E).

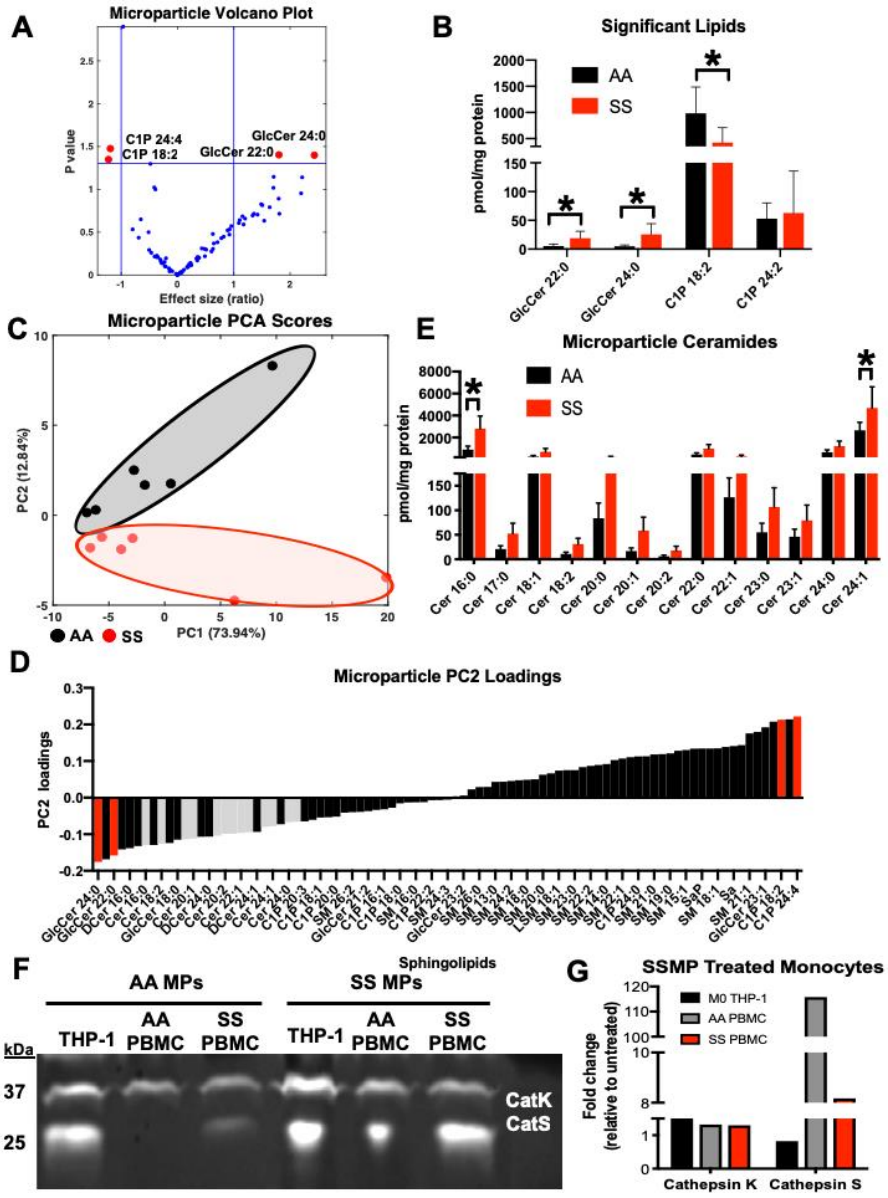

Figure 4.3. SS RBC-derived MPs have a distinct sphingolipid profile and enhance cathepsin activity in monocytes. (A) Volcano plot analysis of 89 sphingolipids characterized for AA and SS MPs (n=6 donors per group). (B) Four lipids that were deemed significant between AA and SS MPs via volcano analysis (n=6 donors per group). (C) 2D scores plot of sphingolipids for AA and SS RBC-derived MPs. AA MPs= black, SS MPs= red (n=6 donors per group). (D) 2D loadings (weight coefficients) plot of the 89 input variables (sphingolipids) in the reduced principal component space. Lipids

deemed significant via volcano analysis are depicted in red. Ceramides are depicted in gray (n=6 donors per group). (E) Fatty acyl chain lengths of ceramide sphingolipid class. Each acyl chain was deemed to add to the variance that separates AA and SS MPs by PCA (n=6 donors per group). (F) Representative cathepsin zymography gel of THP-1 cells and AA and SS human PBMCs treated with AA and SS RBC-derived MPs. (G) Fold change of cat K and S activity relative to untreated cells in THP-1 cells and AA and SS human PBMCs treated with SS RBC MPs. Data expressed as mean ± SD. Statistical significance, * $p < 0.05$, determined by two-way ANOVA. Abbreviations: MP, microparticle; GlcCer, glucosylceramide; Cer, ceramide; DCer, dihydroceramide; SM; sphingomyelin, LSM, lysosphingomyelin; C1P, ceramide 1-phosphate; Sa, sphinganine; SaP, sphinganine 1-phosphate; PCA, principal component analysis; PBMC, peripheral blood mononuclear cells; Cat, cathepsin.

4.3.3 Cathepsin activity is increased in SCD

In our previous work, we saw an increase in inflammatory, osteoclastogenic cytokine production in monocytes incubated with SS MPs [10]. We therefore became interested in the effect that SS MPs have on the activity of cat K and S, both of which have been implicated in bone remodeling [99]. When we incubated human monocytes (THP-1 cells), AA peripheral blood mononuclear cells (PBMCs), and SS PBMCs with SS MPs, we saw an increase in cat K and S activity via enzyme zymography (Figure 4.3F-G). In this technique, protein substrates are loaded into and run through a gel. After electrophoresis, cathepsins can be identified based on the molecular weight and the appearance of white bands is indicative of protease activity as the gelation substrate is removed. When we calculated the fold change in cathepsin activity for each cell type treated with SS MPs relative to their corresponding controls, we found that cathepsin S activity was increased 115 and 8-fold in SS MP-treated AA and SS PBMCs, respectively (Figure 4.3G). Cat K activity was increased approximately 1.3-fold in SS MP-treated AA and SS PBMCs (Figure 4.3G).

With an increase in cat K activity in white blood cells up taking SS MPs and the increase in OPCs within SS BM, we then wanted to investigate if cultured SS BM cells would lead to an increase in osteoclast differentiation in vitro. Interestingly, mostly multinucleated osteoclasts formed from AA BM cells, whereas mature, activated osteoclasts (indicated by the presence of ruffled border) formed from SS cells (Figure 4.4A-D). Similar to the OPC findings, there was a 64% increase in the number of osteoclasts (TRAP+, ≥3 nuclei) per well that developed from SS BM cells relative to AA BM cells (Figure 4.4E). We further characterized these cultured AA and SS osteoclasts cathepsin activity through zymography. As depicted in Figure 4.4F, cat K activity was apparent at the expected 75 kDa. We were also able to visualize other cathepsin activity at higher and lower molecular weights. As determined by quantification through densitometry, SS BM-derived osteoclasts had 267% and 180% more cathepsin activity at 175kDa and 150kDa, respectively, compared to AA BM- derived osteoclasts (Figure 4.4G). Additionally, we performed Western blot analysis to determine the expression of cat K in AA and SS osteoclasts. The expression for each identified molecular weight of cathepsin K, including mature cathepsin K at 37kDa, was also quantified by densitometry (Figure 4.4I). Depicted in Figure 4.4H, SS BM-derived osteoclasts have up to 72% more cat K expression at higher molecular weights of 95kDa and 80kDa compared to AA BM-derived osteoclasts. To further clarify the source of protease activity, we performed zymography on AA and SS osteoclasts in the presence of a broad cathepsin inhibitor E-64. With E-64 incubation, protease activity is completely inhibited, demonstrating that the enzyme activity we see in Figure 4.4F is indeed from cysteine cathepsins (Figure 4.5A). Furthermore, incubation with a cat K inhibitor showed diminished cathepsin

activity from osteoclast samples (Figure 4.5B). Through densitometry, we see that activity at 175kDa is completely inhibited for both AA and SS, but only completely inhibited at 150kDa for AA osteoclasts (Figure 4.5C). When comparing the ratio between cathepsin activity at each molecular weight between control and incubation with cat k inhibitor, we see no difference among AA and SS osteoclasts (Figure 4.5D). With this information, we sectioned distal femurs from all three genotypes to look at the osteoclast activity within the bone by staining for the presence of an enzyme secreted by osteoclast, tartrate-resistant acid phosphatase (TRAP). SS bone had an increase in the TRAP staining in comparison to AA and AS (Figure 4.4J-L). Collectively, this data suggests that SS osteoclasts are more active and produce more cat K than AA osteoclasts and thus elucidates a cause for the imbalance in bone homeostasis in SCD.

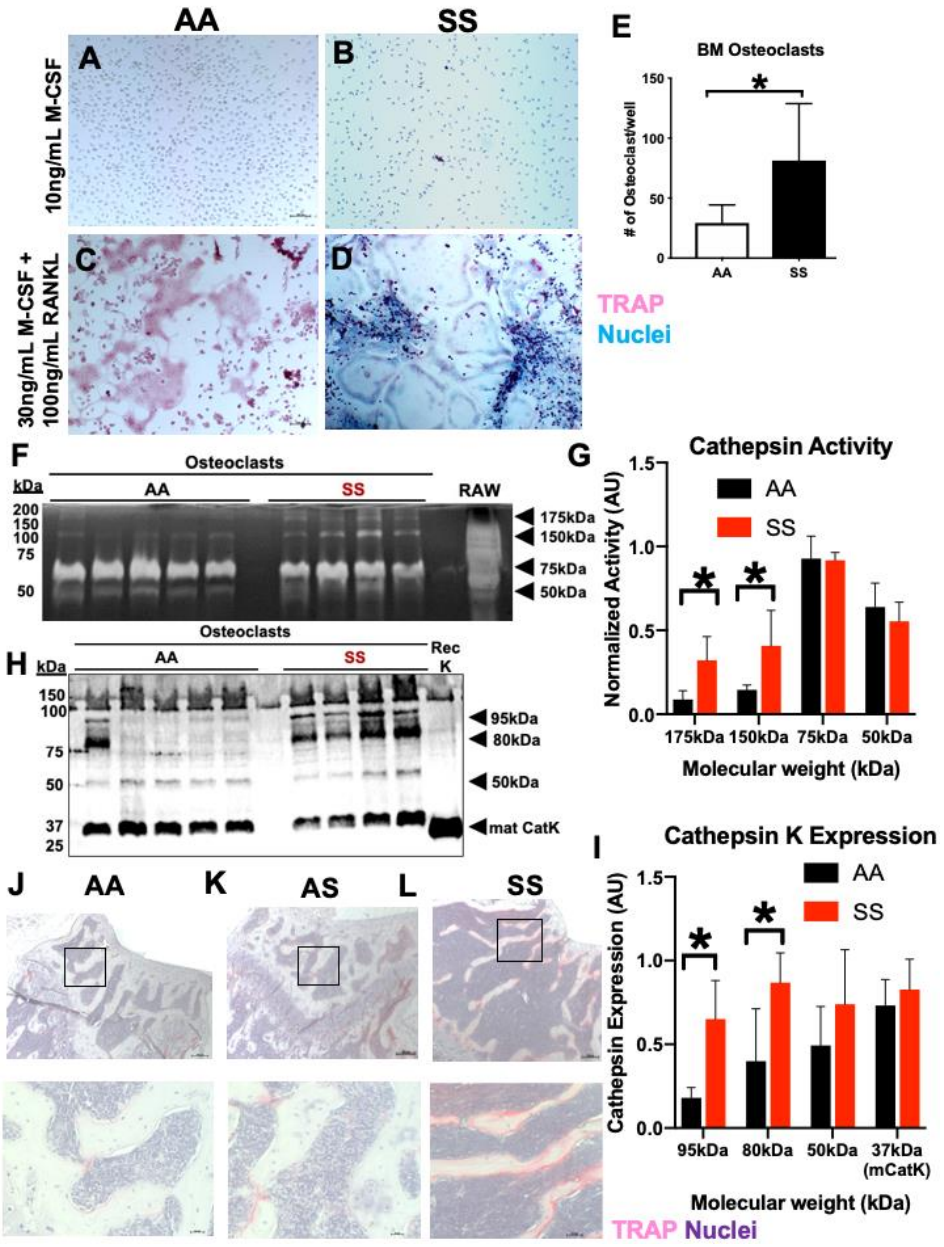

Figure 4.4. Osteoclast differentiation and cathepsin activity is increased in SCD. Representative images of BM cells from (A, C) AA and (B, D) SS mice treated with 10 ng/mL M-CSF (A-B) or 30ng/mL M-CSF + 100ng.mL RANKL (C-D) for 21 days. Osteoclasts are determined as TRAP positive (pink) and at least three nuclei (blue). (E) Quantified number of osteoclasts per well, (n=4 mice and 8 wells per group). (F) Representative cathepsin zymography gel of AA and SS osteoclasts (30ng/mL M-CSF + 100ng/mL RANKL treated). Active protein appears as white bands. Mouse RAW macrophages were used as a positive control. (G) Densitometry quantification of 175kDa, 150kDa, 75kDa, and 50kDa bands of active cathepsin bands in AA and SS osteoclasts, (n=4 mice per group). (H) Representative western of cat K protein in AA and SS osteoclasts. Recombinant cat K was used as a positive control. (I) Densitometry quantification of 95kDa, 80kDa, 50kDa, and 37kDa (mature cathepsin K) bands of cat K

protein expression in AA and SS osteoclasts, (n=4-5 mice per group). AA=black and SS=red. Histological sections of distal femur (J) AA (K) AS and (L) SS bone stained with TRAP (pink) and counterstained with hematoxylin (purple). 10X images (top) scale bar 100 μm, 40X images (bottom) scale bar 20 μm. Data expressed as mean ± SD. Statistical significance, * p< 0.05, determined by Welch's t-test. Abbreviations: BM, bone marrow; mCatK, mature cathepsin K; Rec, recombinant.

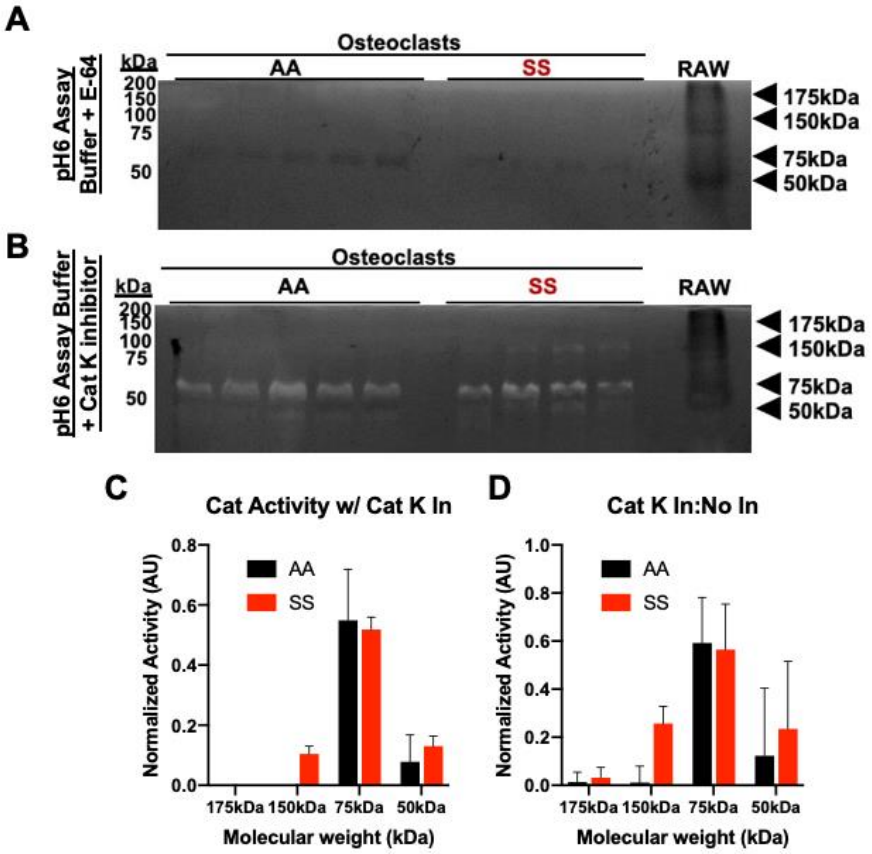

Figure 4.5. Protease activity in bone marrow osteoclasts is executed by cysteine cathepsins, specifically cathepsin K. Representative cathepsin zymography gel of AA and SS osteoclasts (30ng/mL M-CSF + 100ng.mL RANKL treated) incubated with (A) broad cysteine cathepsin inhibitor E-64 or (B) cat K inhibitor. Active protein appears as white bands. Mouse RAW macrophages were used as a positive control. (C) Densitometry quantification of 175kDa, 150kDa, 75kDa, and 50kDa of active cathepsin bands in cathepsin zymography gel treated with cathepsin K inhibitor. (D) Densitometry quantification of ratio of cathepsin zymography gel treated with vehicle or cat k inhibitor of 175kDa, 150kDa, 75kDa, and 50kDa active cathepsin bands (n=4-5 mice per group). AA=black, SS= red. Data expressed as mean ± SD. Abbreviations: In, inhibitor; Cat, cathepsin.

4.3.4 E64 treatment increases cortical bone in SCD mice

Due to previous studies demonstrating reduced cortical bone in SS femurs, we performed microCT analysis in the mid diaphyseal region to elucidate if E-64 treatment had any effect in reducing bone loss. In order to qualitatively analyze the 3D renderings of the mid diaphyseal region from AA, sickle-trait (AS), SS femurs and their corresponding treatment groups, we utilized 5 blind observers to rank the images based on Cort. Th. Unsurprisingly, SS femora ranked lowest in comparison to AA and AS; however, E64-treated SS bones ranked higher than SS bones (Figure 4.64A-B). These observations were further verified with the quantification through microCT of Cort. Th. being reduced in SS bone up to 25% in comparison to AA and AS (Figure 4.6C). However, E-64 treatment significantly increased Cort. Th. in SS mice by 9% (Figure 4.6D). Similarly, there was up to a 22%, 36%, and 4% significant decrease in bone area (BA) (Figure 4.6E), bone area fraction (BA/TA) (Figure 4.6G), and bone tissue mineral density (BMD) (Figure 4.6I), respectively in SS in comparison to AA and AS. E-64 treatment significantly increased BA and BA/TA by 10% (Figure 4.6F, H, J). This data demonstrates that E64 treatment is able attenuate the cortical bone loss that is characteristic of SBD.

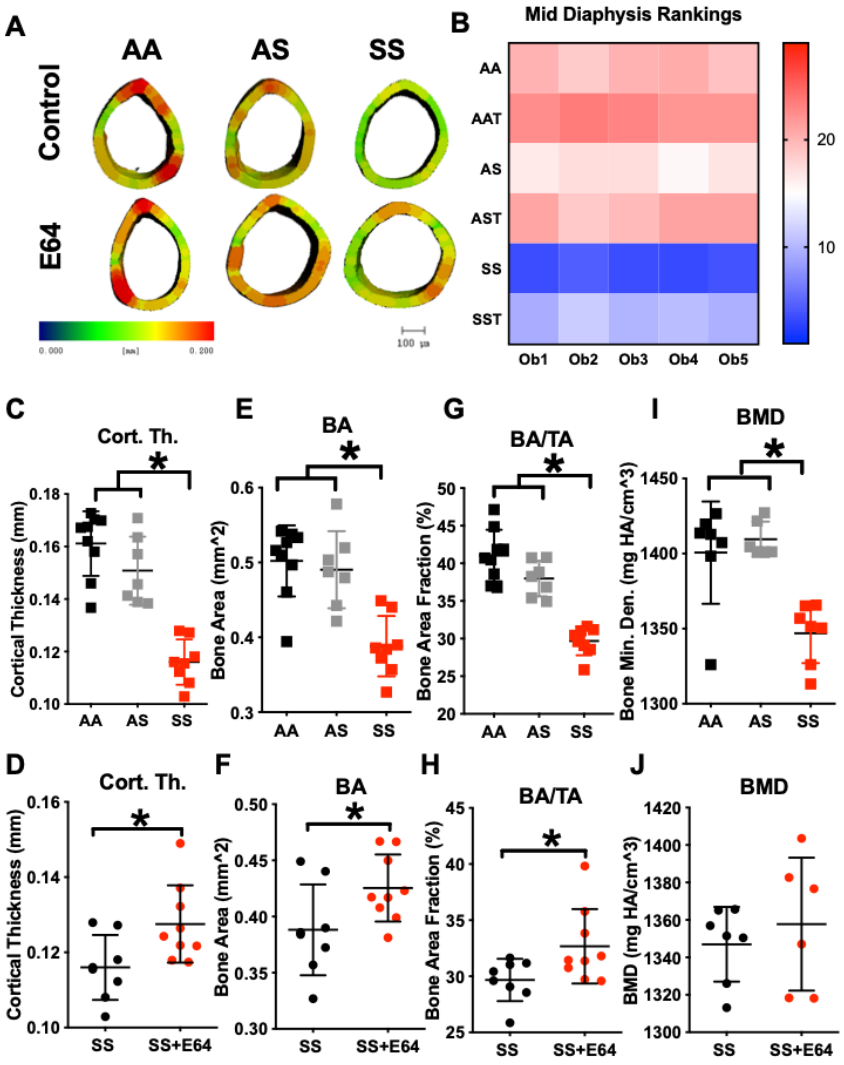

Figure 4.6. E-64 treatment increases cortical bone in SCD mice. A) Representative 3D heat maps of the mid diaphyseal region in AA, AS, and SS 3-month-old mice administered saline (top) or E-64 (bottom). A pseudocolor scale of blue (0 mm) to red (0.2mm) depicts cortical thickness. (B) Ranking of cortical thickness depicted in 3D images generated for 30 mice on a scale ranging from least thick (1) to most thick (30) by 5 blinded observers. (C-J) Cortical bone parameters generated by microCT scans for mice treated with E-64 weekly from 1 month to 3 months of age including (C-D) cortical thickness, (E-F) bone tissue mineral density, (G-H) bone area fraction, (I-J) bone mineral density. (C, E, G, I) Comparison between AA, AS, and SS control via one-way ANOVA with Tukey's post hoc test (n=7-9 mice per group). AA=black, AS= gray, SS= red. (D, F, H, J) SS mice solely compared to SS mice treated with E-64 via t-test. SS=black, SS with E-64=red (n=8-9 mice per group). SS Data expressed as mean ± SD. Statistical significance, * $p < 0.05$, scale bar 100 μm. Abbreviations: Cort. Th., cortical thickness; BA, bone area; BA/TA, bone area fraction; BMD, bone tissue mineral density; Ob, observer.

4.3.5 E-64 treatment increases trabecular bone in SCD mice

We performed further microCT analysis on the distal end of the femurs to look at the effect of E-64 treatment on trabecular bone. In the distal epiphysis, qualitative analysis of the region of interest for AA, AS, SS and their corresponding treatment groups was performed also by 5 blind observers, ranking based on trabecular thickness (Tb.Th). The rankings were quite varied for this region. Surprisingly, AS and SS appeared to rank higher than AA, with a slight increase in rank for both genotypes with E-64 (Figure 4.7A-B). These observations were first contradicted by microCT in that the Tb.Th. was decreased up to 15% in SS femurs in comparison to AA and AS (Figure 4.7C). However, part of our qualitive observations were verified in that E-64 significantly increased SS Tb.Th. by 8% in comparison to untreated SS (Figure 4.7D). Additionally, the trabecular BMD for SS femurs was significantly decreased by 5% in comparison to controls; this parameter was enhanced by 5% with E-64 treatment (Figure 4.7E-F). In the distal metaphysis, however, we saw no difference among the three genotypes for the same bone parameters (Figure 4.8C, E). Furthermore, E-64 had no effect on sickle bones (Figure 4.8D, F). In our qualitative analysis, however, there was at least a visual effect on the bone due to the treated groups being ranked higher than the control samples in all three genotypes (Figure 4.8 6B). This data demonstrates that E64 treatment is able to increase the trabecular bone in certain regions in sickle bone.

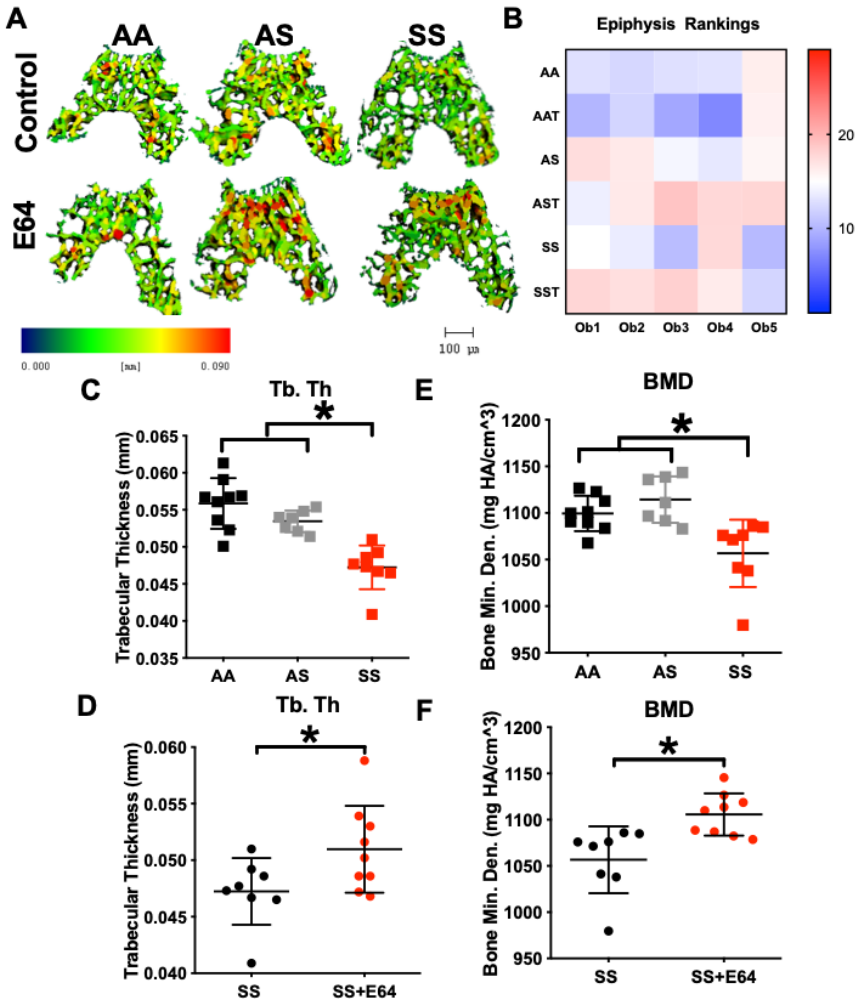

Figure 4.7. E-64 treatment increases epiphyseal trabecular thickness and bone tissue mineral density in the distal femur of SCD mice. (A) Representative 3D heat maps of the epiphysis region in AA, AS, and SS 3-month-old mice administered saline (top) or E64 (bottom). A pseudocolor scale of blue (0 mm) to red (0.09mm) depicts trabecular thickness. (B) Ranking of trabecular bone thickness depicted in 3D images generated for 30 mice on a scale ranging from least thick (1) to most thick (30) by 5 blinded observers. (C-F) Trabecular bone parameters generated by microCT scans of the epiphysis for mice treated with E64 weekly from 1 month to 3 months of age including (C-D) trabecular thickness and (E-F) bone tissue mineral density. (C, E) Comparison between AA, AS, and SS control mice by one-way ANOVA with Tukey's post-hoc test. AA=black, AS= gray, SS= red (n=7-9 mice per group). (D, F) SS mice solely compared to SS mice treated with E64 via t-test. SS=black, SS with E-64=red (n=8-9 mice per group). Data expressed as mean ± SD. Statistical significance, * $p < 0.05$, scale bar 100 µm. Abbreviations: Tb. Th., trabecular thickness; BMD, bone tissue mineral density; Ob, observer.

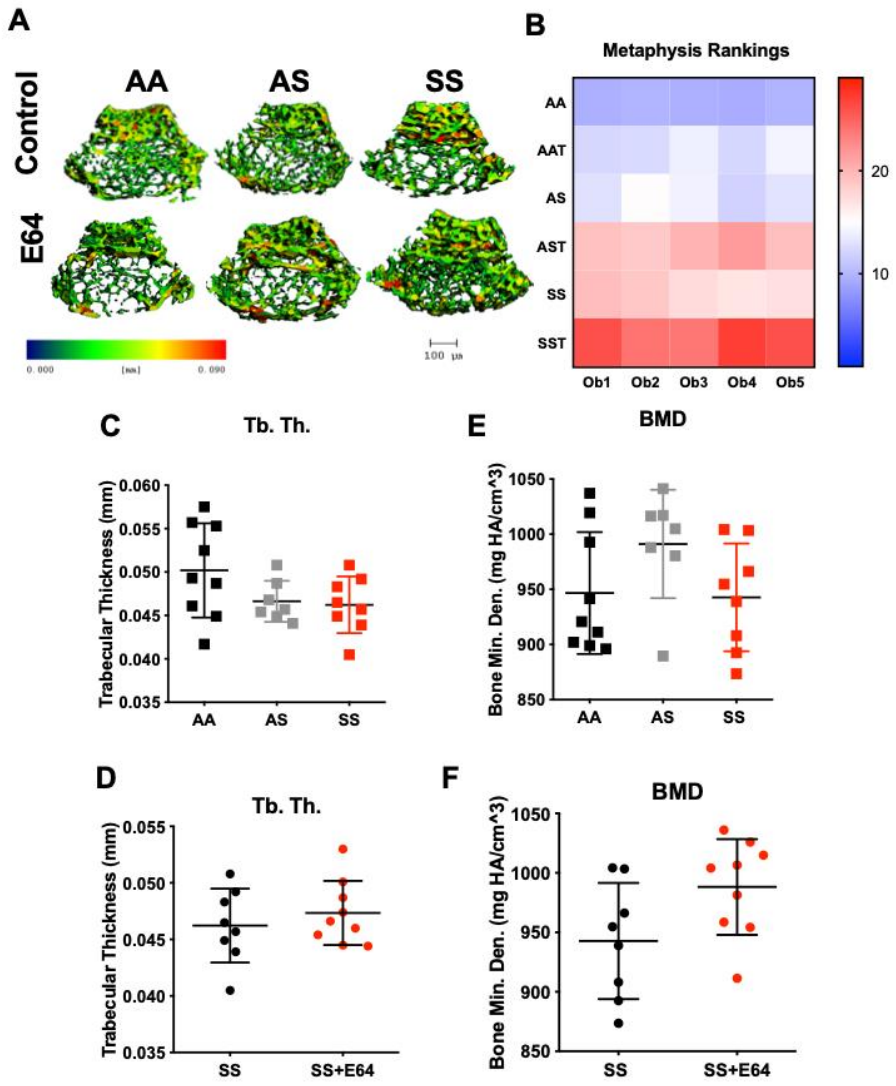

Figure 4.8. E-64 treatment does not impact metaphyseal trabecular bone structure in distal femur of SCD mice. (A)Representative 3D heat maps of the metaphyseal region in AA, AS, and SS 3-month-old mice administered saline (top) or E64 (bottom). A pseudocolor scale of blue (0 mm) to red (0.09mm) depicts trabecular thickness. (B) Ranking of trabecular bone thickness depicted in 3D images generated for 30 mice on a scale ranging from least thick (1) to most thick (30) by 5 blinded observers. (C-F) Trabecular bone parameters generated by microCT scans of metaphysis for mice treated with E-64 weekly from 1 month to 3 months of age including (C-D) trabecular thickness and (E-F) bone mineral density. (C, E) Comparison between AA, AS, and SS control mice by one-way ANOVA with Tukey's post-hoc test. AA=black, AS= gray, SS= red (n=7-9 mice per group). (D, F) SS mice solely compared to SS mice treated with E-64 via t-test. SS= black, SS with E-64= red (n=8-9 mice per group). Data expressed as mean ± SD. Statistical significance, * $p < 0.05$, scale bar 100 µm. Abbreviations: Tb. Th., trabecular thickness; BMD, bone tissue mineral density; Ob, observer.

4.3.6 E-64 treatment improves mechanical properties of sickle bone

To investigate the effect that E-64 treatment has on the mechanical properties of bone, four-point bending was performed on the murine femurs. Without treatment, SS bones were significantly less stiff than AA bones (Figure 4.9A). SS femurs were only capable of tolerating 46% less force and 37% less stress than AA femurs (Figure 4.9B-C). In comparison to AS bones, SS femurs could only withstand approximately 37% less force and 30% less stress (Figure 4.9B-C). The beneficial effect of E-64 is apparent in looking at the correlations between Cort. Th. and BA/TA, two parameters that are enhanced with E-64 in SS bones (Figure 4.6D, H), and the three aforementioned mechanical properties. In normal or AA bones, stiffness, maximum force, and ultimate stress are all positively correlated to Cort. Th. as well as BA/TA (Figure 4.9D-I). All of these correlations are negative (indicated by the negative slope of the fitted lines) for SS femurs (Figure 4.9D-I), which speaks to an altered physiological state of the bones. However, E-64 treatment of SS bones induces positive correlations for all 6 comparisons, making SS femurs more comparable to AA (Figure 4.9D-I). This effect is most substantial in the ultimate stress property where E-64 treatment induces a significantly positive correlation between ultimate stress and Cort. Th. ($r=0.9489$, $p=0.013$) as well as between the ultimate stress and bone area fraction ($r=0.897$, $p=0.0496$) (Figure 4.9F, I). This data shows that E-64 treatment improves the pathological state of the mechanical properties of sickle bone.

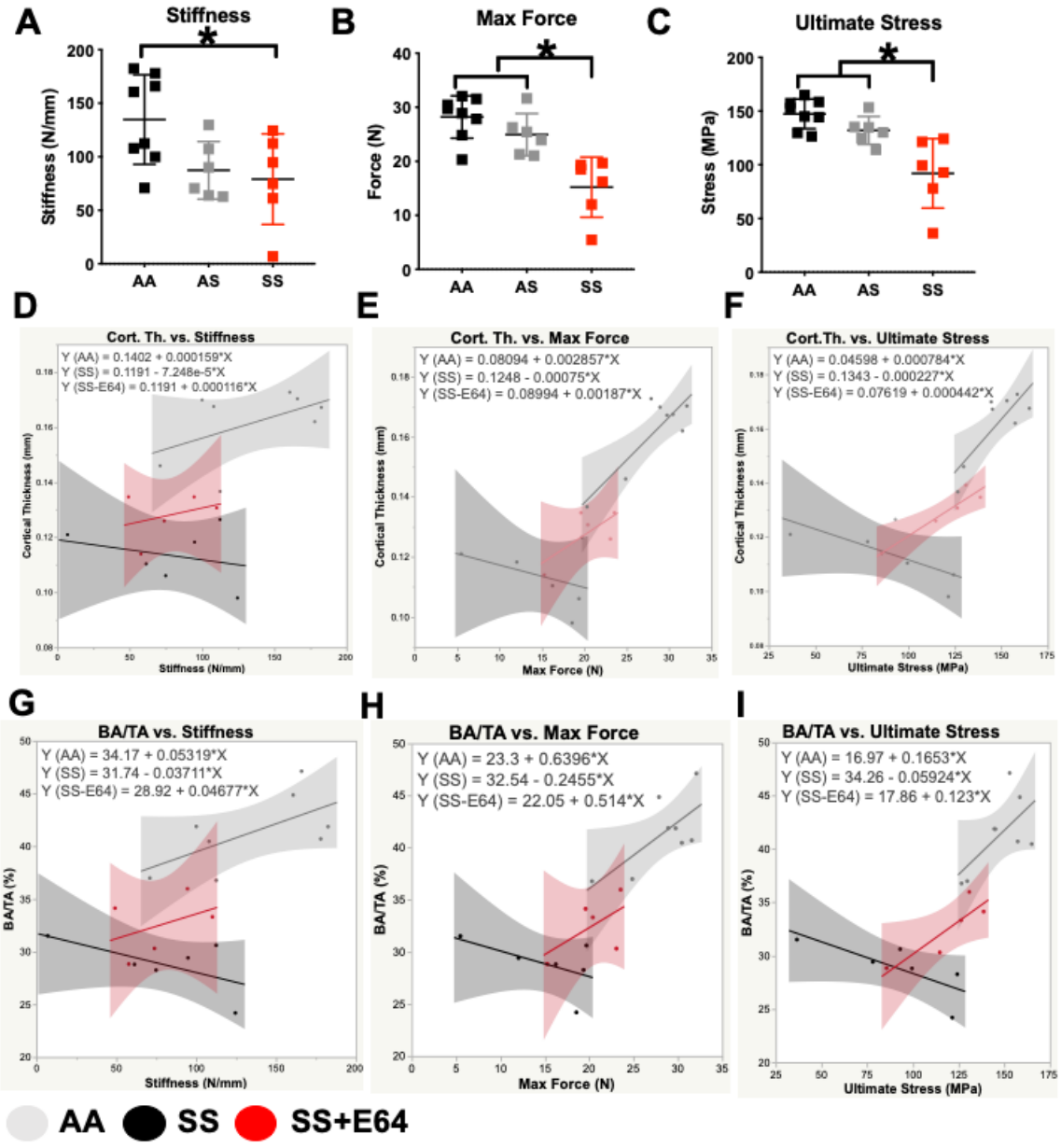

Figure 4.9. E-64 treatment enhances mechanical properties of SS bones. Mechanical properties for 3-month femurs including (A) stiffness, (B) max force, and (C) ultimate stress. AA=black, AS= gray, SS= red. Correlation plots for SS, SS +E64, and AA animals between (D) cortical thickness and stiffness (E) cortical thickness and maximum force (F) cortical thickness and ultimate stress (G) bone area fraction and stiffness (H) bone area fraction and max force (I) bone area fraction and ultimate stress. AA=gray, SS= black, SS with E-64= red. Data expressed as mean ± SD. Statistical significance, * $p < 0.05$, determined by two-way ANOVA with Tukey's post-hoc test or correlation, n=5-8 mice per group. Abbreviations: Cort. Th., cortical thickness; BA/TA bone area fraction.

4.3.7 Stromal cat K does not contribute to SBD

Cat K can not only be secreted by osteoclasts, but also by endothelial cells. Due to interaction with activated PBMCs, endothelial cells in sickle vessels have upregulated cat K activity [17]. We wanted to investigate then if the cat K secretion by stromal cells could be further enhancing the increased bone resorption present in SCD. To study this, we performed BMT studies in which wild-type C57BL6 mice and mice with a genetic knock-out for cat K (CatK -/-) received BM from AA or SS mice following lethal irradiation (Figure 4.10A) at 2 months of age. In the mid diaphyseal region, C57BL/6 mice that were given SS BM had Cort. Th. that decreased by 5% in comparison to C57BL/6 given AA BM (Figure 4.10C). Cort. Th. was also reduced by 12% in CatK-/- mice that received SS BM in comparison to mice that were reconstituted with AA BM (Figure 4.10C). In the distal epiphyseal region, C57BL/6 mice that were given SS BM had 35% less mineralized tissue or BV/TV in comparison to wild-type mice given AA BM (Figure 4.10E). Again, we saw a similar pattern for CatK-/- mice given SS BM, with a 26% reduction in BV/TV in comparisons to CatK-/- mice reconstituted with AA BM (Figure 4.10E). Collectively, this data suggests that active cat K in the hematopoietic cells leads to the bone loss that is present in SCD and not cathepsins that are active within stromal cells.

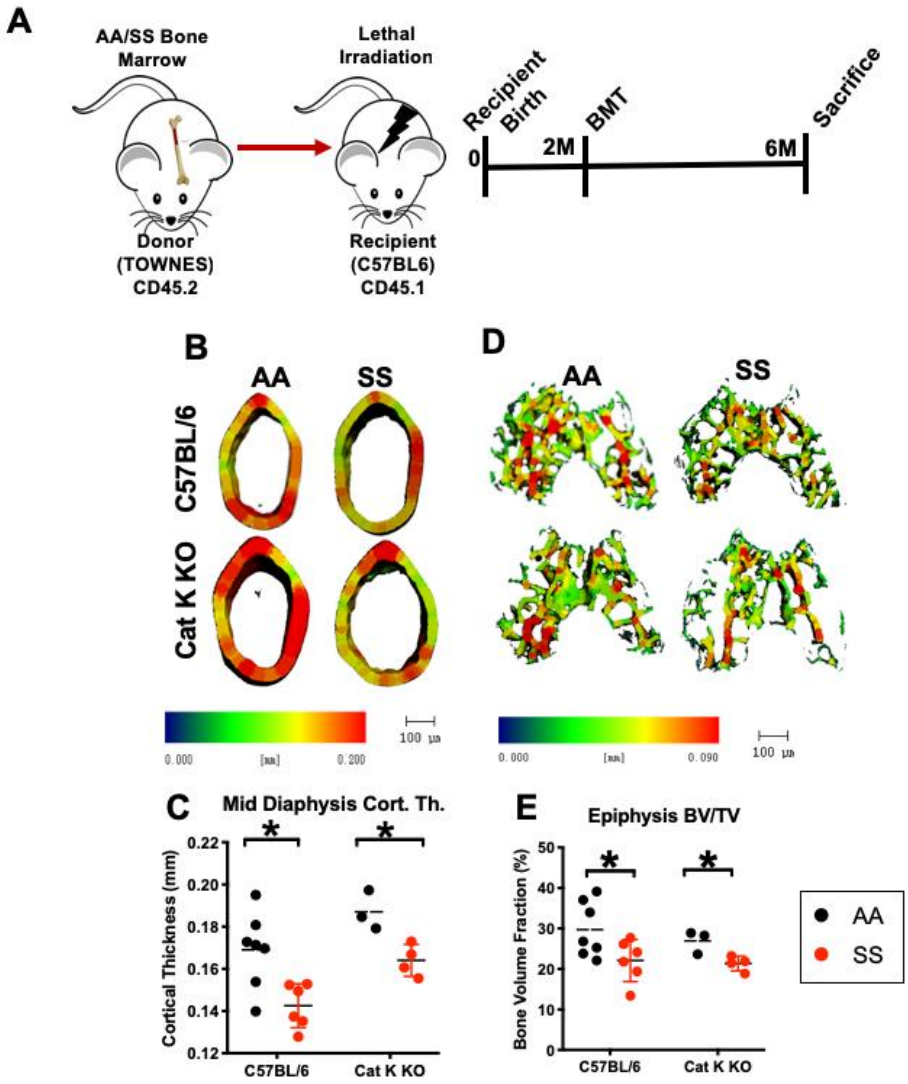

Figure 4.10. Cathepsin K inhibition in stromal cells does not increase SS bone. (A) Schematic and timeline of bone marrow transfer studies. (B) Representative 3D heat maps of cortical thickness in the mid diaphyseal region in C57BL/6 (top) and CatK -/- (bottom) that received AA or SS bone marrow. A pseudocolor scale of blue (0 mm) to red (0.2mm) depicts cortical thickness. (C) Cortical thickness in the mid diaphyseal region generated by microCT. (D) Representative 3D heat maps of trabecular morphology in the epiphysis region of the distal femur in C57BL/6 (top) and CatK -/- (bottom) that received AA or SS bone marrow. A pseudocolor scale of blue (0 mm) to red (0.09 mm) depicts trabecular thickness. (E)Trabecular bone volume fraction in the epiphyseal region generated by microCT. AA bone marrow= black, SS bone marrow = red. Data expressed as mean ± SD. Statistical significance, * $p < 0.05$, determined by multiple t-tests with Holm-Sidak's post-hoc test, n=3-7 mice per group, scale bar 100 µm. Abbreviations: Cort. Th., cortical thickness; BV/TV, bone volume fraction; BMT, bone marrow transfer.

4.4 Discussion

In this work we have shown that sphingolipid metabolism and increased cathepsin activity in SCD are linked and serve as novel targets to combat SBD. Through lipidomics, we demonstrated that sphingolipid metabolism is dysregulated in the blood of a sickle mouse model. We demonstrate that this change in the blood also affects the BM niche in leading to the dysregulation of sphingolipids in MSCs, as well as increased OPCs in the BM of sickle mice. We see the further effect of sphingolipids in that SS MPs have a distinct sphingolipid profile, due to differences in glucosylceramide and ceramide species, that differentiates them from AA MPs. Furthermore, we demonstrate functionality differences in the MPs via SS MPs increasing the cathepsin activity of SS and to even a greater extent AA PBMCs. We see further increased cat K activity in cultured SS osteoclasts as well as increased osteoclast differentiation in SCD. With these findings, we implored a cysteine cathepsin inhibitor, E-64; this treatment increased the cortical and trabecular bone as well improved the mechanical strength of sickle femurs. Finally, through BMT studies, we demonstrated that this elevation in cathepsin activity contributes to the bone loss in SCD and is indeed due to cells of the hematopoietic lineage and not stromal cells.

We found that sphingolipid metabolism is dysregulated in sickle mouse model. Similarly, to the findings of Zhang et al. [12], we saw an increase in S1P before hypoxia in SS mice in comparison to wild-type (Figure 4.1B). This coincides with our and others' findings that S1P is increased in the blood, RBCs, and plasma of sickle human donors [10, 191]. We also found an increase in S1P in SS blood after hypoxic conditioning in comparison to control. The S1P levels did increase in SS with hypoxic conditioning,

although not significantly (Figure 4.1B). The precursor to S1P, sphingosine (So), decreased in SS mice with hypoxia (Figure 4.1A). It has been established that there is an increase in sphingosine kinase 1 (SK1) activity in SS human and murine erythrocytes [12]. SK1 phosphorylates So in order to produce S1P. These observations suggest that in states of hypoxia or sickle crisis, So is extensively converted into S1P. This further corroborates early findings in which we saw an increase acid SMase activity under normoxic and hypoxic conditions in SS mice [10]. Acid SMase acts upstream of So on the sphingolipid SM to produce Cer, which is then converted into So by the enzyme ceramidase [46] . We have shown earlier that an increase in acid SMase activity increases under hypoxia, demonstrating that the sickling of erythrocytes happens before the increased activation of acid SMase [10]. Furthermore, one study showed an increase in SMase activity due to extensive RBC membrane bending [56]. However, Zhang et al. argues that SK1 and S1P actually increase the sickling of RBCs and that inhibition of SK1 leads to an increase in the RBC lifespan, thus reducing the enlarged spleen characteristic of SCD [12]. These combined findings suggest that sickling of erythrocytes in hypoxia increases acid SMase activity that further increases SK1 activation. The membrane changes that occur with the increased conversion of So to S1P further enhances sickling of RBCs. These conclusions are further substantiated by Sun et al.'s findings that increased RBC S1P in SCD binds to deoxygenated sickle hemoglobin (HbS) and further enhances HbS polymerization and therefore erythrocyte sickling as well [192]. Our current findings show that the sickling of erythrocytes further propagates the dysregulation of sphingolipid metabolism in SCD.

The dysregulation of sphingolipid metabolism in the blood has an effect on the BM microenvironment in SCD. We found that sphingolipid metabolism is dysregulated in sickle MSCs (Figure 4.1C-D). In the past, bone and blood formation have been thought to be mutually exclusive processes. However, there has been shown ample communication between stromal and hemopoietic cells, with osteoblasts and MSCs controlling hematopoiesis. Additionally, the two aforementioned cell types' communication is enhanced through cell adhesion molecules [193]. We hypothesize that this close relationship between bone and blood cells thus results in SS MSCs' function being compromised by the sphingolipid changes in the blood due to RBC sickling. Pradas et al. argues that lipid profiles are tissue-specific, but that lipids must remain adaptive in order to change biological properties and functions of cells based on their environmental cues [194]. For example, during chondrocyte differentiation, MSCs change their lipid profile, with sphingomyelins being expressed mostly during day 2 and 14, and S1P expression peaking on day 14 due to increased SK1 activity [195]. Interestingly, MSCs isolated from sickle mice have demonstrated diminished osteogenic potential in comparison to AA MSCs [134, 137]. Further study is needed in order to elucidate if our observed changes in the sphingolipid profile of SS MSCs impacts their osteogenic differentiation. Additionally, our data displays an increased number of OPCs in the BM of SS mice (Figure 4.2B). We hypothesize that the increase of S1P blood in SCD is the cause for this. S1P controls the migration of OPCs from the BM and the blood. OPCs possess the receptors S1PR1 and S1PR2. S1PR1 leads OPCs toward increased S1P in the blood. S1PR2 however initiates negative chemotaxis of OPCs away from high levels of S1P toward the BM [70]. Once in the BM, OPCs can attach to the bone and differentiate

into mature osteoclasts to resorb bone. In an area where there is minimal S1P, such as the BM, OPCs restore their S1PR1 expression to their outer membrane in order to migrate back into the blood by the S1P gradient [62]. In the blood, where S1P expression is significant, S1PR1is activated on OPCs and then quickly internalized to allow S1PR2 to dominate [62]. We hypothesize that due to the increased level of S1P in SCD, S1PR1 is overly internalized in OPCs, therefore causing for their increased chemotaxis to the BM where they can then lead to the increased bone resorption seen in SCD. For example, Ishii et al. found that S1PR2 knock out in mice led to osteopetrosis, suggesting that inhibition of S1PR2 causes a decrease in OPCs that are allowed to attach the bone surface [70]. Further studies should investigate the S1PR1 and S1PR2 expression on SS OPCs as well as intravital imaging to track the migration OPCs from the BM into the blood over time. Overall, our studies show that dysregulation in sphingolipid metabolism in SCD leads to changes in the BM microenvironment.

We further discovered that SS MPs also have a different sphingolipid profile in comparison AA MPs that possibly contributes to differences in their functionality. When we performed PCA on all 89 sphingolipids that we characterized with HPLC-MS, we found that complex sphingolipids, GlcCers and Cers, separated MPs based on genotype along PC2 (Figure 4.3C-D). Complex sphingolipids contain a constant sphingoid backbone as well as a variable side fatty acyl chain that varies in the number of carbons, which usually range from 13 to 26, and double bonds. Among the complex sphingolipids, small differences in acyl chain length or unsaturation can be functionally consequential; for example, the production of different Cer species in cell membranes impacts membrane morphology and fluidity [49, 50]. We found GlcCer 22:0 and 24:0 to

be increased in SS MPs (Figure 4.3A-B). GlcCers and other Cer derivatives promote osteoclastogenesis by increasing RANK production in osteoclasts [196, 197]. RANK production has in fact been found to be increased in SCD [134, 137]. Furthermore, Cer has been shown to induce apoptosis in several cell types, including osteoblasts and their precursors [198, 199]. RUNX2 and osteonectin, osteogenic markers, were found to be downregulated in SCD [137]. For the individual acyl chains, we found C16 and C24:1 are increased in SS MPs (Figure 4.3E). Interestingly, C16 and C24 ceramide fabrication ensues neutrophil and hepatocyte apoptosis [200, 201]. Our current findings regarding the sphingolipid profile of SS MPs gives some insight into how the sickle environment could lead to increased osteoclastogenesis and reduced osteoblast differentiation that has been characterized in sickle mouse models [134, 137].

Inflammation contributes to bone remodeling, and SCD induces chronic inflammation due to frequent sickling of RBCs and endothelial interactions that may prolong osteoclast activity [202]. The result is an abnormally high concentration of inflammatory proteins circulating in plasma of non-sickle individuals [203], with TNF-α and IL-6 being important ones. We previously found that SS MPs increase the production of the inflammatory cytokines TNF-α and IL-6 in monocytes and macrophages [10]. TNF-α and IL-6 are osteoclastogenic cytokines [204-207] and the latter has been implicated in increasing the expression of RANKL to attenuate osteoclast apoptosis in sickle patients as well to be increased in SS mice [137, 208]. Additionally, TNF-α incites the expression of the cat K gene (CTSK) in osteoclast precursors and has increased cat K activity in endothelial cells in SCD [17, 209]. Cat K is a potent collagenase released by osteoclasts to degrade bone matrix in both mice and humans [210]. Cat S is mainly

present in antigen presenting immune cells and cleaves collagen as well as other extracellular matrix (ECM) proteins like laminin, fibronectin, and osteocalcin (a bone protein produced by osteoblasts). Consequentially, inhibition of cat S has been shown to increase osteoblastic differentiation as well as bone turn over [211]. Disruption of these proteins can impair bone formation and contribute to the unbalance between bone formation and bone resorption. Both cathepsins are expressed in osteoclasts during bone development in mice [212] as well as have been implicated in several orthopedic-related diseases such as osteoporosis and osteoarthritis [99]. We found that SS MPs increased the cat K and S activity in SS and AA PBMCs in comparison to untreated cells (Figure 4.3F-G). This data suggest that monocytes and macrophages may play a role bone resorption in SCD due to the uptake of SS MPs. Blair et al. discovered that macrophages are able to absorb bone in acidic environment [213] . It has previously been shown that monocytes and macrophages are involved in bone resorption or display increased osteoclastogenesis in other chronic inflammatory diseases such as rheumatoid arthritis or osteoarthritis [214, 215]. Furthermore, Zhao et al. discovered that increased S1P in SCD led to an increase in the production of the osteoclastogenic cytokine IL-6 in macrophages and subsequent tissue damage [57]. We hypothesize that difference in the sphingolipid profile in SS MPs contribute to the increase in inflammatory response of immune cells and thus increased cathepsin activation as well. Future studies are needed to further elucidate if sphingolipids in SS MPs are solely responsible for the increased cathepsin activity.

If the bone loss in SCD is due to increased osteoclastogenesis and/or osteoclast activity has been up for debate. In adult and pediatric SCD patients, TRACP 5b, an enzyme that is a marker of osteoclast activity, is increased in the serum [208, 216].

However, in female SS mice, the mRNA for TRAP was decreased in comparison to control, and there was no increase in the bone resorption marker CTX-1 [134]. Moreover, increased osteoclast activity and osteoclast differentiation in sickle mice was surmised through upregulation of the genes RANK and RANKL, respectively, as well as through the increase in the number of osteoclasts present on the femoral bone surface [137]. In this work, we found evidence of increased osteoclastogenesis and activity in SCD. BM cells cultured from AA and SS femurs resulted in increased osteoclast differentiation in SS samples (Figure 4.4E). Furthermore, by the appearance of the cells, SS cells appeared to differentiate into full activated osteoclasts, apparent by the presence of a ruffled border, while AA cells look to be more so in the multinucleated osteoclast stage of osteoclastogenesis [184] (Figure 4.4C-D). Xiao et al. reported that SS osteoclasts did not have an increase in bone resorption activity in vitro [134]. However, our data display increased osteoclast activity through the increased presence of TRAP in the distal end of SS femurs (Figure 4.4J-L). Increased osteoclast activity in SCD is further demonstrated in increased cathepsin activity and cat K expression shown via enzyme zymography and western blot (Figure 4.4F-I). Additionally, we see no proteases activity at any molecular weight with the addition of the cysteine cathepsin inhibitor E-64 (Figure 4.5A). Zymography and Western blot data taken together suggests that the higher active bands (175kDa, 150kDa) in the zymography are cat K. The Western shows expression of mature cat K in addition to increased expression of heavy chain versions of cat K in SS (and one AA) BM-derived osteoclasts, which provides insight as to why we see increased activity in SS osteoclasts at 175kDa and 150kDa in the zymography gel (Figure 4.4F, H). With the addition of a cat K inhibitor, activity at 175kDa disappears for AA and SS

osteoclasts while the signal at 150kDa only diminishes for SS osteoclasts (Figure 4.5B-C). This data shows that indeed the increased cathepsin activity in SS osteoclasts in Figure 4.4F-G at 175kDa and 150kDa is cat K. Future studies are needed to fully elucidate if the higher bands in the zymography are potentially cat K bound to tissue, causing for its activity to show up in the gel at molecular weights higher than the anticipated 75kDa. Additionally, the higher bands in the Western are potentially pro-cathepsin K that has not been fully cleaved by other proteases to be fully active, or mature. This deduction is further supported by recombinant cat K being present at 150kDa. Our data demonstrates that SS BM- derived osteoclasts produce more cat K compared to AA BM-derived osteoclasts. This gives some in sight about cat K production in SCD and gives a discernible reason for the decreased bone density that plagues sickle patients.

Our BMT studies further substantiate our inference that the increased cathepsin activity in SS osteoclasts and PBMCs contribute to the bone loss in SCD. Keegan et al. found that there is increased cat K activity in SS endothelial cells [17]. We wanted to demonstrate that the cathepsin activity present within cells of a hematological lineage contributes to SBD and not the cathepsins from stromal cells. When we reconstituted the BM of wild-type mice with AA and SS BM, we saw a decrease in Cort. Th. and trabecular BV/TV in mice that received SS BM in comparison to those that received AA BM (Figure 4.10C, E). However, even when cat K is genetically knocked down, we still see a significant decrease in the aforementioned bone parameters in Cat K-/- mice given SS BM in comparison to those given AA BM (Figure 4.10C, E). This demonstrates that even when cat K is not active in the stromal cells, there is still bone loss present due to

the overactive cathepsins in the hematological cells in SS BM. Overall, our data demonstrates that cathepsins should be targeted to reduce the bone loss present in SCD.

By inhibiting cysteine cathepsins with E-64 treatment, we saw an increase in cortical and trabecular bone in sickle mice. In previous studies combating osteoporotic bone loss, inhibition of cat k has been the main strategy [217-219]. However, a total genetic knockout of cat K has been shown to increase the production of other proteases such as matrix metalloproteinases (MMPs), modify osteoblast function, and lead to brittle bones [127, 220]. This finding is possibly due to the fact that, even though at minor level, osteoblasts produce cathepsin K [221]. Furthermore, in humans there is a lysosomal disease called pycnodysostosis that is caused by a mutation in the cat K gene; people with this disorder have increased bone density but suffer from brittle bones [123]. Additionally, osteoclasts use cathepsins other than cat K such as B and L to resorb bone in mice and rats [73, 127, 222]. Moreover, broad cysteine cathepsin inhibition had a significant reduction in the amount of digested bone matrix in comparison to a specific cat K inhibitor [127]. Therefore, we utilized the drug E-64, which inhibits the activity of several cysteine proteases such as cathepsin K, S, L, B, and H to attenuate the bone loss in SCD [223]. In 3-month old mice, SCD caused for decreased Cort. Th., BA, BA/TA, and BMD within the mid diaphyseal region (Figure 4.6C, E, G, I). According to Bonnet et al., the strength of bones primarily comes from the Cort. Th. and BA [147]. Unsurprisingly, SS femurs were able to withstand significantly less force and stress in comparison to AA and AS bones during four-point bending mechanical testing (Figure 4.9B-C). E-64 treatment increased Cort. Th., BA, and BA/TA in SS mice (Figure 4.6D, F, H). Consequentially, this enhancement in cortical bone structure due to E-64 treatment

leads to improved mechanical properties in SS bones. In regard to the relationship between the Cort. Th. and the mechanical properties of stiffness, ultimate stress and max force, SS femurs have a negative correlation; this shows that as stiffness, maximum force or ultimate stress increases, the Cort. Th. decreases. However, with E64 treatment, SS femurs had a significant positive correlation of their Cor. Th. to the latter two aforementioned properties (Figure 4.9E-F). A similar pattern was observed for stiffness and BA/TA, but E-64 resulted in a positive although not significant correlation (Figure 4.9G-I). Furthermore, other studies have shown that the mechanical strength of bone can also vary due to changes in trabecular architecture [171]. In the distal end of the femur, SS mice have reduced Tb. Th. and BMD in the epiphyseal but not the metaphyseal region (Figure 4.7C, E, Figure 4.8 C, E). This difference could be due to the fact that the distal epiphysis in mice is nourished from an independent vasculature from the metaphysis until 5 months of age [130]. This would cause the epiphysis to be at an elevated risk for vaso-occlusions that would result in bone loss. E-64 treatment significantly increased Tb. Th. and BMD in the distal epiphysis in SS mice (Figure 4.7D, F). Overall, E-64 treatment lead to increased cortical and trabecular bone and thus increased mechanical strength of SS femurs; this demonstrates that the inhibition of cysteine cathepsins is a viable target to attenuate SBD.

In conclusion, we have shown that there is a mechanistic link between the dysregulation in sphingolipid metabolism and increased cathepsin activity that leads to bone loss in SCD. We have made the novel discovery that targeting cathepsin activity is a viable treatment to attenuate bone loss, especially within the cortical bone, in SBD.

CHAPTER 5 Novel Lipid Signaling Mediators for Mesenchymal Stem Cell Mobilization During Bone Repair[2]

5.1 Abstract

Mesenchymal stem and progenitor cells (MSCs), which normally reside in the bone marrow, are critical to bone health and can be recruited to sites of traumatic bone injury, contributing to new bone formation. The ability to control the trafficking of MSCs provides therapeutic potential for improving traumatic bone healing and therapy for genetic bone diseases such as hypophosphatasia. In this study, we explored the sphingosine-1-phosphate (S1P) signaling axis as a means to control the mobilization of MSCs into blood and possibly to recruit MSCs enhancing bone growth. Loss of S1P receptor 3 (S1PR3) leads to an increase in circulating CD45-/CD29+/CD90+/Sca1 putative mesenchymal progenitor cells, suggesting that blocking S1PR3 may stimulate MSCs to leave the bone marrow. Antagonism of S1PR3 with the small molecule VPC01091 stimulated acute migration of CD45-/CD29+/CD90+/Sca1+ MSCs into the blood as early as 1.5 hours after treatment. VPC01091 administration also increased ectopic bone formation induced by BMP-2 and significantly increased new bone formation in critically sized rat cranial defects, suggesting that mobilized MSCs may home to injuries to contribute to healing. We also explored the possibility of combining

---

[2] Adapted from: J.M. Selma, A. Das, A.O. Awojoodu, T. Wang, A.P. Kaushik, Q. Cui, H. Song, M.E. Ogle, C.E. Olingy, E.G. Pendleton, K.F. Tehrani, L.J. Mortensen, E.A. Botchwey, Novel Lipid Signaling Mediators for Mesenchymal Stem Cell Mobilization during Bone Repair, Cell Mol Bioeng 11(4) (2018) 241-253. Reprinted with permission from Springer Nature

S1P manipulation of endogenous host cell occupancy with exogenous MSC transplantation for potential use in combination therapies. Importantly, reducing niche occupancy of host MSCs with VPC01091 does not impede engraftment of exogenous MSCs. Our studies suggest that MSC mobilization through S1PR3 antagonism is a promising strategy for endogenous tissue engineering and improving MSC delivery to treat bone diseases.

5.2 Introduction

After traumatic bone injury, including long bone fractures and ischemic injuries, a population of MSCs exit the bone marrow (BM) and migrate to the wound to differentiate into osteoblastic cells and support new bone formation [75, 76, 224, 225]. The mobilization and recruitment of these cells are critical phases of tissue regeneration and a decreased mesenchymal stem cell (MSC) response is correlated with deficits in bone healing in human patients [73, 226, 227]. Dysfunction of MSCs through genetic defects such as in hypophosphatasia can also lead to improper bone development and homeostasis [228]. Delivery of exogenous BM-derived MSCs after bone injury enhances repair [229-231]. However, exogenous cell-based therapies are not widely available yet, can be time-intensive, and cost-prohibitive. Since there is an established role for MSCs in bone tissue repair, we sought to increase their mobilization and recruitment to the defect site to enhance bone healing. We also pursued utilizing endogenous MSC mobilization as a method to enhance the engraftment of exogenous MSCs in the BM.

Sphingosine 1-phosphate (S1P) is a biologically active signaling lipid that is present at high concentrations in blood where it binds to serum albumin or high-density lipoproteins. It binds to 5 high affinity G-coupled receptors (S1PR1-S1PR5) that direct a

wide range of biological processes [59, 62, 232-235] such as a chemoattractant for many cell types including MSCs [18, 19] and hematopoietic stem cells, guiding their egress from BM into the peripheral blood (PB) along the S1P gradient [20-22]. While the network of S1PR signaling is extremely complex, S1PR1 and S1PR3 in particular, have been shown to have significant effects on stem cell homing and mobilization. BM-derived cells are recruited by S1PR3 to inflamed tissues and induce a reduction in proinflammatory cytokine secretion and microvascular remodeling [95]. SEW2871, an S1PR1 agonist, enhances the motility and mobilization of osteoclast precursors *in vivo* and regulates bone homeostasis[62]. S1PR3 activation on human endothelial progenitor cells (EPCs) resulted in phosphorylation of the chemokine receptor 4 (CXCR4) and enhanced SDF-1 mediated chemotaxis and homing to ischemic tissues [61]. S1PR3 activation with a small molecule analogue of sphingosine, FTY720, resulted in enhanced CXCR4 function in hematopoietic stem and progenitor cells (HSPCs) *in vitro* and *in vivo* as well as enhanced homing and proliferation [94]. Recently, we found that antagonizing S1PR3, which phosphorylates CXCR4, mobilizes HSPCs out of the BM and into circulation [96]. Since MSCs express CXCR4, we hypothesized that S1PR3 antagonism could be utilized to mobilize MSCs as well [236].

In this study, we show that use of VPC01091 [237], a small molecule analogue of S1P that is a weak agonist of S1PR1 and strong antagonist of S1PR3, in a systemic manner enhances the mobilization of progenitor and mesenchymal stem cells and favors mesenchymal stem mobilization over hematopoietic stem cell mobilization. Using a subcutaneous bone formation assay, we demonstrate that osteogenic differentiation of the progenitor cells contributes to this process. We also determined that VPC01091

administration increases new bone formation in critical size cranial defects. In this work, we demonstrate for the first time that utilizing small molecule antagonism in S1PR3 signaling is sufficient for rapidly mobilizing MSCs into the PB and has broad implications for advancing therapy for bone fractures/defects and bone metabolic diseases.

5.3 Materials and Methods

5.3.1 Animals

Animal surgeries and procedures were performed in accordance and with approval from the University of Virginia, Georgia Institute of Technology, or University of Georgia Institutional Animal Care and Use Committees. Murine model studies were performed using C57BL/6 male mice from Jackson Laboratories and S1PR3 knockout mice (S1PR3-/-) on C57BL/6 background (a kind gift of Dr. Richard Proia at the National Institutes of Health). The subcutaneous ectopic bone model and the cranial defect model were performed in female Sprague Daley rats aged 8-10 weeks which were obtained from Charles River Laboratories International, Inc. (Wilmington, MA).

5.3.2 Analysis of MSC and LSK Mobilization

C57BL/6 or age-matched S1PR3-/- mice were euthanized by CO_2 inhalation. PB was harvested by cardiac puncture. For analysis of MSC trafficking in response to S1P signaling and other small molecules, mice were injected intraperitoneally (IP) with 5 mg/kg AMD3100 (Sigma) in saline or VPC0109 (Avanti) or FTY720 (Cayman Chemical) in sterile saline with 5% DMSO, 3% fatty-acid-free bovine serum albumin. For MSC trafficking time course analysis, C57BL/6 mice were treated IP with 5 or 10 mg/kg of VPC01091, and PB was collected by jugular vein draw at 1.5, 3, or 24 hours

after anesthesia. After blood collection, red blood cells were lysed with ammonium chloride, and PB mononuclear cells were stained for FACS analysis. Flow cytometry immunophenotyping was performed according to standard procedures and was analyzed on a CyAn ADP flow cytometer or BD FACS Aria II cytometer. Fluorophore conjugated monoclonal antibodies to Sca1, CD45, CD105, CD11b, CD90, and/or CD29 were used in studies to identify MSCs while antibodies for stem cell antigen-1 (Sca1), C-kit, and Lineage were used for LSK (Lineage- Sca1+ C-kit+) cells. The absolute number of cells mobilized were determined by utilizing AccuCheck Counting Beads (Thermo).

5.3.3 S1PR1 and S1PR3 Expression

S1PR1 and S1PR3 expression was measured by western blotting utilizing antibodies (S1PR1/EDG-1, S1PR3/EDG-3, Novus Biologicals) against the sphingolipid receptors. An equivalent quantity of protein from each group was injected into the gels and the bands were stained with near IR dyes

5.3.4 Ectopic Bone Model

Sprague Daley rats of age 8-10 weeks were anesthesia with isoflurane gas and continued with Ketamine/Xylazine (80/8 mg/kg via IP injection). To study ectopic bone formation, rats were injected subcutaneously, as described by Scott et al., with a Matrigel plug doped with BMP-2 [238]. Rats were randomly assigned to three different groups: control-subcutaneous Matrigel plug with BMP-2 only; subcutaneous Matrigel plug with BMP-2 plus a systemic IP dose of 1 mg/kg or 5 mg/kg VPC01091 (Lynch lab) every other week. Tissue surrounding the Matrigel was taken at week 1 and week 3 following implantation and digested for flow cytometry. At the end of 6 weeks, the ectopic implants

were removed, and the bone volume was measured with micro-computed tomography (microCT).

5.3.5 Cranial Defect Model

Following anesthetization, cranial defect surgery was performed as previously described [239, 240]. Briefly, after sterilization, a longitudinal incision was made through skin and periosteum, over the dorsum of the skull. The periosteum was reflected laterally. A 3-mm round burr was used to create an 8-mm defect in the bone with constant saline irrigation using a Hall® Surgical E900® System and Coolflex® High Speed Drill (CONMED Linvatec, Largo FL). The animals were treated with an IP dose of 1 mg/kg VPC01091 (Lynch lab) 24 hours and 3 weeks after surgery or left untreated for control. In all cases, the periosteum was closed with a 5-0 running nylon suture. The skin was closed with a running subcuticular vicryl suture, and VetClose™ (Butler Animal Health Supply, Dublin OH) was applied on the incision. Ketoprofen (3 mg/kg SC) was given after closure and for three days post-surgery to minimize pain. Rats were given free access to food and water and monitored for complications or abnormalities. At 9 weeks post-surgery, rats were anesthetized with 2.5% isoflurane gas and injected in the heart with 1 mL Nembutal for euthanasia.

5.3.6 Histology

Calvarial bones were extracted, fixed in 10% buffered formalin for 7 days and decalcified using an HCl and EDTA decalcifying solution (Richard-Allan Scientific, Kalamazoo MI) for 3 days at 4^{o}C. The calvarial bones were cut in half, perpendicular to the sagittal suture and centered at the defect. The rostral section was embedded in paraffin and sliced and stained with Mason's Trichrome. Bone sections were then washed and mounted

with PBS and glycerol solution (1:1) and visualized under a bright field microscope for positive staining. All images were evaluated by a blinded researcher.

5.3.7 MicroCT Analysis

MicroCT of the ectopic bone formation was conducted on explanted tissue after sacrifice. MicroCT of for the critical-sized defect studies was performed longitudinally at weeks 2, 4, 6 and 8 under ketamine/ xylazine induced anesthesia. 2D images were segmented by drawing the region of interest to comprise only parietal bone by including all bone inside the ridges separating parietal from temporal bone. Animals were scanned with the following parameters: 38 μm voxel size, 55 kVp, 145 μA, medium resolution, 38.9 mm diameter field of view, and 200 ms integration time (73 mGy radiation per scan). Slice number was set for each animal throughout the study to include the whole defect and an equal length both anterior and posterior of the defect (≈300 slices). Bone was thresholded at 470.1-1000 mg hydroxyapatite (HA)/cm^3, and bone volume was measured with the microCT software. 3D volume renderings were either done with SCANCO software after segmentation, or OsiriX 3.9 (Pixmeo, Geneva, Switzerland) from DICOM files of the region of interest. OsiriX images were thresholded and colored appropriately with the 16-bit color look up table (CLUT). All images were evaluated by a blinded researcher.

5.3.8 MSC In Vitro Culture

MSCs from 6-week-old wild type C57BL/6 mice were isolated according to a previous protocol [186]. Briefly, filtered BM-derived cells were collected in alpha-MEM media supplemented with 10% heat-inactivated fetal bovine serum, 1% penicillin-streptomycin (Gibco), and plated in a tissue culture flask at $1.5x10^6$ cells/cm^2. The media was changed every 3-4 days and cells were passaged at 60-80% confluence.

5.3.9 BM Niche Pre-clearance for MSC Engraftment

C57BL/6 mice aged 6-8 weeks were obtained from Jackson Laboratories. Mice were treated IP with saline or 5 mg/kg of VPC01091 (Avanti) in saline containing 5% DMSO and 3% fatty-acid-free BSA. Three hours later, MSCs (isolated and cultured from 6-week-old C57BL/6 mice BM) stained with lipophilic DiD membrane dye according to manufacturer protocols (Invitrogen) were injected into the retro-orbital sinus at a dose of $1x10^5$ cells per 20g of recipient mouse weight. Mice were euthanized 24 hours later, and the craniums were imaged with 2-photon microscopy to quantify MSC engraftment.

5.3.10 Optical Setup

A custom-built two-photon microscope was used. [241-243]. A 1550 nm, 370 femtosecond pulsed fiber laser (Calmar Cazadero) with wavelength of 1550 nm and repetition rate of 10 MHz was used. The beam was frequency doubled using a second harmonic generation (SHG) crystal (Newlight Photonics), to produce a 150mW 775 nm beam for two-photon excitation of the sample. Beam power was modulated using a Pockels cell (Conoptics) and scanned over the sample by a resonant-galvanometer (fast axis – slow axis) scanner (Sutter instruments MDR-R), which enables imaging at a rate of 30 frames per second. A 60x Olympus (LUMFLN60x) water immersion objective with NA of 1.1 was used for imaging. Z-scanning was performed using an X-Y-Z stage from the Sutter Instruments (MPC-200). MSCs stained with DiD were imaged using a 697/58 nm filter, autofluorescence from the endogenous bone marrow cells were captured using a 525/50 nm filter, and second harmonic generation from bone collagen fibers was measured using a 390/18 nm filter. Photon multiplier tubes (PMTs) from Hamamatsu were used for collection of the signal, and their signal amplified with a transimpedance

amplifier (Edmund Optics 59-178). A National Instruments DAQ card and FPGA module were used for control and synchronization of the system and digitizing of the amplified SHG signal. MATLAB-based Open-source software Scanimage [244] was used to control the microscope.

5.3.11 Statistical Analysis

Statistical comparisons were performed utilizing GraphPad Prism (La Jolla, CA). The resulting analysis is conveyed as mean ± standard error of the mean (SEM). Two-tailed t-test was used for column analysis. For grouped analyses, one-way ANOVA with Holm-Sidak's multiple comparison test was utilized. For grouped analyses comparing data over time or between treatment and control, two-way ANOVA with Tukey's multiple comparisons test was used. A *p*-value less than 0.05 was considered statistically significant.

5.4 Results

5.4.1 The S1P signaling axis controls progenitor cell trafficking from the BM

Due to our previous finding that S1PR3 plays a role in hematopoietic stem and progenitor cell (HSPC) retention within the BM niche, we hypothesized that S1PR3 may play a similar role in other progenitors such as MSCs and that the loss of S1PR3 mobilizes them into the blood. To analyze circulating progenitor cells by flow cytometry, blood was drawn from wild type and S1PR3-/- mice. S1PR3-/- mice have a significantly higher proportion of Sca1+ (a marker widely expressed on progenitor populations of the BM including MSCs and HSPCs[245]) cells in the PB compared to age matched wildtype controls (Figure 5.1A) and similarly display a larger percentage of CD45-/CD29+/Sca1+/CD90+ cells (MSCs) in the blood (Figure 5.1B) via the gating strategy

depicted in (Figure 5.2A-D). Acute pharmacological targeting of S1PR3 with a small molecule antagonist, VPC01091 [237], significantly enhanced the percentage of Sca1+ progenitor cells in the blood of wild type mice compared to AMD3100 (a CXCR4 antagonist and known stem cell mobilizer) while FTY720, an agonist of S1PR3, reduced Sca1+ progenitor cell circulation (Figure 5.1C).

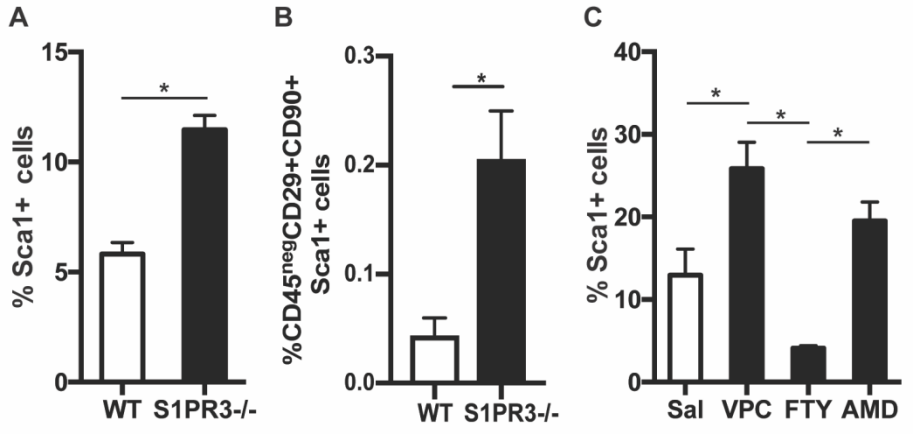

Figure 5.1. Genetic and pharmacological S1PR3 suppression mobilizes progenitor cells into circulation. (A) S1PR3-/- mice show an increase in percentage of Sca1+ (n=3 mice per group) and (B) CD45-/C29+/CD90+/Sca1+ cells in circulation (n=4 mice per group). (C) The percentage of Sca1+ cells mobilized into circulation increases in one hour by pharmacological S1PR3 antagonism via VPC01091 (n=4 mice per group). Data expressed as mean ± SEM. *p<0.05. Abbreviations: WT, wild type; Sal, saline; AMD, AMD3100; VPC, VPC01091; FTY, FTY720.

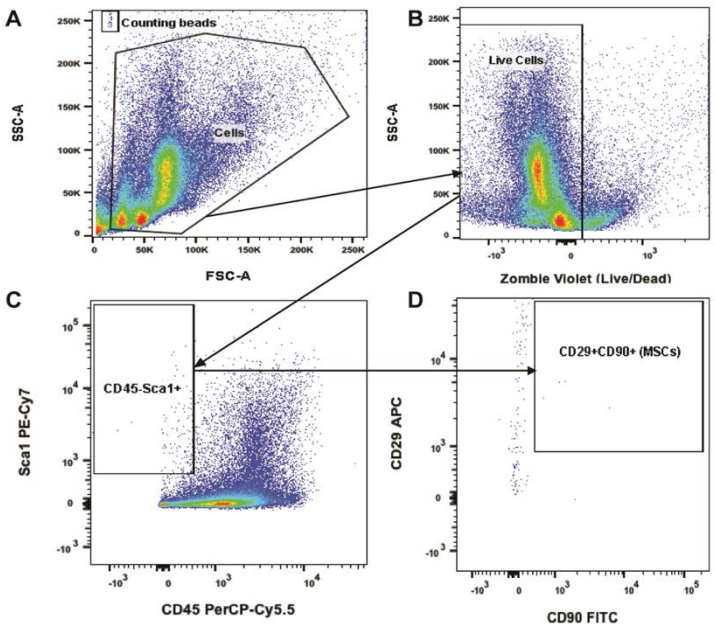

Figure 5.2. Flow cytometry gating for MSCs. MSCs are identified in the blood by gating for (A) cells, (B) live cells (C) CD45-/Sca1+cells and finally (D) CD90+/CD29+ cells**.**

Additionally, BM cells were harvested from wild type mice and Sca1+/CD105+ cells were sorted via FACS. Western blotting was used to detect S1PR1 and S1PR3 expression. Both receptors were present in these mouse mesenchymal cells (Figure 5.3A). In order to determine if Sca1+/CD105+ cells were in the pool of cells in the PB of S1PR3-/- mice, we employed antibodies against Sca1 and CD105, putative murine MSC markers. We quantified the proportion of Sca1+/CD105+ cells in blood and found that, similar to Sca1+ progenitors, untreated S1PR3-/- mice showed an increase in Sca1+/CD105+ cells in the blood (Figure 5.3B).

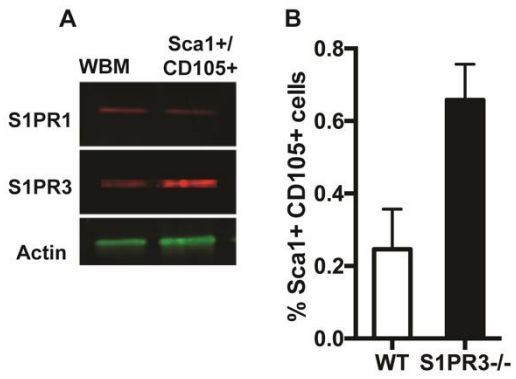

Figure 5.3. S1P receptor expression for MSCs. (A) Sca1+/CD105+ cells isolated from wild type mice express relatively more S1PR3 compared to whole bone marrow cells. (B) S1PR3-/- mice have more Sca1+/CD105+ cells in circulation (n=2 mice per group).

5.4.2 Systemic antagonism of S1PR3 increases MSC mobilization

To further examine whether pharmacological inhibition of S1PR3 could mobilize MSCs into the PB, we treated wildtype C57BL/6 mice with 5 mg/kg or 10mg/kg doses of VPC01091 (Figure 5.4A-B).

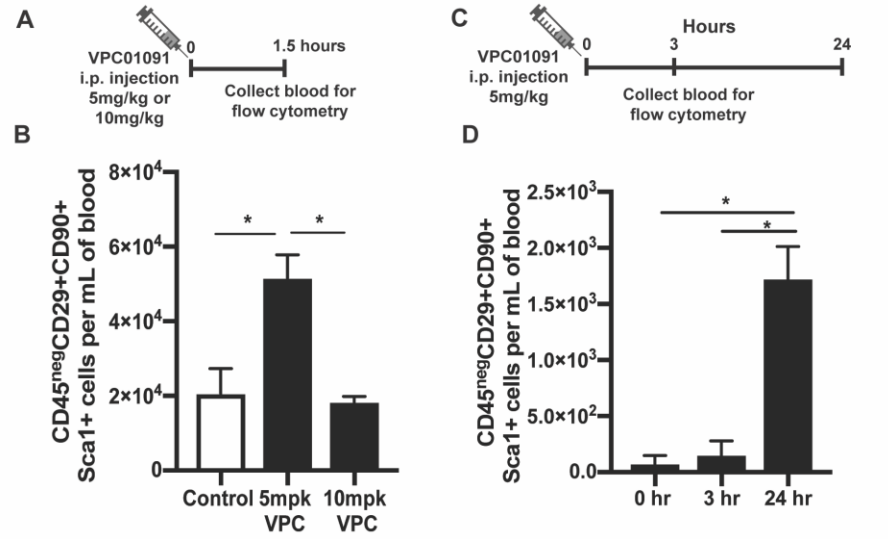

Figure 5.4. VPC01091 increases the mobilization of MSCs into circulation. (A) Schematic of animal studies. (B) 5 mg/kg of VPC01091 increases the number of CD45-/C29+/CD90+/Sca1+ cells (MSCs) in the blood after 1.5 hours in comparison to control and 10mg/kg of VPC01091 (n=3-4 mice per group). (C) Schematic of animal studies. (D) The number of CD45-/C29+/CD90+/Sca1+ cells (MSCs) in the blood increases following twenty-four hours after 5mg/kg VPC01091 dose (n=4 mice per group). Data

expressed as mean ± SEM. * $p<0.05$. Abbreviations: WT, wild type; BM, bone marrow; VPC, VPC01091; mpk, milligram per kilogram; I.P., intraperitoneal.

VPC01091 increased the number of MSCs in the blood at a concentration of 5 mg/kg. Similarly, we tested these dosages on the effect of mobilizing LSK (Lineage-/Sca1+/C-kit+) cells and observed a significant increase in the number of MSCs mobilized in comparison to LSK cells (Figure 5.5A) by utilizing the gating strategy depicted in (Figure 5.5B-E).

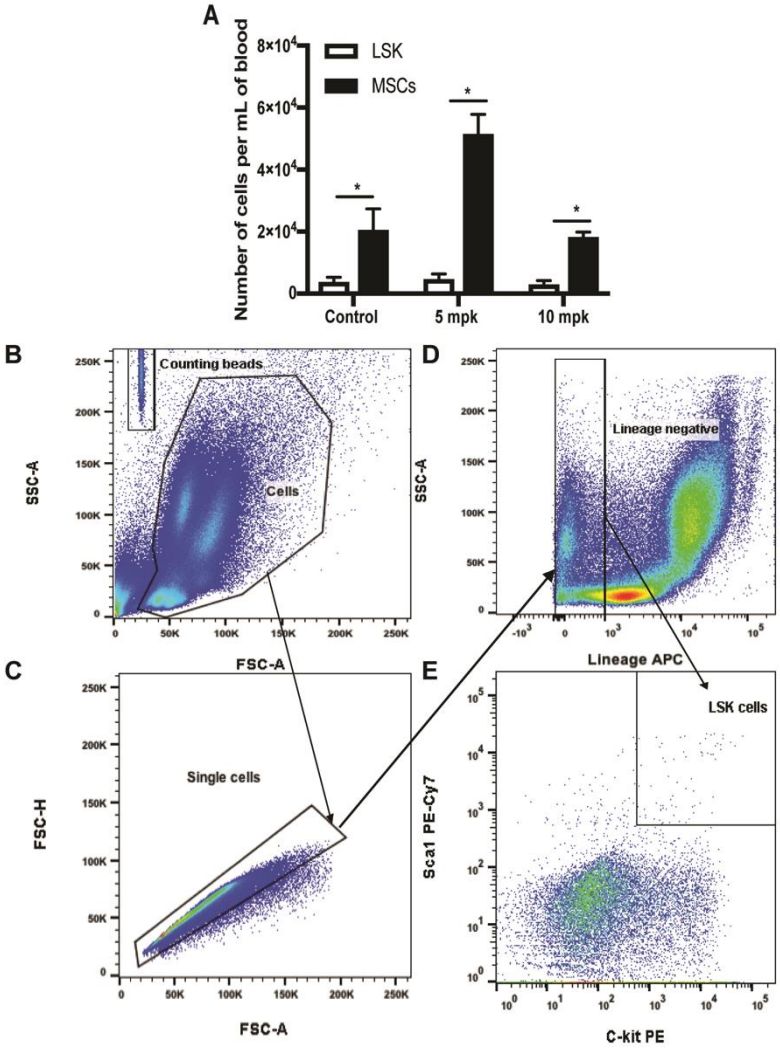

Figure 5.5. VPC01091 increases the mobilization of MSCs into circulation over LSK cells. (A)5mg/kg of VPC01091 increases the mobilization of MSCs into the blood more than LSK cells (n=4 mice per group). LSK cells are identified in the blood by gating for (B) cells, (C) single cells, (D) lineage- cells and (E) Sca1+/C-kit+ cells. Data expressed as mean ± SEM. * $p<0.05$. Abbreviations: VPC, VPC01091; mpk, milligram per kilogram.

To further examine whether pharmacological inhibition of S1PR3 could mobilize MSCs into the PB over a longer time course, wildtype C57Bl/6 mice were treated with vehicle control or 5 mg/kg VPC01901 by IP injection and tracked the expression of CD45-

/Sca1+/CD90+/CD29+ cells in the blood at 0, 3, and 24-hour intervals after injection (Figure 5.4C-D). MSCs were increased in the blood at 24 hours after (Figure 5.4D) by utilizing the gating strategy depicted in (Figure 5.2A-D).

5.4.3 Systemic antagonism of S1PR3 increases ectopic bone formation

Since MSCs have osteogenic potential, we investigated whether VPC01091 has an effect on ectopic bone formation. In Sprague Daley rats, we performed an ectopic bone assay with BMP-2 laden matrigel. Under control conditions, after 6 weeks, a very small amount of mineralized bone is formed in the BMP-2 matrigel implant. However, if VPC01091 is injected once weekly over the 6-week experiment, there is substantially increased bone formation as measured by microCT imaging (Figure 5.6A-C).

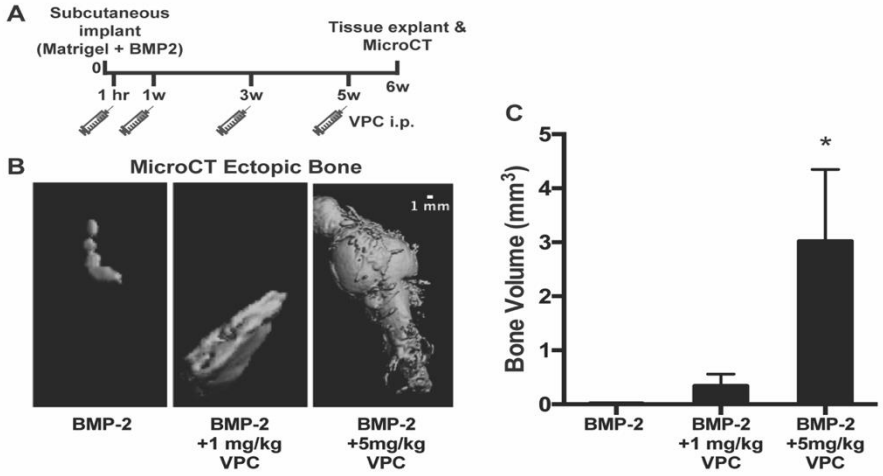

Figure 5.6. Amount of ectopic bone 6 weeks after matrigel + BMP-2 implantation increases with weekly systemic VPC01091 treatment. (A) Schematic of animal studies. (B) Representative MicroCT images of ectopic bone after 6 weeks of 1 or 5 mg/kg dose of VPC01091. (C) Every other week treatment of 1 or 5 mg/kg of systemic VPC01091 increases the ectopic bone formation in the presence of BMP-2 (n=6 mice per group). Data expressed as mean ± SEM. * $p<0.05$. Abbreviations: BMP-2, bone morphogenetic protein 2; VPC, VPC01091; mpk, milligram per kilogram.

Moreover, the tissue surrounding the ectopic bone site shows an increased recruitment of CD29+/CD90+ cells at weeks 1 and 3 post implantation (Figure 5.7A-B). This suggests that systemic delivery of VPC01091 encourages ectopic bone formation and that this could be related its S1PR3 antagonism inducing the circulation of MSCs.

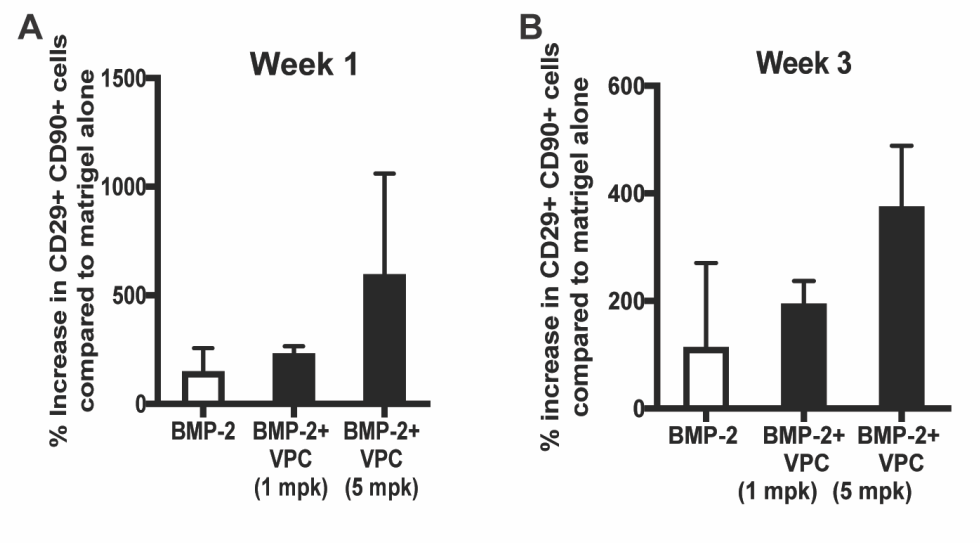

Figure 5.7. More MSC-like cells migrate to ectopic bone site with systemic VPC01091. Percentage of CD29+/CD90+ cells surrounding ectopic bone site increases with systemic VPC01091 treatment at 1 week (A) and (B) 3 weeks after matrigel + BMP-2 implantation (n= 3 mice per group). Data expressed as mean ± SEM. * $p<0.05$. Abbreviations: VPC, VPC01091; mpk, milligram per kilogram.

5.4.4 S1PR3 antagonism improves regeneration of a critical-sized bone defect

To further explore S1PR3 antagonism as a means to enhance bone forming capacity, we tested the effect of systemic VPC01091 treatment after a critical sized cranial bone defect (Figure 5.8A).

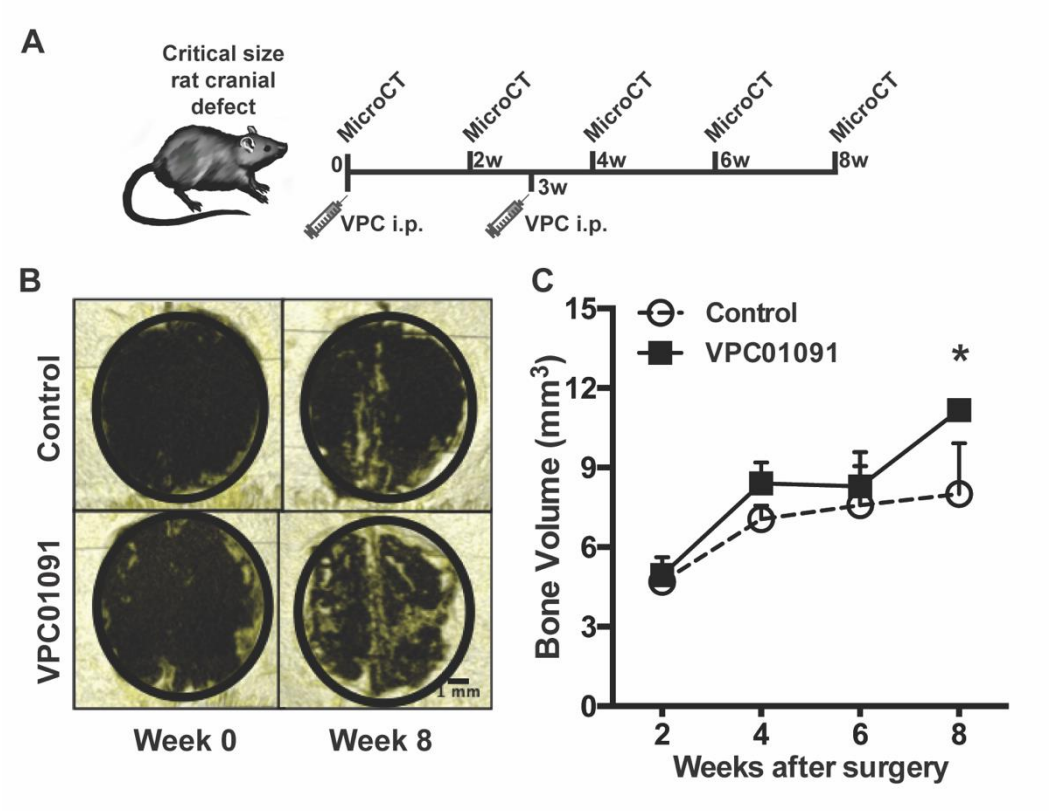

Figure 5.8. Systemic therapy with VPC01091 (at week 0 and week 3) after critical-sized cranial defect results in an increase in defect site bone volume. (A) Schematic of animal studies. (B) Representative MicroCT images before and 8 weeks after cranial defect surgery. (C) Systemic treatment with 1 mg/kg of VPC01091 increases bone volume at defect site at 8 weeks (n=4-9 mice per group). Data expressed as mean ± SEM. *p<0.05 week 8 empty compared to week 2 empty, week 8 VPC01091 compared to week 2 VPC01091. Abbreviations: VPC, VPC01091; mpk, milligram per kilogram; I.P., intraperitoneal.

Rats were treated with either vehicle or 5mg/kg VPC01091 on the day of the defect surgery and again at 3 weeks following the surgery. After 8 weeks, the animals treated with VPC01091 demonstrated increases in the amount of new bone formation by microCT analysis (Figure 5.8B-C) and Masson's trichrome histology (Figure 5.9). Histological evaluations show animals treated with VPC01091 had tissue in the defect

region that appears more like regenerating bone, including the presence of more osteoid bodies and more collagen than in the control animals (Figure 5.9A-D).

This treatment does not require any local implants and is modulated by the fact that VPC01091 mobilizes stem and progenitor cells from the bone barrow into circulation. These cells can then be recruited to the defect site where they can differentiate into bone. Moreover, CD90+/ CD11b- cells were recruited to the defect site in animals that received the systemic dose of VPC01091 (Figure 5.9E).

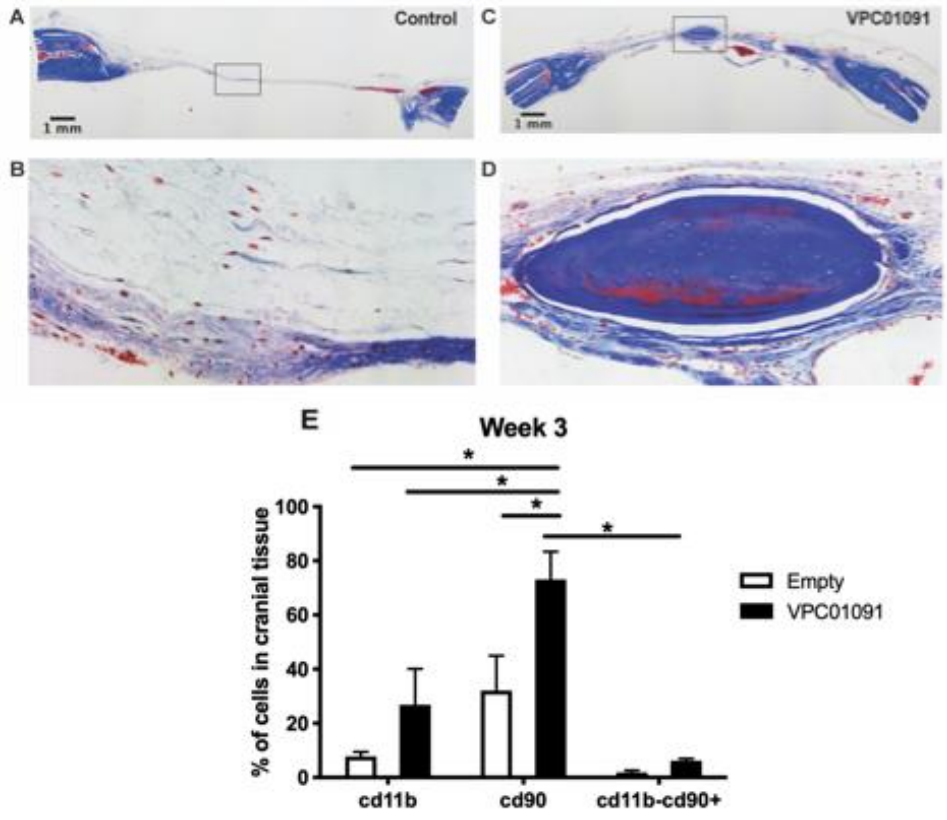

Figure 5.9. Increase in osteoid body formation and fibroblast-like cell migration to defect site with systemic VPC01091. Representative images of Masson's trichrome staining of calvarial bone after 8 weeks of saline (A) or 1 mg/kg VPC01091 treatment (C) showing osteoid bodies (red) within the bone (blue). Magnified sections (squared off segments in A, C) of Masson's trichrome staining of calvarial bone after 8 weeks of saline (B) or 1 mg/kg VPC01091 treatment (D). (E) 3 weeks after treatment, there is an

increase in the percentage of CD90+ and CD11b-/CD90+ cells in the defect region (n=3 mice per group). Data expressed as mean ± SEM. * $p<0.05$.

5.4.5 S1PR3 antagonism to pre-clear the BM niche does not impede donor MSC engraftment

With bone fractures and some metabolic bone diseases being treated via MSC therapies, we were interested to see the effect that VPC01091 has on allogenic MSCs homing to bone. An injection of VPC01091 three hours before MSC administration yielded transplanted MSC engraftment into the cranial bone of wild-type mice (Figure 5.10A-B). Importantly, treatment with VPC01091 did not impede external MSC engraftment ($p=0.4905$). DiD stained MSCs were visualized in the skull 24 hours after injection (Figure 5.10C-D). This data suggests that manipulating sphingolipid signaling in order to mobilize endogenous BM-residing MSCs can be utilized in a combination with delivering allogenic MSCs without damaging the host bone marrow or compromising bone homeostasis.

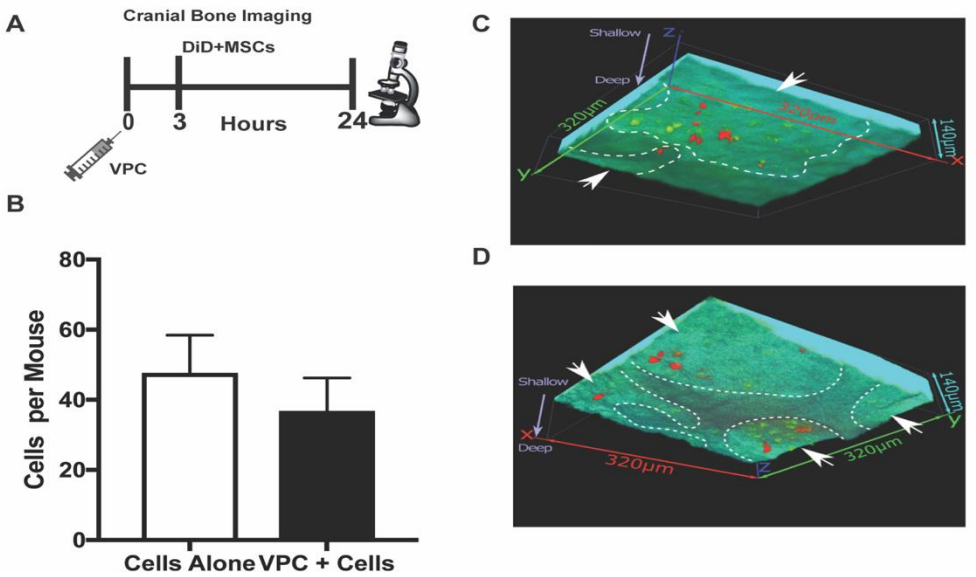

Figure 5.10. Mobilizing endogenous MSCs with VPC01091 does not inhibit transplanted MSC engraftment into bone. (A) Schematic of animal studies. (B) Number of donor MSCs engrafted per mouse into the cranial bone does not increase 24 hours after 5 mg/kg treatment of VPC01091 (n=3 mouse per group). Representative images of donor DiD-stained engrafted into the cranial bone of host mice 24 hours after saline (C) or 5 mg/kg VPC01091treatment (D). Green cells are endogenous bone marrow cells. Red cells are transplanted MSCs, quantified in the bone marrow cavities (indicated by arrow with dotted line borders). Cyan colored areas are second harmonic generation signal from bone collagen. Data expressed as mean ± SEM. Abbreviations: VPC, VPC01091; mpk, milligram per kilogram.

5.5 Discussion

Autologous or allogenic bone grafts are the gold standard remedies to repair critical-size bone defects; however, there are several limitations. In addition to causing chronic residual pain, autografts harvested from patients' iliac crests have up to a 20% chance of causing major complications such as pelvic instability, nerve injury, and haematoma formation [246]. Due to the risk of transmitting disease, allografts have to undergo a sterilization process that affects the structural integrity and eliminates the intrinsic osteogenic potential of the grafts [246, 247]. As an alternative, researchers have

investigated cellular approaches to bone tissue engineering, such locally implanted autologous MSC-seeded constructs [248]. Despite some debate in MSC therapy leading to vascular calcification, utilizing MSCs over other stem cell types such as embryonic stem cells is advantageous in that they can be isolated from various sources including but not limited to BM, adipose tissue, dental pulp, and PB [249, 250]. However, it takes an estimated 4-6 weeks to obtain enough MSCs for clinical application [249]. Additionally, long-term *in vitro* culture of MSCs decreases their mineralization and immunosuppression capacity [251, 252]. Hence, research studies have begun to place emphasis on finding a therapy to quickly mobilize and amplify a patient's own endogenous stem cells to the site of the bone injury.

The presence of MSCs in PB is controversial. Hoogduijn et al. claimed that human patients with organ injury had no circulating MSCs unless the bone marrow cavity was broken open by way of a skeletal fracture [253]. However, Kassis et al. discovered that with the use of G-CSF, MSCs could be isolated from human PB with the use of fibrin microbeads [254]. Furthermore, MSCs taken from the PB were found to be successful in contributing to new bone formation in cranial critical sized defects in Sprague Dawley rats [255]. Future studies will be required to track endogenous MSCs after administering VPC01091 to a cranial defect site, utilizing our previous cell tracking methods, to verify that the new bone formation we witnessed with VPC01091 administration in Figure 5.6 and Figure 5.8 is indeed due to mobilized MSCs [256]. Additional studies will also be required to examine whether mobilized cells give rise to mesenchymal lineages such as osteocytes, chondrocytes, and adipocytes in vitro as do MSCs from other tissue depots such as BM and adipose tissues.

A steep gradient of S1P exists between BM and blood and is used by many cell types to navigate the path from marrow to circulation [21, 60, 62, 96, 257]. MSCs, osteoprogenitors, and osteoclast progenitors express S1P receptors and are chemotactically sensitive to S1P gradients [18, 62, 70] and biomaterial strategies incorporating S1P receptor targeting molecules increase bone regeneration [239, 240, 258-260]. We have recently demonstrated that S1PR3 is a critical signal for HSPC retention within the BM niche and that loss or antagonism of S1PR3 mobilizes these cells to the blood [96]. Additionally, we discovered that HSPCs and MSCs have different relative expression levels of S1PR1and S1PR3 mRNA [96]. Because MSCs may react distinctively to S1P signalling, we utilized flow cytometry to determine that S1PR3 -/- mice have an increased basal level of circulating progenitor cells in comparison to wildtype (Figure 5.1A). We therefore hypothesized MSCs can be mobilized into the blood through pharmacological inhibition of S1PR3 by VPC010191 treatment and serve in bone repair.

It has been speculated that due to their greater size and superior ability to remain in their stem cell niche, MSCs are more difficult to mobilize than HSPCs [261]. However, in this study we were able to demonstrate with VPC01091 that we can mobilize a greater number of MSCs into circulation in comparison to LSK cells (Figure 5.5A). For these in vivo mobilization studies, we utilized a single isomer (3d-P) of VPC01091 that has greater inhibitory activity at S1PR3 and little to no activity at S1PR1 [237]. This finding can possibly be explained by the results in (Figure 5.3A) that show more relative expression of S1PR3 in cells positive for the MSC markers Scal and CD105 in comparison to whole bone marrow cells. Furthermore, we verified through flow

cytometry that 5mg/kg of VPC01091 transiently induces mobilization of CD45-/CD29+/C90+/Sca-1+ cells (MSCs) as early as 1.5 hours after injection (Figure 5.4B). Interestingly, at 3 hours the level of MSCs in the blood drops and then increases again at 24 hours (Figure 5.4D). This suggests that the cell population is traveling to other parts of the body, but the location is unclear. It has been found that BM-derived MSCs migrate to sites of injury to aid in tissue repair and regeneration in various kinds of wounds including myocardial infarction and bone fracture [236]. Therefore, we utilized a cranial defect model to test whether mobilized MSCs were indeed moving to an injured site. Through microCT imaging, we determined that injections of VPC01091 at week 0 and week 3 increased bone volume and CD90+ cells at the defect site (Figure 5.8C, Figure 5.9E). Furthermore, ectopic bone development created by BMP-2 releasing matrigels was enhanced due to cells mobilized by VP01091 (Figure 5.6C). According to Otsuru et al., there is a mechanistic links between osteoprogenitors circulating in the blood and the formation of ectopic bone via BMP-2 [93]. Additionally, VPC01091 treatment increased the percentage of CD29+/CD90+ cells present in the tissue surrounding the matrigel as early as one-week post-implantation (Figure 5.7A-B). This combined data suggests that bone-forming MSCs are capable of being mobilized from the bone marrow niche through S1P signalling.

Recently, Fu et al utilized G-CSF in rabbits to mobilize MSCS into the blood to be harvested and cultured to treat osteonecrosis (ON) [81]. Deng et al. mobilized MSCs with G-CSF into the PB and found that they can aid in repair of injured cerebral tissue [82]. However, in certain populations, such as cancer patients undergoing chemotherapy or other hematological disorders, G-CSF has proven to be an ineffective drug [83-85].

MSCs are positive for the chemokine receptor 4 (CXCR4), which aids in the stem cells remaining in the SDF-1 rich BM. AMD3100, being a CXCR4 antagonist, can therefore disturb this linkage and mobilize MSCs into circulation. Toupadakis et al., showed that AMD3100 treatment increased the number of MSCs in the blood 24 hours after injection and that a 3-day AMD3100 dosing regimen increased bone volume 84 days after injury in a murine femur fracture model [262]. We, however, were able to show that with biweekly injects of VPC01091, bone volume significantly increased as early as 8 weeks (56 days) (Figure 5.8C). Additionally, we found that VPC01091 induces more progenitor cells into circulation that with AMD3100 (Figure 5.1C).

Systemically administered allogeneic MSCs are a promising therapeutic approach to prevent or ameliorate metabolic bone diseases, such as hypophosphatasia or osteoporosis. Limited success has been reported involving MSC therapies to enhance skeletal mineralization and halt disease progression; healthy donor MSC survival and integration in bone is a challenge. The treatment of a few patients with MSCs supported by myeloablation and bone marrow transplants resulted in some desired clinical outcomes, but only provided low levels of stromal cell engraftment in the bone [228, 263-266]. Therefore, we hypothesized that mobilization of endogenous MSCs with VPC01091 could be combined with MSC transplantation to yield enhanced treatment of bone defects and metabolic bone diseases. Our results demonstrate that VPC01091 does not obstruct donor MSC transplantation (Figure 5.10B). We plan to do further studies in order to determine if mobilizing endogenous MSCs with VPC01091 and combining with MSC transplantation aids in decreasing the negative effects of allogenic treatment that has been seen in some combination bone graft therapies [267-269].

We noted previously that VPC01091 and AMD3100 have different (and in many ways complimentary) mechanisms of action [96]. While VPC01091 indirectly affects CXCR4 by preventing its phosphorylation via S1PR3, AMD3100 directly binds to three acid residues in the main ligand-binding pocket [61, 270]. We found that LSK cells pre-treated with VPC01091 had greater BM engraftment capacity in comparison to pre-treated AMD3100 cells [96]. Consequently, Granero-Molto et al. and Osturu et al., states that the CXCR4/SDF-1 pathway is necessary for MSCs to home bone and then differentiate into osteoblasts [92, 93]. More CXCR4+ MSCs may be present in circulation after VPC01091 treatment (as we saw previously with HSPCs) than with AMD3100, allowing for more cells to migrate to the site of injury and enhance bone repair [96]. Moreover, as our data suggests that this treatment does not hinder engraftment of transplanted MSCs, (Figure 5.10B), we believe our approach strikes an important balance between transient mobilization signals to evacuate the niche and preservation of niche signaling elements to facilitate homing and engraftment into bone. Finding technologies that will effectively manage this compromise may be key to successful translation and treatment of skeletal diseases caused by errors in bone metabolism.

CHAPTER 6 CONCLUSIONS AND FUTURE DIRECTIONS

6.1 Major Findings

The work presented in this thesis represents a significant contribution to the field of sickle cell disease (SCD) by elucidating the under-characterized sickle bone phenotype of weakened biomechanical strength due to reduced trabecular and cortical bone, discovering cysteine cathepsins as a viable target to relegate bone loss, and establishing endogenous (mesenchymal stem cell) MSC mobilization as potential therapy for bone disorders. This work expands the understanding of the relationship between dysregulated sphingolipid metabolism in SCD and subsequent increased cathepsin activation; we identify methods in which this relationship can be utilized as a potential therapy for sickle bone disease (SBD) to promote bone growth and development. This thesis also demonstrates that modulating sphingolipid signaling increases bone repair.

In Aim 1, we characterize novel differences in bone development as well as bone architecture for the sickle Townes mouse model. We discovered that SBD leads to delayed proximal epiphyseal fusion and therefore stunted skeletal maturation and overall growth. Furthermore, we discovered that while cortical bone deficiency is present in both sexes, trabecular bone growth is impaired in SS females while increases with age in SS males. Interestingly, our work also displays that the sickle bone phenotype varies in the trabecular bone depending on the anatomical structure (e.g. femoral neck, distal epiphysis). For example, in female SS mice only the trabecular thickness (Tb.Th.) is reduced in the femoral neck, but in the distal epiphysis, the Tb.Th. as well as the bone tissue mineral density (BMD) was decreased. Through multivariate analysis we were able to determine that trabecular bone parameters had the most significant effect in separating

the sickle bone phenotype from normal and sickle trait, regardless of sex. Overall, we were able to determine that when characterizing the sickle bone phenotype, trabecular bone morphometry is the most important factor and should be depicted at various anatomical sites when investigating potential therapies for SBD.

In Aim 2, we show a connection between sphingolipid metabolism and increased cathepsin activity that leads to bone loss in SCD. We demonstrate that sphingosine 1-phosphate (S1P) is increased in the blood of a sickle transgenic mouse model. We elucidate that increased S1P in the blood of our sickle mouse model causes for an increase in osteoclast progenitors (OPCs) in the bone marrow (BM) and subsequent increased bone resorption. This finding is further evident in the increased TRAP staining in sickle femurs as well as increased osteoclastogenesis from SS BM cells. Furthermore, we demonstrated that the dysregulated sphingolipid metabolism in SCD that produces more proinflammatory microparticles (MPs), also leads to increased osteoclast activity by amplifying the cathepsin K (cat K) activity of osteoclast precursors. Moreover, we discovered that cat K activity and production in SS osteoclasts is increased. We were able to connect this increase in cathepsin activity to the sickle bone phenotype that we characterized in Aim 1 by showing that cathepsin inhibition results in improved bone strength and cortical and trabecular bone growth in SCD. Overall, we show a novel connection between sphingolipid metabolism and cathepsin activity that leads to the pathological bone resorption characteristic of SBD.

In Aim 3, we were able to demonstrate for the first time that S1P signaling could be utilized to mobilize MSCs into the peripheral blood (PB). We prove that the antagonism of sphingosine 1-phosphate receptor 3 (S1PR3) through the drug VPC01091

increases the circulation of MSCs into the PB and thus leads to increased bone growth in the context of an orthopedic injury. With the administration of VPC01091, MSCs increased in circulation as early as 1.5 hours and remained in circulation at 24 hours. Through ectopic bone and cranial critical-defect models, we were able to demonstrate that treatment with VPC01091increases bone growth. These findings relay a potential treatment strategy to combat the bone loss characterized in SCD in Aim 1.

6.2 Future Directions

6.2.1 Utilization of endogenous MSC mobilization to enhance bone regeneration in SCD

We believe that mobilized autologous MSCs are a promising therapeutic approach to treat SBD. Allogenic MSC therapy has yielded improvements in metabolic bone disorders such as hypophosphatasia and osteogenesis imperfecta [228, 263-266, 271]. Although external MSC administration has been therapeutic, low and inconsistent rates of engraftment lead to poorer outcomes. In looking at autologous therapy for SBD, human SS MSCs did not have diminished osteogenic potential [23]. In one study, MSCs harvested from the iliac crest of sickle patients suffering from early stage osteonecrosis (ON) were able to delay the progression of bone death in the femoral head for 5 years [228, 263-266, 271]. However, in more advanced stages of ON, there is more bone loss, and thus more stem cells are needed in order to fully regenerate the bone than can be safely harvested from patients at one time. Therefore, ex vivo expansion of MSCs would be necessary, a process which takes anywhere from 4-6 weeks and decreases the cells' mineralization capacity [249, 252]. It would be interesting to see the effects of utilizing VPC01091 to mobilize endogenous MSCs on bone morphology and growth in our sickle

Townes mouse model as an alternative therapy for SBD. With the occlusions that occur in the microvasculature of the BM due to the sickling of erythrocytes, it is possible that poor circulation of MSCs to the site of injury, as presumed by Lebouvier et al., is also aiding in the bone loss in SCD that we characterized in Aim 1. We have shown in Aim 3 that the administration of VPC01091 leads to an increase in circulating MSCs as well an increase in bone growth in a bone defect model. Furthermore, this thesis work highlights an important role for S1PRs in MSC niche occupancy and trafficking that can be harnessed for rapid endogenous MSC mobilization and homing into the diseased osseous tissues of sickle bone for subsequent bone regeneration.

6.2.2 Utilization of acid SMase inhibition to reduce RBC MPs in order to attenuate bone loss in SCD

We have shown previously that acid sphingomyelinase (SMase) inhibition with the tricyclic antidepressant amitriptyline reduces red blood cell (RBC)-derived MPs in vitro as well as in wild type mice [10]. We have established in Aim 2 that RBC MPs increase the activity of cat K, an enzyme that aids in bone resorption, in SS and AA peripheral blood mononuclear cells (PBMCs). Additionally, others have shown that sphingosine kinase 1 (SK1) inhibition leads to less sickling of RBCs [12]. Reduced RBC sickling would lead to decreased vaso-occulsions in the microvasculature of bone and thus diminished bone loss. Acid SMase converts sphingomyelin (SM) into ceramide (Cer), which can then be converted into sphingosine (So) in order to be phosphorylated by SK. Acid SMase therefore is an upstream target of SK. Therefore, we find it imperative that acid SMase inhibition be explored as potential treatment in reducing proteolytic MPs, RBC sickling, and thus subsequent bone loss in SCD.

6.2.3 Investigation of the role of MSC sphingolipid metabolism in osteoblast differentiation in SBD pathology

In Aim 2 we have shown that SS MSCs have a different sphingolipid profile in comparison to AA and AS MSCs. Sphingolipids have been shown to be tissue specific and even alter during cellular processes such as differentiation [194, 195]. We have demonstrated that sphingolipid metabolism is dysregulated in SS RBCs, blood, and plasma [10]. Changes in RBC membrane morphology drive alterations in the activity of sphingolipid-metabolizing enzymes; increases in SK1 and subsequent elevated blood sphingosine 1-phosphate (S1P) increases the sickling and membrane distortions in SS RBCs [10, 12]. Changes in MSC morphology have been linked to their osteogenic potential/mineralization capacity [252, 272, 273]. Additionally, MSC osteoblast differentiation is enhanced with S1P and FTY720 treatment as well as their morphology is altered [63, 64, 181]. In the transgenic sickle Townes model, MSCs isolated from SS MSCs have a lower incidence of osteoblast differentiation when compared to AA MSCs; additionally, the mRNA expression of osteogenic genes osterix, RUNX2, osteocalcin, and osteonectin are decreased in SS mice [134, 137]. With SCD pathology including femoral and vertebral infarcts, ON, osteoporosis, and increased risk of bone fracture, there is a need to discover the mechanism behind this decrease in SS MSCs progression towards osteogenic lineage [2, 4, 274]. We believe that studies should be conducted to test if the difference in sphingolipid profile of SS MSCs causes reduced osteogenic differentiation in the sickle transgenic model.

REFERENCES

[1] F.B. Piel, S.I. Hay, S. Gupta, D.J. Weatherall, T.N. Williams, Global burden of sickle cell anaemia in children under five, 2010-2050: modelling based on demographics, excess mortality, and interventions, PLoS Med 10(7) (2013) e1001484.

[2] A. Almeida, I. Roberts, Bone involvement in sickle cell disease, Br J Haematol 129(4) (2005) 482-90.

[3] V.C. Ejindu, A.L. Hine, M. Mashayekhi, P.J. Shorvon, R.R. Misra, Musculoskeletal manifestations of sickle cell disease, Radiographics 27(4) (2007) 1005-21.

[4] C. Aguilar, E. Vichinsky, L. Neumayr, Bone and joint disease in sickle cell disease, Hematol Oncol Clin North Am 19(5) (2005) 929-41, viii.

[5] P.F. Milner, A.P. Kraus, J.I. Sebes, L.A. Sleeper, K.A. Dukes, S.H. Embury, R. Bellevue, M. Koshy, J.W. Moohr, J. Smith, Sickle cell disease as a cause of osteonecrosis of the femoral head, N Engl J Med 325(21) (1991) 1476-81.

[6] K.M. Mahadeo, S. Oyeku, B. Taragin, S.N. Rajpathak, K. Moody, R. Santizo, M.C. Driscoll, Increased prevalence of osteonecrosis of the femoral head in children and adolescents with sickle-cell disease, Am J Hematol 86(9) (2011) 806-8.

[7] P. Hernigou, D. Bachir, F. Galacteros, The natural history of symptomatic osteonecrosis in adults with sickle-cell disease, J Bone Joint Surg Am 85-A(3) (2003) 500-4.

[8] E.P. Vichinsky, L.D. Neumayr, C. Haberkern, A.N. Earles, J. Eckman, M. Koshy, D.M. Black, The perioperative complication rate of orthopedic surgery in sickle cell disease: report of the National Sickle Cell Surgery Study Group, Am J Hematol 62(3) (1999) 129-38.

[9] S. Adam, J. Jonassaint, H. Kruger, M. Kail, E.P. Orringer, J.R. Eckman, A. Ashley-Koch, M.J. Telen, L.M. De Castro, Surgical and obstetric outcomes in adults with sickle cell disease, Am J Med 121(10) (2008) 916-21.

[10] A.O. Awojoodu, P.M. Keegan, A.R. Lane, Y. Zhang, K.R. Lynch, M.O. Platt, E.A. Botchwey, Acid sphingomyelinase is activated in sickle cell erythrocytes and contributes to inflammatory microparticle generation in SCD, Blood 124(12) (2014) 1941-50.

[11] A. Marsh, R. Schiffelers, F. Kuypers, S. Larkin, G. Gildengorin, W. van Solinge, C. Hoppe, Microparticles as biomarkers of osteonecrosis of the hip in sickle cell disease, Br J Haematol 168(1) (2015) 135-8.

[12] Y. Zhang, V. Berka, A. Song, K. Sun, W. Wang, W. Zhang, C. Ning, C. Li, Q. Zhang, M. Bogdanov, D.C. Alexander, M.V. Milburn, M.H. Ahmed, H. Lin, M. Idowu, J. Zhang, G.J. Kato, O.Y. Abdulmalik, W. Zhang, W. Dowhan, R.E. Kellems, P. Zhang, J. Jin, M. Safo, A.L. Tsai, H.S. Juneja, Y. Xia, Elevated sphingosine-1-phosphate promotes sickling and sickle cell disease progression, J Clin Invest 124(6) (2014) 2750-61.

[13] S.T. Price, T.H. Beckham, J.C. Cheng, P. Lu, X. Liu, J.S. Norris, Sphingosine 1-Phosphate Receptor 2 Regulates the Migration, Proliferation, and Differentiation of Mesenchymal Stem Cells, Int J Stem Cell Res Ther 2(2) (2015).

[14] K. Higashi, E. Matsuzaki, Y. Hashimoto, F. Takahashi-Yanaga, A. Takano, H. Anan, M. Hirata, F. Nishimura, Sphingosine-1-phosphate/S1PR2-mediated signaling triggers Smad1/5/8 phosphorylation and thereby induces Runx2 expression in osteoblasts, Bone 93 (2016) 1-11.

[15] J. Ryu, H.J. Kim, E.J. Chang, H. Huang, Y. Banno, H.H. Kim, Sphingosine 1-phosphate as a regulator of osteoclast differentiation and osteoclast-osteoblast coupling, EMBO J 25(24) (2006) 5840-51.

[16] S. Lotinun, R. Kiviranta, T. Matsubara, J.A. Alzate, L. Neff, A. Luth, I. Koskivirta, B. Kleuser, J. Vacher, E. Vuorio, W.C. Horne, R. Baron, Osteoclast-specific cathepsin K deletion stimulates S1P-dependent bone formation, J Clin Invest 123(2) (2013) 666-81.

[17] P.M. Keegan, S. Surapaneni, M.O. Platt, Sickle cell disease activates peripheral blood mononuclear cells to induce cathepsins k and v activity in endothelial cells, Anemia 2012 (2012) 201781.

[18] Y. Kong, H. Wang, T. Lin, S. Wang, Sphingosine-1-phosphate/S1P receptors signaling modulates cell migration in human bone marrow-derived mesenchymal stem cells, Mediators Inflamm 2014 (2014) 565369.

[19] M. Meriane, S. Duhamel, L. Lejeune, J. Galipeau, B. Annabi, Cooperation of matrix metalloproteinases with the RhoA/Rho kinase and mitogen-activated protein kinase kinase-1/extracellular signal-regulated kinase signaling pathways is required for the sphingosine-1-phosphate-induced mobilization of marrow-derived stromal cells, Stem cells 24(11) (2006) 2557-65.

[20] M.Z. Ratajczak, M. Suszynska, S. Borkowska, J. Ratajczak, G. Schneider, The role of sphingosine-1 phosphate and ceramide-1 phosphate in trafficking of normal stem cells and cancer cells, Expert opinion on therapeutic targets 18(1) (2014) 95-107.

[21] M.Z. Ratajczak, H. Lee, M. Wysoczynski, W. Wan, W. Marlicz, M.J. Laughlin, M. Kucia, A. Janowska-Wieczorek, J. Ratajczak, Novel insight into stem cell mobilization-plasma sphingosine-1-phosphate is a major chemoattractant that directs the egress of hematopoietic stem progenitor cells from the bone marrow and its level in peripheral blood increases during mobilization due to activation of complement cascade/membrane attack complex, Leukemia 24(5) (2010) 976-85.

[22] C.H. Kim, W. Wu, M. Wysoczynski, A. Abdel-Latif, M. Sunkara, A. Morris, M. Kucia, J. Ratajczak, M.Z. Ratajczak, Conditioning for hematopoietic transplantation activates the complement cascade and induces a proteolytic environment in bone marrow: a novel role for bioactive lipids and soluble C5b-C9 as homing factors, Leukemia 26(1) (2012) 106-16.

[23] A. Lebouvier, A. Poignard, L. Coquelin-Salsac, J. Leotot, Y. Homma, N. Jullien, P. Bierling, F. Galacteros, P. Hernigou, N. Chevallier, H. Rouard, Autologous bone marrow stromal cells are promising candidates for cell therapy approaches to treat bone degeneration in sickle cell disease, Stem Cell Res 15(3) (2015) 584-594.

[24] K.L. Hassell, Population estimates of sickle cell disease in the U.S, Am J Prev Med 38(4 Suppl) (2010) S512-21.

[25] M. Azuma, K. Kato, Y. Ikarashi, R. Asada-Mikami, H. Maruoka, Y. Takaue, A. Saito, H. Wakasugi, Cytokines production of U5A2-13-positive T cells by stimulation with glycolipid alpha-galactosylceramide, Eur J Immunol 30(8) (2000) 2138-46.

[26] G.A. Barabino, M.O. Platt, D.K. Kaul, Sickle cell biomechanics, Annu Rev Biomed Eng 12 (2010) 345-67.

[27] F.A. Ferrone, Polymerization and sickle cell disease: a molecular view, Microcirculation 11(2) (2004) 115-28.

[28] P. Connes, S. Verlhac, F. Bernaudin, Advances in understanding the pathogenesis of cerebrovascular vasculopathy in sickle cell anaemia, Br J Haematol 161(4) (2013) 484-98.

[29] O. Barrett, Jr., D.E. Saunders, Jr., D.E. McFarland, J.O. Humphries, Myocardial infarction in sickle cell anemia, Am J Hematol 16(2) (1984) 139-47.

[30] K.F. Baum, D.T. Dunn, G.H. Maude, G.R. Serjeant, The painful crisis of homozygous sickle cell disease. A study of the risk factors, Arch Intern Med 147(7) (1987) 1231-4.

[31] M.T. Gladwin, A.N. Schechter, F.P. Ognibene, W.A. Coles, C.D. Reiter, W.H. Schenke, G. Csako, M.A. Waclawiw, J.A. Panza, R.O. Cannon, 3rd, Divergent nitric oxide bioavailability in men and women with sickle cell disease, Circulation 107(2) (2003) 271-8.

[32] O.S. Platt, D.J. Brambilla, W.F. Rosse, P.F. Milner, O. Castro, M.H. Steinberg, P.P. Klug, Mortality in sickle cell disease. Life expectancy and risk factors for early death, N Engl J Med 330(23) (1994) 1639-44.

[33] O.S. Platt, Hydroxyurea for the treatment of sickle cell anemia, N Engl J Med 358(13) (2008) 1362-9.

[34] C.P. Minniti, l-Glutamine and the Dawn of Combination Therapy for Sickle Cell Disease, N Engl J Med 379(3) (2018) 292-294.

[35] J. Tsay, Z. Yang, F.P. Ross, S. Cunningham-Rundles, H. Lin, R. Coleman, P. Mayer-Kuckuk, S.B. Doty, R.W. Grady, P.J. Giardina, A.L. Boskey, M.G. Vogiatzi, Bone loss caused by iron overload in a murine model: importance of oxidative stress, Blood 116(14) (2010) 2582-9.

[36] A. Shander, M.D. Cappellini, L.T. Goodnough, Iron overload and toxicity: the hidden risk of multiple blood transfusions, Vox Sang 97(3) (2009) 185-97.

[37] T.L. Kauf, T.D. Coates, L. Huazhi, N. Mody-Patel, A.G. Hartzema, The cost of health care for children and adults with sickle cell disease, Am J Hematol 84(6) (2009) 323-7.

[38] V. Sebastiano, M.L. Maeder, J.F. Angstman, B. Haddad, C. Khayter, D.T. Yeo, M.J. Goodwin, J.S. Hawkins, C.L. Ramirez, L.F. Batista, S.E. Artandi, M. Wernig, J.K. Joung, In situ genetic correction of the sickle cell anemia mutation in human induced pluripotent stem cells using engineered zinc finger nucleases, Stem Cells 29(11) (2011) 1717-26.

[39] G. Socie, J. Ritz, Current issues in chronic graft-versus-host disease, Blood 124(3) (2014) 374-84.

[40] E.Y. Chiang, P.S. Frenette, Sickle cell vaso-occlusion, Hematol Oncol Clin North Am 19(5) (2005) 771-84, v.

[41] S.K. Kim, J.H. Miller, Natural history and distribution of bone and bone marrow infarction in sickle hemoglobinopathies, J Nucl Med 43(7) (2002) 896-900.

[42] M.R. Brinker, K.A. Thomas, S.J. Meyers, T. Texada, J.R. Humbert, S.D. Cook, R. Gitter, Bone mineral density of the lumbar spine and proximal femur is decreased in children with sickle cell anemia, Am J Orthop (Belle Mead NJ) 27(1) (1998) 43-9.

[43] G.J. Lonergan, D.B. Cline, S.L. Abbondanzo, Sickle cell anemia, Radiographics 21(4) (2001) 971-94.

[44] D.M. Deely, M.E. Schweitzer, MR imaging of bone marrow disorders, Radiol Clin North Am 35(1) (1997) 193-212.

[45] M. Green, I. Akinsami, A. Lin, S. Banton, S. Ghosh, B. Chen, M. Platt, I. Osunkwo, S. Ofori-Acquah, R. Guldberg, G. Barabino, Microarchitectural and mechanical characterization of the sickle bone, J Mech Behav Biomed Mater 48 (2015) 220-8.

[46] Y.A. Hannun, L.M. Obeid, Principles of bioactive lipid signalling: lessons from sphingolipids, Nat Rev Mol Cell Biol 9(2) (2008) 139-50.

[47] S. Gupta, M.R. Maurya, A.H. Merrill, Jr., C.K. Glass, S. Subramaniam, Integration of lipidomics and transcriptomics data towards a systems biology model of sphingolipid metabolism, BMC Syst Biol 5 (2011) 26.

[48] M.J. Hernandez-Corbacho, M.F. Salama, D. Canals, C.E. Senkal, L.M. Obeid, Sphingolipids in mitochondria, Biochim Biophys Acta Mol Cell Biol Lipids 1862(1) (2017) 56-68.

[49] S.N. Pinto, L.C. Silva, A.H. Futerman, M. Prieto, Effect of ceramide structure on membrane biophysical properties: the role of acyl chain length and unsaturation, Biochim Biophys Acta 1808(11) (2011) 2753-60.

[50] S. Grosch, S. Schiffmann, G. Geisslinger, Chain length-specific properties of ceramides, Prog Lipid Res 51(1) (2012) 50-62.

[51] F. Bianco, C. Perrotta, L. Novellino, M. Francolini, L. Riganti, E. Menna, L. Saglietti, E.H. Schuchman, R. Furlan, E. Clementi, M. Matteoli, C. Verderio, Acid sphingomyelinase activity triggers microparticle release from glial cells, EMBO J 28(8) (2009) 1043-54.

[52] R.W. Jenkins, D. Canals, Y.A. Hannun, Roles and regulation of secretory and lysosomal acid sphingomyelinase, Cell Signal 21(6) (2009) 836-46.

[53] M.L. Wong, B. Xie, N. Beatini, P. Phu, S. Marathe, A. Johns, P.W. Gold, E. Hirsch, K.J. Williams, J. Licinio, I. Tabas, Acute systemic inflammation up-regulates secretory sphingomyelinase in vivo: a possible link between inflammatory cytokines and atherogenesis, Proc Natl Acad Sci U S A 97(15) (2000) 8681-6.

[54] A.S. Shet, O. Aras, K. Gupta, M.J. Hass, D.J. Rausch, N. Saba, L. Koopmeiners, N.S. Key, R.P. Hebbel, Sickle blood contains tissue factor-positive microparticles derived from endothelial cells and monocytes, Blood 102(7) (2003) 2678-83.

[55] S.M. Camus, B. Gausseres, P. Bonnin, L. Loufrani, L. Grimaud, D. Charue, J.A. De Moraes, J.M. Renard, A. Tedgui, C.M. Boulanger, P.L. Tharaux, O.P. Blanc-Brude, Erythrocyte microparticles can induce kidney vaso-occlusions in a murine model of sickle cell disease, Blood 120(25) (2012) 5050-8.

[56] D.J. Lopez, M. Egido-Gabas, I. Lopez-Montero, J.V. Busto, J. Casas, M. Garnier, F. Monroy, B. Larijani, F.M. Goni, A. Alonso, Accumulated bending energy elicits neutral sphingomyelinase activity in human red blood cells, Biophys J 102(9) (2012) 2077-85.

[57] S. Zhao, M.G. Adebiyi, Y. Zhang, J.P. Couturier, X. Fan, H. Zhang, R.E. Kellems, D.E. Lewis, Y. Xia, Sphingosine-1-phosphate receptor 1 mediates elevated IL-6 signaling to promote chronic inflammation and multitissue damage in sickle cell disease, FASEB J 32(5) (2018) 2855-2865.

[58] H. Rosen, P.J. Gonzalez-Cabrera, M.G. Sanna, S. Brown, Sphingosine 1-phosphate receptor signaling, Annual review of biochemistry 78 (2009) 743-68.

[59] J. Rivera, R.L. Proia, A. Olivera, The alliance of sphingosine-1-phosphate and its receptors in immunity, Nat Rev Immunol 8(10) (2008) 753-63.

[60] K. Golan, Y. Vagima, A. Ludin, T. Itkin, S. Cohen-Gur, A. Kalinkovich, O. Kollet, C. Kim, A. Schajnovitz, Y. Ovadya, K. Lapid, S. Shivtiel, A.J. Morris, M.Z. Ratajczak, T. Lapidot, S1P promotes murine progenitor cell egress and mobilization via S1P1-mediated ROS signaling and SDF-1 release, Blood 119(11) (2012) 2478-88.

[61] D.H. Walter, U. Rochwalsky, J. Reinhold, F. Seeger, A. Aicher, C. Urbich, I. Spyridopoulos, J. Chun, V. Brinkmann, P. Keul, B. Levkau, A.M. Zeiher, S. Dimmeler, J. Haendeler, Sphingosine-1-phosphate stimulates the functional capacity of progenitor cells by activation of the CXCR4-dependent signaling pathway via the S1P3 receptor, Arterioscler Thromb Vasc Biol 27(2) (2007) 275-82.

[62] M. Ishii, J.G. Egen, F. Klauschen, M. Meier-Schellersheim, Y. Saeki, J. Vacher, R.L. Proia, R.N. Germain, Sphingosine-1-phosphate mobilizes osteoclast precursors and regulates bone homeostasis, Nature 458(7237) (2009) 524-8.

[63] K. Marycz, A. Smieszek, M. Jelen, K. Chrzastek, J. Grzesiak, J. Meissner, The effect of the bioactive sphingolipids S1P and C1P on multipotent stromal cells--new opportunities in regenerative medicine, Cell Mol Biol Lett 20(3) (2015) 510-33.

[64] Y. Hashimoto, E. Matsuzaki, K. Higashi, F. Takahashi-Yanaga, A. Takano, M. Hirata, F. Nishimura, Sphingosine-1-phosphate inhibits differentiation of C3H10T1/2 cells into adipocyte, Mol Cell Biochem 401(1-2) (2015) 39-47.

[65] S. Weske, M. Vaidya, A. Reese, K. von Wnuck Lipinski, P. Keul, J.K. Bayer, J.W. Fischer, U. Flogel, J. Nelsen, M. Epple, M. Scatena, E. Schwedhelm, M. Dorr, H. Volzke, E. Moritz, A. Hannemann, B.H. Rauch, M.H. Graler, G. Heusch, B. Levkau, Targeting sphingosine-1-phosphate lyase as an anabolic therapy for bone loss, Nat Med 24(5) (2018) 667-678.

[66] M.T. Valenti, L. Dalle Carbonare, M. Mottes, Osteogenic Differentiation in Healthy and Pathological Conditions, Int J Mol Sci 18(1) (2016).

[67] J. Keller, P. Catala-Lehnen, A.K. Huebner, A. Jeschke, T. Heckt, A. Lueth, M. Krause, T. Koehne, J. Albers, J. Schulze, S. Schilling, M. Haberland, H. Denninger, M. Neven, I. Hermans-Borgmeyer, T. Streichert, S. Breer, F. Barvencik, B. Levkau, B. Rathkolb, E. Wolf, J. Calzada-Wack, F. Neff, V. Gailus-Durner, H. Fuchs, M.H. de Angelis, S. Klutmann, E. Tsourdi, L.C. Hofbauer, B. Kleuser, J. Chun, T. Schinke, M. Amling, Calcitonin controls bone formation by inhibiting the release of sphingosine 1-phosphate from osteoclasts, Nat Commun 5 (2014) 5215.

[68] C. Huang, R. Ling, F.J. Li, E.C. Li, Q.K. Huang, B.G. Liu, Y. Ding, S.W. You, FTY720 enhances osteogenic differentiation of bone marrow mesenchymal stem cells in ovariectomized rats, Mol Med Rep 14(1) (2016) 927-35.

[69] S.H. Lee, S.Y. Lee, Y.S. Lee, B.J. Kim, K.H. Lim, E.H. Cho, S.W. Kim, J.M. Koh, G.S. Kim, Higher circulating sphingosine 1-phosphate levels are associated with lower bone mineral density and higher bone resorption marker in humans, J Clin Endocrinol Metab 97(8) (2012) E1421-8.

[70] M. Ishii, J. Kikuta, Y. Shimazu, M. Meier-Schellersheim, R.N. Germain, Chemorepulsion by blood S1P regulates osteoclast precursor mobilization and bone remodeling in vivo, J Exp Med 207(13) (2010) 2793-8.

[71] D.H. Livingston, D. Anjaria, J. Wu, C.J. Hauser, V. Chang, E.A. Deitch, P. Rameshwar, Bone marrow failure following severe injury in humans, Ann Surg 238(5) (2003) 748-53.

[72] T. Takahashi, C. Kalka, H. Masuda, D. Chen, M. Silver, M. Kearney, M. Magner, J.M. Isner, T. Asahara, Ischemia- and cytokine-induced mobilization of bone marrow-derived endothelial progenitor cells for neovascularization, Nat Med 5(4) (1999) 434-8.

[73] S. Kumar, S. Ponnazhagan, Mobilization of bone marrow mesenchymal stem cells in vivo augments bone healing in a mouse model of segmental bone defect, Bone 50(4) (2012) 1012-8.

[74] R. Schofield, The relationship between the spleen colony-forming cell and the haemopoietic stem cell, Blood Cells 4(1-2) (1978) 7-25.

[75] X.X. Wang, R.J. Allen, Jr., J.P. Tutela, A. Sailon, A.C. Allori, E.H. Davidson, G.K. Paek, P.B. Saadeh, J.G. McCarthy, S.M. Warren, Progenitor cell mobilization enhances bone healing by means of improved neovascularization and osteogenesis, Plast Reconstr Surg 128(2) (2011) 395-405.

[76] T. Matsumoto, A. Kawamoto, R. Kuroda, M. Ishikawa, Y. Mifune, H. Iwasaki, M. Miwa, M. Horii, S. Hayashi, A. Oyamada, H. Nishimura, S. Murasawa, M. Doita, M. Kurosaka, T. Asahara, Therapeutic potential of vasculogenesis and osteogenesis

promoted by peripheral blood CD34-positive cells for functional bone healing, Am J Pathol 169(4) (2006) 1440-57.

[77] R.S. Carvalho, T.A. Einhorn, W. Lehmann, C. Edgar, A. Al-Yamani, A. Apazidis, D. Pacicca, T.L. Clemens, L.C. Gerstenfeld, The role of angiogenesis in a murine tibial model of distraction osteogenesis, Bone 34(5) (2004) 849-61.

[78] D.Y. Lee, T.J. Cho, J.A. Kim, H.R. Lee, W.J. Yoo, C.Y. Chung, I.H. Choi, Mobilization of endothelial progenitor cells in fracture healing and distraction osteogenesis, Bone 42(5) (2008) 932-41.

[79] A.J. Laing, J.P. Dillon, E.T. Condon, J.C. Coffey, J.T. Street, J.H. Wang, A.J. McGuinness, H.P. Redmond, A systemic provascular response in bone marrow to musculoskeletal trauma in mice, J Bone Joint Surg Br 89(1) (2007) 116-20.

[80] A.J. Laing, J.P. Dillon, E.T. Condon, J.T. Street, J.H. Wang, A.J. McGuinness, H.P. Redmond, Mobilization of endothelial precursor cells: systemic vascular response to musculoskeletal trauma, J Orthop Res 25(1) (2007) 44-50.

[81] Q. Fu, N.N. Tang, Q. Zhang, Y. Liu, J.C. Peng, N. Fang, L.M. Yu, J.W. Liu, T. Zhang, Preclinical Study of Cell Therapy for Osteonecrosis of the Femoral Head with Allogenic Peripheral Blood-Derived Mesenchymal Stem Cells, Yonsei Med J 57(4) (2016) 1006-15.

[82] J. Deng, Z.M. Zou, T.L. Zhou, Y.P. Su, G.P. Ai, J.P. Wang, H. Xu, S.W. Dong, Bone marrow mesenchymal stem cells can be mobilized into peripheral blood by G-CSF in vivo and integrate into traumatically injured cerebral tissue, Neurol Sci 32(4) (2011) 641-51.

[83] L.B. To, J.P. Levesque, K.E. Herbert, How I treat patients who mobilize hematopoietic stem cells poorly, Blood 118(17) (2011) 4530-40.

[84] B.K. Adler, D.E. Salzman, M.H. Carabasi, W.P. Vaughan, V.V. Reddy, J.T. Prchal, Fatal sickle cell crisis after granulocyte colony-stimulating factor administration, Blood 97(10) (2001) 3313-4.

[85] A.P. Grigg, Granulocyte colony-stimulating factor-induced sickle cell crisis and multiorgan dysfunction in a patient with compound heterozygous sickle cell/beta+ thalassemia, Blood 97(12) (2001) 3998-9.

[86] L. Ding, S.J. Morrison, Haematopoietic stem cells and early lymphoid progenitors occupy distinct bone marrow niches, Nature 495(7440) (2013) 231-5.

[87] A. Greenbaum, Y.M. Hsu, R.B. Day, L.G. Schuettpelz, M.J. Christopher, J.N. Borgerding, T. Nagasawa, D.C. Link, CXCL12 in early mesenchymal progenitors is required for haematopoietic stem-cell maintenance, Nature 495(7440) (2013) 227-30.

[88] H.E. Broxmeyer, C.M. Orschell, D.W. Clapp, G. Hangoc, S. Cooper, P.A. Plett, W.C. Liles, X. Li, B. Graham-Evans, T.B. Campbell, G. Calandra, G. Bridger, D.C. Dale, E.F. Srour, Rapid mobilization of murine and human hematopoietic stem and progenitor cells with AMD3100, a CXCR4 antagonist, The Journal of experimental medicine 201(8) (2005) 1307-18.

[89] A. Peled, I. Petit, O. Kollet, M. Magid, T. Ponomaryov, T. Byk, A. Nagler, H. Ben-Hur, A. Many, L. Shultz, O. Lider, R. Alon, D. Zipori, T. Lapidot, Dependence of human stem cell engraftment and repopulation of NOD/SCID mice on CXCR4, Science 283(5403) (1999) 845-8.

[90] O. Kollet, A. Spiegel, A. Peled, I. Petit, T. Byk, R. Hershkoviz, E. Guetta, G. Barkai, A. Nagler, T. Lapidot, Rapid and efficient homing of human CD34(+)CD38(-/low)CXCR4(+) stem and progenitor cells to the bone marrow and spleen of NOD/SCID and NOD/SCID/B2m(null) mice, Blood 97(10) (2001) 3283-91.

[91] C.A. Toupadakis, A. Wong, D.C. Genetos, D.J. Chung, D. Murugesh, M.J. Anderson, G.G. Loots, B.A. Christiansen, A.S. Kapatkin, C.E. Yellowley, Long-term administration of AMD3100, an antagonist of SDF-1/CXCR4 signaling, alters fracture repair, J Orthop Res 30(11) (2012) 1853-9.

[92] F. Granero-Molto, J.A. Weis, M.I. Miga, B. Landis, T.J. Myers, L. O'Rear, L. Longobardi, E.D. Jansen, D.P. Mortlock, A. Spagnoli, Regenerative effects of transplanted mesenchymal stem cells in fracture healing, Stem Cells 27(8) (2009) 1887-98.

[93] S. Otsuru, K. Tamai, T. Yamazaki, H. Yoshikawa, Y. Kaneda, Circulating bone marrow-derived osteoblast progenitor cells are recruited to the bone-forming site by the CXCR4/stromal cell-derived factor-1 pathway, Stem Cells 26(1) (2008) 223-34.

[94] T. Kimura, A.M. Boehmler, G. Seitz, S. Kuci, T. Wiesner, V. Brinkmann, L. Kanz, R. Mohle, The sphingosine 1-phosphate receptor agonist FTY720 supports CXCR4-dependent migration and bone marrow homing of human CD34+ progenitor cells, Blood 103(12) (2004) 4478-86.

[95] A.O. Awojoodu, M.E. Ogle, L.S. Sefcik, D.T. Bowers, K. Martin, K.L. Brayman, K.R. Lynch, S.M. Peirce-Cottler, E. Botchwey, Sphingosine 1-phosphate receptor 3 regulates recruitment of anti-inflammatory monocytes to microvessels during implant arteriogenesis, Proc Natl Acad Sci U S A 110(34) (2013) 13785-90.

[96] M.E. Ogle, C.E. Olingy, A.O. Awojoodu, A. Das, R.A. Ortiz, H.Y. Cheung, E.A. Botchwey, Sphingosine-1-Phosphate Receptor-3 Supports Hematopoietic Stem and Progenitor Cell Residence Within the Bone Marrow Niche, Stem Cells 35(4) (2017) 1040-1052.

[97] B. Turk, D. Turk, V. Turk, Lysosomal cysteine proteases: more than scavengers, Biochim Biophys Acta 1477(1-2) (2000) 98-111.

[98] V. Turk, V. Stoka, O. Vasiljeva, M. Renko, T. Sun, B. Turk, D. Turk, Cysteine cathepsins: from structure, function and regulation to new frontiers, Biochim Biophys Acta 1824(1) (2012) 68-88.

[99] M. Fonovic, B. Turk, Cysteine cathepsins and extracellular matrix degradation, Biochim Biophys Acta 1840(8) (2014) 2560-70.

[100] M.E. McGrath, The lysosomal cysteine proteases, Annu Rev Biophys Biomol Struct 28 (1999) 181-204.

[101] M.M. Mohamed, B.F. Sloane, Cysteine cathepsins: multifunctional enzymes in cancer, Nat Rev Cancer 6(10) (2006) 764-75.

[102] X.W. Cheng, G.P. Shi, M. Kuzuya, T. Sasaki, K. Okumura, T. Murohara, Role for cysteine protease cathepsins in heart disease: focus on biology and mechanisms with clinical implication, Circulation 125(12) (2012) 1551-62.

[103] G.K. Sukhova, G.P. Shi, D.I. Simon, H.A. Chapman, P. Libby, Expression of the elastolytic cathepsins S and K in human atheroma and regulation of their production in smooth muscle cells, J Clin Invest 102(3) (1998) 576-83.

[104] W.S. Hou, W. Li, G. Keyszer, E. Weber, R. Levy, M.J. Klein, E.M. Gravallese, S.R. Goldring, D. Bromme, Comparison of cathepsins K and S expression within the rheumatoid and osteoarthritic synovium, Arthritis Rheum 46(3) (2002) 663-74.

[105] Y. Yasuda, J. Kaleta, D. Bromme, The role of cathepsins in osteoporosis and arthritis: rationale for the design of new therapeutics, Adv Drug Deliv Rev 57(7) (2005) 973-93.

[106] D. Bromme, F. Lecaille, Cathepsin K inhibitors for osteoporosis and potential off-target effects, Expert Opin Investig Drugs 18(5) (2009) 585-600.

[107] T. Castro-Gomes, M. Corrotte, C. Tam, N.W. Andrews, Plasma Membrane Repair Is Regulated Extracellularly by Proteases Released from Lysosomes, PLoS One 11(3) (2016) e0152583.

[108] B. Turk, D. Turk, V. Turk, Protease signalling: the cutting edge, EMBO J 31(7) (2012) 1630-43.

[109] G. Dubin, Proteinaceous cysteine protease inhibitors, Cell Mol Life Sci 62(6) (2005) 653-69.

[110] A.A.G. Tantawy, A.A.M. Adly, E.A.R. Ismail, M. Abdelazeem, Clinical Predictive Value of Cystatin C in Pediatric Sickle Cell Disease: A Marker of Disease Severity and Subclinical Cardiovascular Dysfunction, Clin Appl Thromb Hemost 23(8) (2017) 1010-1017.

[111] A. Littlewood-Evans, T. Kokubo, O. Ishibashi, T. Inaoka, B. Wlodarski, J.A. Gallagher, G. Bilbe, Localization of cathepsin K in human osteoclasts by in situ hybridization and immunohistochemistry, Bone 20(2) (1997) 81-6.

[112] T. Yamaza, T. Goto, T. Kamiya, Y. Kobayashi, H. Sakai, T. Tanaka, Study of immunoelectron microscopic localization of cathepsin K in osteoclasts and other bone cells in the mouse femur, Bone 23(6) (1998) 499-509.

[113] P. Garnero, O. Borel, I. Byrjalsen, M. Ferreras, F.H. Drake, M.S. McQueney, N.T. Foged, P.D. Delmas, J.M. Delaisse, The collagenolytic activity of cathepsin K is unique among mammalian proteinases, J Biol Chem 273(48) (1998) 32347-52.

[114] M.F. Young, J.M. Kerr, K. Ibaraki, A.M. Heegaard, P.G. Robey, Structure, expression, and regulation of the major noncollagenous matrix proteins of bone, Clin Orthop Relat Res (281) (1992) 275-94.

[115] B.R. Troen, The regulation of cathepsin K gene expression, Ann N Y Acad Sci 1068 (2006) 165-72.

[116] L. Kramer, D. Turk, B. Turk, The Future of Cysteine Cathepsins in Disease Management, Trends Pharmacol Sci 38(10) (2017) 873-898.

[117] M.T. Drake, B.L. Clarke, M.J. Oursler, S. Khosla, Cathepsin K Inhibitors for Osteoporosis: Biology, Potential Clinical Utility, and Lessons Learned, Endocr Rev 38(4) (2017) 325-350.

[118] C. Jerome, M. Missbach, R. Gamse, Balicatib, a cathepsin K inhibitor, stimulates periosteal bone formation in monkeys, Osteoporos Int 22(12) (2011) 3001-11.

[119] J.P. Falgueyret, S. Desmarais, R. Oballa, W.C. Black, W. Cromlish, K. Khougaz, S. Lamontagne, F. Masse, D. Riendeau, S. Toulmond, M.D. Percival, Lysosomotropism of basic cathepsin K inhibitors contributes to increased cellular potencies against off-target cathepsins and reduced functional selectivity, J Med Chem 48(24) (2005) 7535-43.

[120] P.J. Masarachia, B.L. Pennypacker, M. Pickarski, K.R. Scott, G.A. Wesolowski, S.Y. Smith, R. Samadfam, J.E. Goetzmann, B.B. Scott, D.B. Kimmel, L.T. Duong, Odanacatib reduces bone turnover and increases bone mass in the lumbar spine of skeletally mature ovariectomized rhesus monkeys, J Bone Miner Res 27(3) (2012) 509-23.

[121] H.G. Bone, M.R. McClung, C. Roux, R.R. Recker, J.A. Eisman, N. Verbruggen, C.M. Hustad, C. DaSilva, A.C. Santora, B.A. Ince, Odanacatib, a cathepsin-K inhibitor for osteoporosis: a two-year study in postmenopausal women with low bone density, J Bone Miner Res 25(5) (2010) 937-47.

[122] A. Mullard, Merck &Co. drops osteoporosis drug odanacatib, Nat Rev Drug Discov 15(10) (2016) 669.

[123] B.D. Gelb, G.P. Shi, H.A. Chapman, R.J. Desnick, Pycnodysostosis, a lysosomal disease caused by cathepsin K deficiency, Science 273(5279) (1996) 1236-8.

[124] P.A. Hill, D.J. Buttle, S.J. Jones, A. Boyde, M. Murata, J.J. Reynolds, M.C. Meikle, Inhibition of bone resorption by selective inactivators of cysteine proteinases, J Cell Biochem 56(1) (1994) 118-30.

[125] O. Ishibashi, T. Inui, Y. Mori, T. Kurokawa, T. Kokubo, M. Kumegawa, Quantification of the expression levels of lysosomal cysteine proteinases in purified human osteoclastic cells by competitive RT-PCR, Calcif Tissue Int 68(2) (2001) 109-16.

[126] K.Y. Park, W.A. Li, M.O. Platt, Patient specific proteolytic activity of monocyte-derived macrophages and osteoclasts predicted with temporal kinase activation states during differentiation, Integr Biol (Camb) 4(12) (2012) 1459-69.

[127] V. Everts, W. Korper, K.A. Hoeben, I.D. Jansen, D. Bromme, K.B. Cleutjens, S. Heeneman, C. Peters, T. Reinheckel, P. Saftig, W. Beertsen, Osteoclastic bone degradation and the role of different cysteine proteinases and matrix metalloproteinases: differences between calvaria and long bone, J Bone Miner Res 21(9) (2006) 1399-408.

[128] M.T. Acurio, R.J. Friedman, Hip arthroplasty in patients with sickle-cell haemoglobinopathy, J Bone Joint Surg Br 74(3) (1992) 367-71.

[129] R. Gupta, A.D. Adekile, MRI follow-up and natural history of avascular necrosis of the femoral head in Kuwaiti children with sickle cell disease, J Pediatr Hematol Oncol 26(6) (2004) 351-3.

[130] H.A. Cole, M. Yuasa, G. Hawley, J.M. Cates, J.S. Nyman, J.G. Schoenecker, Differential development of the distal and proximal femoral epiphysis and physis in mice, Bone 52(1) (2013) 337-46.

[131] J. Emons, A.S. Chagin, L. Savendahl, M. Karperien, J.M. Wit, Mechanisms of growth plate maturation and epiphyseal fusion, Horm Res Paediatr 75(6) (2011) 383-91.

[132] P.F. Collett-Solberg, R.E. Ware, S.M. O'Hara, Asymmetrical closure of epiphyses in a patient with sickle cell anemia, J Pediatr Endocrinol Metab 15(8) (2002) 1207-12.

[133] R. Vaishya, A.K. Agarwal, E.O. Edomwonyi, V. Vijay, Musculoskeletal Manifestations of Sickle Cell Disease: A Review, Cureus 7(10) (2015) e358.

[134] L. Xiao, B. Andemariam, P. Taxel, D.J. Adams, W.T. Zempsky, V. Dorcelus, M.M. Hurley, Loss of Bone in Sickle Cell Trait and Sickle Cell Disease Female Mice Is Associated With Reduced IGF-1 in Bone and Serum, Endocrinology 157(8) (2016) 3036-46.

[135] H. Chen, X. Zhou, H. Fujita, M. Onozuka, K.Y. Kubo, Age-related changes in trabecular and cortical bone microstructure, Int J Endocrinol 2013 (2013) 213234.

[136] S.M. Chung, A. Alavi, M.O. Russell, Management of osteonecrosis in sickle-cell anemia and its genetic variants, Clin Orthop Relat Res (130) (1978) 158-74.

[137] L. Dalle Carbonare, A. Matte, M.T. Valenti, A. Siciliano, A. Mori, V. Schweiger, G. Zampieri, L. Perbellini, L. De Franceschi, Hypoxia-reperfusion affects osteogenic lineage and promotes sickle cell bone disease, Blood 126(20) (2015) 2320-8.

[138] J.E. Aaron, N.B. Makins, K. Sagreiya, The microanatomy of trabecular bone loss in normal aging men and women, Clin Orthop Relat Res (215) (1987) 260-71.

[139] I.A. Akinsanmi, A. Lin, R. Guldberg, M. Platt, G. Barabino, Age and Sex Determinants of Bone Phenotype in a Transgenic Mouse Model of Sickle Cell Disease, Blood 120(21) (2012) 3249-3249.

[140] R. Gupta, R. Marouf, A. Adekile, Pattern of bone mineral density in sickle cell disease patients with the high-Hb F phenotype, Acta Haematol 123(1) (2010) 64-70.

[141] A. Lal, E.B. Fung, Z. Pakbaz, E. Hackney-Stephens, E.P. Vichinsky, Bone mineral density in children with sickle cell anemia, Pediatr Blood Cancer 47(7) (2006) 901-6.

[142] M. Sarrai, H. Duroseau, J. D'Augustine, S. Moktan, R. Bellevue, Bone mass density in adults with sickle cell disease, Br J Haematol 136(4) (2007) 666-72.

[143] T.M. Ryan, D.J. Ciavatta, T.M. Townes, Knockout-transgenic mouse model of sickle cell disease, Science 278(5339) (1997) 873-6.

[144] G. Robertson, C. Xie, D. Chen, H. Awad, E.M. Schwarz, R.J. O'Keefe, R.E. Guldberg, X. Zhang, Alteration of femoral bone morphology and density in COX-2-/- mice, Bone 39(4) (2006) 767-72.

[145] H.R. Buie, G.M. Campbell, R.J. Klinck, J.A. MacNeil, S.K. Boyd, Automatic segmentation of cortical and trabecular compartments based on a dual threshold technique for in vivo micro-CT bone analysis, Bone 41(4) (2007) 505-15.

[146] T. Hildebrand, P. Ruegsegger, Quantification of Bone Microarchitecture with the Structure Model Index, Comput Methods Biomech Biomed Engin 1(1) (1997) 15-23.

[147] N. Bonnet, C.L. Benhamou, B. Brunet-Imbault, A. Arlettaz, M.N. Horcajada, O. Richard, L. Vico, K. Collomp, D. Courteix, Severe bone alterations under beta2 agonist treatments: bone mass, microarchitecture and strength analyses in female rats, Bone 37(5) (2005) 622-33.

[148] M.L. Bouxsein, S.K. Boyd, B.A. Christiansen, R.E. Guldberg, K.J. Jepsen, R. Muller, Guidelines for assessment of bone microstructure in rodents using micro-computed tomography, J Bone Miner Res 25(7) (2010) 1468-86.

[149] Naseer, A. Parmar, S. Mudaliar, N. Shah, M. Desai, A. Swami, B. Agrawal, Multiple pathological fractures as presentation in a 18 month old child of sickle cell disease, 2016.

[150] C.D. Flory, Sex Differences in Skeletal Development, Child Development 6(3) (1935) 205-212.

[151] O. Nilsson, J. Baron, Fundamental limits on longitudinal bone growth: growth plate senescence and epiphyseal fusion, Trends Endocrinol Metab 15(8) (2004) 370-4.

[152] M. Ding, A. Odgaard, I. Hvid, Accuracy of cancellous bone volume fraction measured by micro-CT scanning, J Biomech 32(3) (1999) 323-6.

[153] C.E. Farnum, N.J. Wilsman, Cellular turnover at the chondro-osseous junction of growth plate cartilage: analysis by serial sections at the light microscopical level, J Orthop Res 7(5) (1989) 654-66.

[154] H.P. Gerber, T.H. Vu, A.M. Ryan, J. Kowalski, Z. Werb, N. Ferrara, VEGF couples hypertrophic cartilage remodeling, ossification and angiogenesis during endochondral bone formation, Nat Med 5(6) (1999) 623-8.

[155] O.O. IIesanmi, Gender Differences in Sickle Cell Crises: Implications for Geneic Counseling and Psychotherapy, Journal of Pyschology & Psychotherapy 3(4) (2013) 1-12.

[156] J. Emons, A.S. Chagin, T. Malmlof, M. Lekman, A. Tivesten, C. Ohlsson, J.M. Wit, M. Karperien, L. Savendahl, Expression of vascular endothelial growth factor in the growth plate is stimulated by estradiol and increases during pubertal development, J Endocrinol 205(1) (2010) 61-8.

[157] M.M. Donohue, M.B. Demay, Rickets in VDR null mice is secondary to decreased apoptosis of hypertrophic chondrocytes, Endocrinology 143(9) (2002) 3691-4.

[158] Z. Schwartz, H. Ehland, V.L. Sylvia, D. Larsson, R.R. Hardin, V. Bingham, D. Lopez, D.D. Dean, B.D. Boyan, 1alpha,25-dihydroxyvitamin D(3) and 24R,25-dihydroxyvitamin D(3) modulate growth plate chondrocyte physiology via protein kinase C-dependent phosphorylation of extracellular signal-regulated kinase 1/2 mitogen-activated protein kinase, Endocrinology 143(7) (2002) 2775-86.

[159] J.B. Arlet, M. Courbebaisse, G. Chatellier, D. Eladari, J.C. Souberbielle, G. Friedlander, M. de Montalembert, D. Prie, J. Pouchot, J.A. Ribeil, Relationship between vitamin D deficiency and bone fragility in sickle cell disease: a cohort study of 56 adults, Bone 52(1) (2013) 206-11.

[160] E. Araldi, E. Schipani, Hypoxia, HIFs and bone development, Bone 47(2) (2010) 190-6.

[161] S.S. Babhulkar, K. Pande, S. Babhulkar, The hand-foot syndrome in sickle-cell haemoglobinopathy, J Bone Joint Surg Br 77(2) (1995) 310-2.

[162] U.T. Iwaniec, R.T. Turner, Influence of body weight on bone mass, architecture and turnover, J Endocrinol 230(3) (2016) R115-30.

[163] R.P. Heaney, S. Abrams, B. Dawson-Hughes, A. Looker, R. Marcus, V. Matkovic, C. Weaver, Peak bone mass, Osteoporos Int 11(12) (2000) 985-1009.

[164] A. Syahrom, M. Al-Fatihhi bin Mohd Szali Januddi, M.N. Harun, A. Öchsner, Cancellous Bone, in: A. Syahrom, M. Al-Fatihhi bin Mohd Szali Januddi, M.N. Harun, A. Öchsner (Eds.), Cancellous Bone: Mechanical Characterization and Finite Element Simulation, Springer Singapore, Singapore, 2018, pp. 7-20.

[165] R.G. Miller, J.B. Segal, B.H. Ashar, S. Leung, S. Ahmed, S. Siddique, T. Rice, S. Lanzkron, High prevalence and correlates of low bone mineral density in young adults with sickle cell disease, Am J Hematol 81(4) (2006) 236-41.

[166] M. Green, I. Akinsami, A. Lin, S. Banton, S. Ghosh, B. Chen, M. Platt, I. Osunkwo, S. Ofori-Acquah, R. Guldberg, G. Barabino, Microarchitectural and mechanical characterization of the sickle bone, J Mech Behav Biomed Mater 48 (2015) 220-228.

[167] P.L. Salmon, C. Ohlsson, S.J. Shefelbine, M. Doube, Structure Model Index Does Not Measure Rods and Plates in Trabecular Bone, Front Endocrinol (Lausanne) 6 (2015) 162.

[168] Y.N. Yeni, M.J. Zinno, J.S. Yerramshetty, R. Zauel, D.P. Fyhrie, Variability of trabecular microstructure is age-, gender-, race- and anatomic site-dependent and affects stiffness and stress distribution properties of human vertebral cancellous bone, Bone 49(4) (2011) 886-94.

[169] D.H. Birkenhager-Frenkel, P. Courpron, E.A. Hupscher, E. Clermonts, M.F. Coutinho, P.I. Schmitz, P.J. Meunier, Age-related changes in cancellous bone structure. A two-dimensional study in the transiliac and iliac crest biopsy sites, Bone Miner 4(2) (1988) 197-216.

[170] D. Ulrich, T. Hildebrand, B. Van Rietbergen, R. Muller, P. Ruegsegger, The quality of trabecular bone evaluated with micro-computed tomography, FEA and mechanical testing, Stud Health Technol Inform 40 (1997) 97-112.

[171] J. Galante, W. Rostoker, R.D. Ray, Physical properties of trabecular bone, Calcif Tissue Res 5(3) (1970) 236-46.

[172] J.H. Cole, M.C.H. van der Meulen, Biomechanics of Bone, in: R.A. Adler (Ed.), Osteoporosis: Pathophysiology and Clinical Management, Humana Press, Totowa, NJ, 2010, pp. 157-179.

[173] B.M. Mulvihill, P.J. Prendergast, Mechanobiological regulation of the remodelling cycle in trabecular bone and possible biomechanical pathways for osteoporosis, Clin Biomech (Bristol, Avon) 25(5) (2010) 491-8.

[174] M. Ding, A. Odgaard, C.C. Danielsen, I. Hvid, Mutual associations among microstructural, physical and mechanical properties of human cancellous bone, J Bone Joint Surg Br 84(6) (2002) 900-7.

[175] E. Mittra, C. Rubin, Y.X. Qin, Interrelationship of trabecular mechanical and microstructural properties in sheep trabecular bone, J Biomech 38(6) (2005) 1229-37.
[176] J. Kabel, A. Odgaard, B. van Rietbergen, R. Huiskes, Connectivity and the elastic properties of cancellous bone, Bone 24(2) (1999) 115-20.

[177] L. Mosekilde, L. Mosekilde, C.C. Danielsen, Biomechanical competence of vertebral trabecular bone in relation to ash density and age in normal individuals, Bone 8(2) (1987) 79-85.

[178] J.H. Kinney, A.J. Ladd, The relationship between three-dimensional connectivity and the elastic properties of trabecular bone, J Bone Miner Res 13(5) (1998) 839-45.

[179] R.W. Goulet, S.A. Goldstein, M.J. Ciarelli, J.L. Kuhn, M.B. Brown, L.A. Feldkamp, The relationship between the structural and orthogonal compressive properties of trabecular bone, J Biomech 27(4) (1994) 375-89.

[180] G.J. Kato, F.B. Piel, C.D. Reid, M.H. Gaston, K. Ohene-Frempong, L. Krishnamurti, W.R. Smith, J.A. Panepinto, D.J. Weatherall, F.F. Costa, E.P. Vichinsky, Sickle cell disease, Nat Rev Dis Primers 4 (2018) 18010.

[181] C. Sato, T. Iwasaki, S. Kitano, S. Tsunemi, H. Sano, Sphingosine 1-phosphate receptor activation enhances BMP-2-induced osteoblast differentiation, Biochem Biophys Res Commun 423(1) (2012) 200-5.

[182] J.R. Claybaugh, A.K. Sato, L.K. Crosswhite, L.H. Hassell, Effects of time of day, gender, and menstrual cycle phase on the human response to a water load, Am J Physiol Regul Integr Comp Physiol 279(3) (2000) R966-73.

[183] S. Dinkla, K. Wessels, W.P. Verdurmen, C. Tomelleri, J.C. Cluitmans, J. Fransen, B. Fuchs, J. Schiller, I. Joosten, R. Brock, G.J. Bosman, Functional consequences of sphingomyelinase-induced changes in erythrocyte membrane structure, Cell Death Dis 3 (2012) e410.

[184] D.S. Amarasekara, H. Yun, S. Kim, N. Lee, H. Kim, J. Rho, Regulation of Osteoclast Differentiation by Cytokine Networks, Immune Netw 18(1) (2018) e8.

[185] C. Paszty, C.M. Brion, E. Manci, H.E. Witkowska, M.E. Stevens, N. Mohandas, E.M. Rubin, Transgenic knockout mice with exclusively human sickle hemoglobin and sickle cell disease, Science 278(5339) (1997) 876-8.

[186] D.G. Phinney, Isolation of mesenchymal stem cells from murine bone marrow by immunodepletion, Methods Mol Biol 449 (2008) 171-86.

[187] M.C. Sullards, Y. Liu, Y. Chen, A.H. Merrill, Jr., Analysis of mammalian sphingolipids by liquid chromatography tandem mass spectrometry (LC-MS/MS) and tissue imaging mass spectrometry (TIMS), Biochim Biophys Acta 1811(11) (2011) 838-53.

[188] C. Jacquin, D.E. Gran, S.K. Lee, J.A. Lorenzo, H.L. Aguila, Identification of multiple osteoclast precursor populations in murine bone marrow, J Bone Miner Res 21(1) (2006) 67-77.

[189] C.L. Wilder, K.Y. Park, P.M. Keegan, M.O. Platt, Manipulating substrate and pH in zymography protocols selectively distinguishes cathepsins K, L, S, and V activity in cells and tissues, Arch Biochem Biophys 516(1) (2011) 52-7.

[190] K. Kupai, G. Szucs, S. Cseh, I. Hajdu, C. Csonka, T. Csont, P. Ferdinandy, Matrix metalloproteinase activity assays: Importance of zymography, J Pharmacol Toxicol Methods 61(2) (2010) 205-9.

[191] S. Agarwal, L. Zhao, R. Zhang, L. Hassell, FaceTime validation study: Low-cost streaming video for cytology adequacy assessment, Cancer Cytopathol 124(3) (2016) 213-20.

[192] K. Sun, A. D'Alessandro, M.H. Ahmed, Y. Zhang, A. Song, T.P. Ko, T. Nemkov, J.A. Reisz, H. Wu, M. Adebiyi, Z. Peng, J. Gong, H. Liu, A. Huang, Y.E. Wen, A.Q.

Wen, V. Berka, M.V. Bogdanov, O. Abdulmalik, L. Han, A.L. Tsai, M. Idowu, H.S. Juneja, R.E. Kellems, W. Dowhan, K.C. Hansen, M.K. Safo, Y. Xia, Structural and Functional Insight of Sphingosine 1-Phosphate-Mediated Pathogenic Metabolic Reprogramming in Sickle Cell Disease, Sci Rep 7(1) (2017) 15281.

[193] R.S. Taichman, Blood and bone: two tissues whose fates are intertwined to create the hematopoietic stem-cell niche, Blood 105(7) (2005) 2631-9.

[194] I. Pradas, K. Huynh, R. Cabre, V. Ayala, P.J. Meikle, M. Jove, R. Pamplona, Lipidomics Reveals a Tissue-Specific Fingerprint, Front Physiol 9 (2018) 1165.

[195] B. Rocha, B. Cillero-Pastor, G. Eijkel, A.L. Bruinen, C. Ruiz-Romero, R.M. Heeren, F.J. Blanco, Characterization of lipidic markers of chondrogenic differentiation using mass spectrometry imaging, Proteomics 15(4) (2015) 702-13.

[196] S. Fukumoto, T. Iwamoto, E. Sakai, K. Yuasa, E. Fukumoto, A. Yamada, T. Hasegawa, K. Nonaka, Y. Kato, Current topics in pharmacological research on bone metabolism: osteoclast differentiation regulated by glycosphingolipids, J Pharmacol Sci 100(3) (2006) 195-200.

[197] T. Iwamoto, S. Fukumoto, K. Kanaoka, E. Sakai, M. Shibata, E. Fukumoto, J. Inokuchi Ji, K. Takamiya, K. Furukawa, K. Furukawa, Y. Kato, A. Mizuno, Lactosylceramide is essential for the osteoclastogenesis mediated by macrophage-colony-stimulating factor and receptor activator of nuclear factor-kappa B ligand, J Biol Chem 276(49) (2001) 46031-8.

[198] S. Olivier, M. Fillet, M. Malaise, J. Piette, V. Bours, M.P. Merville, N. Franchimont, Sodium nitroprusside-induced osteoblast apoptosis is mediated by long chain ceramide and is decreased by raloxifene, Biochem Pharmacol 69(6) (2005) 891-901.

[199] P.A. Hill, A. Tumber, Ceramide-induced cell death/survival in murine osteoblasts, J Endocrinol 206(2) (2010) 225-33.

[200] Y. Osawa, H. Uchinami, J. Bielawski, R.F. Schwabe, Y.A. Hannun, D.A. Brenner, Roles for C16-ceramide and sphingosine 1-phosphate in regulating hepatocyte apoptosis in response to tumor necrosis factor-alpha, J Biol Chem 280(30) (2005) 27879-87.

[201] G. Seumois, M. Fillet, L. Gillet, C. Faccinetto, C. Desmet, C. Francois, B. Dewals, C. Oury, A. Vanderplasschen, P. Lekeux, F. Bureau, De novo C16- and C24-ceramide generation contributes to spontaneous neutrophil apoptosis, J Leukoc Biol 81(6) (2007) 1477-86.

[202] R. Hardy, M.S. Cooper, Bone loss in inflammatory disorders, J Endocrinol 201(3) (2009) 309-20.

[203] M.H. Qari, U. Dier, S.A. Mousa, Biomarkers of inflammation, growth factor, and coagulation activation in patients with sickle cell disease, Clin Appl Thromb Hemost 18(2) (2012) 195-200.

[204] R. Axmann, C. Bohm, G. Kronke, J. Zwerina, J. Smolen, G. Schett, Inhibition of interleukin-6 receptor directly blocks osteoclast formation in vitro and in vivo, Arthritis Rheum 60(9) (2009) 2747-56.

[205] F. Blanchard, L. Duplomb, M. Baud'huin, B. Brounais, The dual role of IL-6-type cytokines on bone remodeling and bone tumors, Cytokine Growth Factor Rev 20(1) (2009) 19-28.

[206] Y.H. Zhang, A. Heulsmann, M.M. Tondravi, A. Mukherjee, Y. Abu-Amer, Tumor necrosis factor-alpha (TNF) stimulates RANKL-induced osteoclastogenesis via coupling of TNF type 1 receptor and RANK signaling pathways, J Biol Chem 276(1) (2001) 563-8.

[207] Y. Azuma, K. Kaji, R. Katogi, S. Takeshita, A. Kudo, Tumor necrosis factor-alpha induces differentiation of and bone resorption by osteoclasts, J Biol Chem 275(7) (2000) 4858-64.

[208] M. Nouraie, K. Cheng, X. Niu, E. Moore-King, M.F. Fadojutimi-Akinsi, C.P. Minniti, C. Sable, S. Rana, N. Dham, A. Campbell, G. Ensing, G.J. Kato, M.T. Gladwin, O.L. Castro, V.R. Gordeuk, Predictors of osteoclast activity in patients with sickle cell disease, Haematologica 96(8) (2011) 1092-8.

[209] M. Komine, A. Kukita, T. Kukita, Y. Ogata, T. Hotokebuchi, O. Kohashi, Tumor necrosis factor-alpha cooperates with receptor activator of nuclear factor kappaB ligand in generation of osteoclasts in stromal cell-depleted rat bone marrow cell culture, Bone 28(5) (2001) 474-83.

[210] M. Asagiri, H. Takayanagi, The molecular understanding of osteoclast differentiation, Bone 40(2) (2007) 251-64.

[211] M. Rauner, U. Foger-Samwald, M.F. Kurz, C. Brunner-Kubath, D. Schamall, A. Kapfenberger, P. Varga, S. Kudlacek, A. Wutzl, H. Hoger, P.K. Zysset, G.P. Shi, L.C. Hofbauer, W. Sipos, P. Pietschmann, Cathepsin S controls adipocytic and osteoblastic differentiation, bone turnover, and bone microarchitecture, Bone 64 (2014) 281-7.

[212] M. Soderstrom, H. Salminen, V. Glumoff, H. Kirschke, H. Aro, E. Vuorio, Cathepsin expression during skeletal development, Biochim Biophys Acta 1446(1-2) (1999) 35-46.

[213] H.C. Blair, L. Ghandur-Mnaymneh, Macrophage-mediated bone resorption occurs in an acidic environment, Calcif Tissue Int 37(5) (1985) 547-50.

[214] Y. Fujikawa, A. Sabokbar, S. Neale, N.A. Athanasou, Human osteoclast formation and bone resorption by monocytes and synovial macrophages in rheumatoid arthritis, Ann Rheum Dis 55(11) (1996) 816-22.

[215] M. Durand, S.V. Komarova, A. Bhargava, D.P. Trebec-Reynolds, K. Li, C. Fiorino, O. Maria, N. Nabavi, M.F. Manolson, R.E. Harrison, S.J. Dixon, S.M. Sims, M.J. Mizianty, L. Kurgan, S. Haroun, G. Boire, M. de Fatima Lucena-Fernandes, A.J. de Brum-Fernandes, Monocytes from patients with osteoarthritis display increased osteoclastogenesis and bone resorption: the In Vitro Osteoclast Differentiation in Arthritis study, Arthritis Rheum 65(1) (2013) 148-58.

[216] G.M. Mokhtar, A.A. Tantawy, A.A. Hamed, A.A. Adly, E.A. Ismail, S.M. Makkeyah, Tartrate-Resistant Acid Phosphatase 5b in Young Patients With Sickle Cell Disease and Trait Siblings: Relation to Vasculopathy and Bone Mineral Density, Clin Appl Thromb Hemost 23(1) (2017) 64-71.

[217] A.G. Costa, N.E. Cusano, B.C. Silva, S. Cremers, J.P. Bilezikian, Cathepsin K: its skeletal actions and role as a therapeutic target in osteoporosis, Nat Rev Rheumatol 7(8) (2011) 447-56.

[218] M. Gowen, F. Lazner, R. Dodds, R. Kapadia, J. Feild, M. Tavaria, I. Bertoncello, F. Drake, S. Zavarselk, I. Tellis, P. Hertzog, C. Debouck, I. Kola, Cathepsin K knockout mice develop osteopetrosis due to a deficit in matrix degradation but not demineralization, J Bone Miner Res 14(10) (1999) 1654-63.

[219] R. Kiviranta, J. Morko, S.L. Alatalo, R. NicAmhlaoibh, J. Risteli, T. Laitala-Leinonen, E. Vuorio, Impaired bone resorption in cathepsin K-deficient mice is partially compensated for by enhanced osteoclastogenesis and increased expression of other proteases via an increased RANKL/OPG ratio, Bone 36(1) (2005) 159-72.

[220] C.Y. Li, K.J. Jepsen, R.J. Majeska, J. Zhang, R. Ni, B.D. Gelb, M.B. Schaffler, Mice lacking cathepsin K maintain bone remodeling but develop bone fragility despite high bone mass, J Bone Miner Res 21(6) (2006) 865-75.

[221] J. Mandelin, M. Hukkanen, T.F. Li, M. Korhonen, M. Liljestrom, T. Sillat, R. Hanemaaijer, J. Salo, S. Santavirta, Y.T. Konttinen, Human osteoblasts produce cathepsin K, Bone 38(6) (2006) 769-77.

[222] T. Goto, T. Yamaza, T. Tanaka, Cathepsins in the osteoclast, J Electron Microsc (Tokyo) 52(6) (2003) 551-8.

[223] K.M. Porter, F.A. Wieser, C.L. Wilder, N. Sidell, M.O. Platt, Cathepsin Protease Inhibition Reduces Endometriosis Lesion Establishment, Reprod Sci 23(5) (2016) 623-9.

[224] T. Kitaori, H. Ito, E.M. Schwarz, R. Tsutsumi, H. Yoshitomi, S. Oishi, M. Nakano, N. Fujii, T. Nagasawa, T. Nakamura, Stromal cell-derived factor 1/CXCR4 signaling is

critical for the recruitment of mesenchymal stem cells to the fracture site during skeletal repair in a mouse model, Arthritis Rheum 60(3) (2009) 813-23.

[225] D. Shirley, D. Marsh, G. Jordan, S. McQuaid, G. Li, Systemic recruitment of osteoblastic cells in fracture healing, J Orthop Res 23(5) (2005) 1013-21.

[226] M. Mathieu, S. Rigutto, A. Ingels, D. Spruyt, N. Stricwant, I. Kharroubi, V. Albarani, M. Jayankura, J. Rasschaert, E. Bastianelli, V. Gangji, Decreased pool of mesenchymal stem cells is associated with altered chemokines serum levels in atrophic nonunion fractures, Bone 53(2) (2013) 391-8.

[227] E.J. Hannoush, I. Elhassan, Z.C. Sifri, A.A. Mohr, W.D. Alzate, D.H. Livingston, Role of bone marrow and mesenchymal stem cells in healing after traumatic injury, Surgery 153(1) (2013) 44-51.

[228] T. Taketani, C. Oyama, A. Mihara, Y. Tanabe, M. Abe, T. Hirade, S. Yamamoto, R. Bo, R. Kanai, T. Tadenuma, Y. Michibata, S. Yamamoto, M. Hattori, Y. Katsube, H. Ohnishi, M. Sasao, Y. Oda, K. Hattori, S. Yuba, H. Ohgushi, S. Yamaguchi, Ex Vivo Expanded Allogeneic Mesenchymal Stem Cells With Bone Marrow Transplantation Improved Osteogenesis in Infants With Severe Hypophosphatasia, Cell Transplant 24(10) (2015) 1931-43.

[229] R. Hou, F. Chen, Y. Yang, X. Cheng, Z. Gao, H.O. Yang, W. Wu, T. Mao, Comparative study between coral-mesenchymal stem cells-rhBMP-2 composite and auto-bone-graft in rabbit critical-sized cranial defect model, J Biomed Mater Res A 80(1) (2007) 85-93.

[230] R. Hou, T. Mao, Y. Yang, Z. Gao, X. Cheng, S. Chen, F. Chen, [Experimental study on repair of critical-sized cranial defect by tissue engineered bone], Zhongguo Xiu Fu Chong Jian Wai Ke Za Zhi 19(10) (2005) 818-21.

[231] S.J. Stephan, S.S. Tholpady, B. Gross, C.E. Petrie-Aronin, E.A. Botchway, L.S. Nair, R.C. Ogle, S.S. Park, Injectable tissue-engineered bone repair of a rat calvarial defect, Laryngoscope 120(5) (2010) 895-901.

[232] O.H. Lee, Y.M. Kim, Y.M. Lee, E.J. Moon, D.J. Lee, J.H. Kim, K.W. Kim, Y.G. Kwon, Sphingosine 1-phosphate induces angiogenesis: its angiogenic action and signaling mechanism in human umbilical vein endothelial cells, Biochem Biophys Res Commun 264(3) (1999) 743-50.

[233] M.J. Lee, S. Thangada, J.H. Paik, G.P. Sapkota, N. Ancellin, S.S. Chae, M. Wu, M. Morales-Ruiz, W.C. Sessa, D.R. Alessi, T. Hla, Akt-mediated phosphorylation of the G protein-coupled receptor EDG-1 is required for endothelial cell chemotaxis, Mol Cell 8(3) (2001) 693-704.

[234] L.S. Sefcik, C.E. Aronin, A.O. Awojoodu, S.J. Shin, F. Mac Gabhann, T.L. MacDonald, B.R. Wamhoff, K.R. Lynch, S.M. Peirce, E.A. Botchwey, Selective activation of sphingosine 1-phosphate receptors 1 and 3 promotes local microvascular network growth, Tissue Eng Part A 17(5-6) (2011) 617-29.

[235] A. Das, C.E. Segar, B.B. Hughley, D.T. Bowers, E.A. Botchwey, The promotion of mandibular defect healing by the targeting of S1P receptors and the recruitment of alternatively activated macrophages, Biomaterials 34(38) (2013) 9853-62.

[236] C. Hu, X. Yong, C. Li, M. Lu, D. Liu, L. Chen, J. Hu, M. Teng, D. Zhang, Y. Fan, G. Liang, CXCL12/CXCR4 axis promotes mesenchymal stem cell mobilization to burn wounds and contributes to wound repair, J Surg Res 183(1) (2013) 427-34.

[237] R. Zhu, A.H. Snyder, Y. Kharel, L. Schaffter, Q. Sun, P.C. Kennedy, K.R. Lynch, T.L. Macdonald, Asymmetric synthesis of conformationally constrained fingolimod analogues--discovery of an orally active sphingosine 1-phosphate receptor type-1 agonist and receptor type-3 antagonist, J Med Chem 50(25) (2007) 6428-35.

[238] M.A. Scott, B. Levi, A. Askarinam, A. Nguyen, T. Rackohn, K. Ting, C. Soo, A.W. James, Brief review of models of ectopic bone formation, Stem Cells Dev 21(5) (2012) 655-67.

[239] A. Das, S. Tanner, D.A. Barker, D. Green, E.A. Botchwey, Delivery of S1P receptor-targeted drugs via biodegradable polymer scaffolds enhances bone regeneration in a critical size cranial defect, J Biomed Mater Res A 102(4) (2014) 1210-8.

[240] C. Huang, A. Das, D. Barker, S. Tholpady, T. Wang, Q. Cui, R. Ogle, E. Botchwey, Local delivery of FTY720 accelerates cranial allograft incorporation and bone formation, Cell Tissue Res 347(3) (2012) 553-66.

[241] L.J. Mortensen, C. Alt, R. Turcotte, M. Masek, T.M. Liu, D.C. Cote, C. Xu, G. Intini, C.P. Lin, Femtosecond laser bone ablation with a high repetition rate fiber laser source, Biomed Opt Express 6(1) (2015) 32-42.

[242] K.F. Tehrani, P. Kner, L.J. Mortensen, Characterization of wavefront errors in mouse cranial bone using second-harmonic generation, J Biomed Opt 22(3) (2017) 36012.

[243] K.F. Tehrani, P. Kner, L.J. Mortensen, Modeling of optical aberrations caused by light propagation in mouse cranial bone using second harmonic generation imaging SPIE BiOS, San Fransciso, California 2017.

[244] T.A. Pologruto, B.L. Sabatini, K. Svoboda, ScanImage: flexible software for operating laser scanning microscopes, Biomed Eng Online 2 (2003) 13.

[245] C. Holmes, W.L. Stanford, Concise review: stem cell antigen-1: expression, function, and enigma, Stem cells 25(6) (2007) 1339-47.

[246] P.V. Giannoudis, H. Dinopoulos, E. Tsiridis, Bone substitutes: an update, Injury 36 Suppl 3 (2005) S20-7.

[247] C. Petrie, S. Tholpady, R. Ogle, E. Botchwey, Proliferative capacity and osteogenic potential of novel dura mater stem cells on poly-lactic-co-glycolic acid, J Biomed Mater Res A 85(1) (2008) 61-71.

[248] Q. Cui, E.A. Botchwey, Emerging ideas: treatment of precollapse osteonecrosis using stem cells and growth factors, Clin Orthop Relat Res 469(9) (2011) 2665-9.

[249] A.R. Amini, C.T. Laurencin, S.P. Nukavarapu, Bone tissue engineering: recent advances and challenges, Crit Rev Biomed Eng 40(5) (2012) 363-408.

[250] J. Liao, X. Chen, Y. Li, Z. Ge, H. Duan, Y. Zou, J. Ge, Transfer of bone-marrow-derived mesenchymal stem cells influences vascular remodeling and calcification after balloon injury in hyperlipidemic rats, J Biomed Biotechnol 2012 (2012) 165296.

[251] M.W. Klinker, R.A. Marklein, J.L. Lo Surdo, C.H. Wei, S.R. Bauer, Morphological features of IFN-gamma-stimulated mesenchymal stromal cells predict overall immunosuppressive capacity, Proc Natl Acad Sci U S A 114(13) (2017) E2598-E2607.

[252] R.A. Marklein, J.L. Lo Surdo, I.H. Bellayr, S.A. Godil, R.K. Puri, S.R. Bauer, High Content Imaging of Early Morphological Signatures Predicts Long Term Mineralization Capacity of Human Mesenchymal Stem Cells upon Osteogenic Induction, Stem Cells 34(4) (2016) 935-47.

[253] M.J. Hoogduijn, M.M. Verstegen, A.U. Engela, S.S. Korevaar, M. Roemeling-van Rhijn, A. Merino, M. Franquesa, J. de Jonge, J.N. Ijzermans, W. Weimar, M.G. Betjes, C.C. Baan, L.J. van der Laan, No evidence for circulating mesenchymal stem cells in patients with organ injury, Stem Cells Dev 23(19) (2014) 2328-35.

[254] I. Kassis, L. Zangi, R. Rivkin, L. Levdansky, S. Samuel, G. Marx, R. Gorodetsky, Isolation of mesenchymal stem cells from G-CSF-mobilized human peripheral blood using fibrin microbeads, Bone Marrow Transplant 37(10) (2006) 967-76.

[255] G. Wu, M. Pan, X. Wang, J. Wen, S. Cao, Z. Li, Y. Li, C. Qian, Z. Liu, W. Wu, L. Zhu, J. Guo, Osteogenesis of peripheral blood mesenchymal stem cells in self assembling peptide nanofiber for healing critical size calvarial bony defect, Sci Rep 5 (2015) 16681.

[256] J.A. Phillips, L.J. Mortensen, J.P. Ruiz, R. Sridharan, S. Kumar, M. Torres, P. Sharma, C.P. Lin, J.M. Karp, P.V. Hauschka, Advances in Single-cell Tracking of Mesenchymal Stem Cells (MSCs) During Musculoskeletal Regeneration, Orthop J Harv Med Sch 14 (2012) 22-28.

[257] J.G. Juarez, N. Harun, M. Thien, R. Welschinger, R. Baraz, A.D. Pena, S.M. Pitson, M. Rettig, J.F. DiPersio, K.F. Bradstock, L.J. Bendall, Sphingosine-1-phosphate facilitates trafficking of hematopoietic stem cells and their mobilization by CXCR4 antagonists in mice, Blood 119(3) (2012) 707-16.

[258] L.S. Sefcik, C.E. Petrie Aronin, K.A. Wieghaus, E.A. Botchwey, Sustained release of sphingosine 1-phosphate for therapeutic arteriogenesis and bone tissue engineering, Biomaterials 29(19) (2008) 2869-77.

[259] C.E. Petrie Aronin, L.S. Sefcik, S.S. Tholpady, A. Tholpady, K.W. Sadik, T.L. Macdonald, S.M. Peirce, B.R. Wamhoff, K.R. Lynch, R.C. Ogle, E.A. Botchwey, FTY720 promotes local microvascular network formation and regeneration of cranial bone defects, Tissue Eng Part A 16(6) (2010) 1801-9.

[260] A. Das, C.E. Segar, Y. Chu, T.W. Wang, Y. Lin, C. Yang, X. Du, R.C. Ogle, Q. Cui, E.A. Botchwey, Bioactive lipid coating of bone allografts directs engraftment and fate determination of bone marrow-derived cells in rat GFP chimeras, Biomaterials 64 (2015) 98-107.

[261] J.P. Levesque, I.G. Winkler, S.R. Larsen, J.E. Rasko, Mobilization of bone marrow-derived progenitors, Handb Exp Pharmacol (180) (2007) 3-36.

[262] C.A. Toupadakis, J.L. Granick, M. Sagy, A. Wong, E. Ghassemi, D.J. Chung, D.L. Borjesson, C.E. Yellowley, Mobilization of endogenous stem cell populations enhances fracture healing in a murine femoral fracture model, Cytotherapy 15(9) (2013) 1136-47.

[263] M. Tadokoro, R. Kanai, T. Taketani, Y. Uchio, S. Yamaguchi, H. Ohgushi, New bone formation by allogeneic mesenchymal stem cell transplantation in a patient with perinatal hypophosphatasia, J Pediatr 154(6) (2009) 924-30.

[264] E.M. Horwitz, D.J. Prockop, L.A. Fitzpatrick, W.W. Koo, P.L. Gordon, M. Neel, M. Sussman, P. Orchard, J.C. Marx, R.E. Pyeritz, M.K. Brenner, Transplantability and therapeutic effects of bone marrow-derived mesenchymal cells in children with osteogenesis imperfecta, Nat Med 5(3) (1999) 309-13.

[265] J. Galipeau, The mesenchymal stromal cells dilemma--does a negative phase III trial of random donor mesenchymal stromal cells in steroid-resistant graft-versus-host disease represent a death knell or a bump in the road?, Cytotherapy 15(1) (2013) 2-8.

[266] R.F. Pereira, M.D. O'Hara, A.V. Laptev, K.W. Halford, M.D. Pollard, R. Class, D. Simon, K. Livezey, D.J. Prockop, Marrow stromal cells as a source of progenitor cells for nonhematopoietic tissues in transgenic mice with a phenotype of osteogenesis imperfecta, Proc Natl Acad Sci U S A 95(3) (1998) 1142-7.

[267] A. Ateschrang, B.G. Ochs, M. Ludemann, K. Weise, D. Albrecht, Fibula and tibia fusion with cancellous allograft vitalised with autologous bone marrow: first results for infected tibial non-union, Arch Orthop Trauma Surg 129(1) (2009) 97-104.

[268] Z. Kong, D. Tian, H. Yu, W. Feng, C. Liu, [Treatment of traumatic bone defect with graft material of allogenic cancellous combined with autologous red marrow], Zhongguo Xiu Fu Chong Jian Wai Ke Za Zhi 22(10) (2008) 1251-4.

[269] I. Fernandez-Bances, M. Perez-Basterrechea, S. Perez-Lopez, D. Nunez Batalla, M.A. Fernandez Rodriguez, M. Alvarez-Viejo, A. Ferrero-Gutierrez, Y. Menendez-Menendez, J.M. Garcia-Gala, D. Escudero, J. Paz Aparicio, S. Carnero Lopez, P. Lopez Fernandez, D. Gonzalez Suarez, J. Otero Hernandez, Repair of long-bone pseudoarthrosis with autologous bone marrow mononuclear cells combined with allogenic bone graft, Cytotherapy 15(5) (2013) 571-7.

[270] M.M. Rosenkilde, L.O. Gerlach, J.S. Jakobsen, R.T. Skerlj, G.J. Bridger, T.W. Schwartz, Molecular mechanism of AMD3100 antagonism in the CXCR4 receptor: transfer of binding site to the CXCR3 receptor, J Biol Chem 279(4) (2004) 3033-41.

[271] G.C. Daltro, V. Fortuna, E.S. de Souza, M.M. Salles, A.C. Carreira, R. Meyer, S.M. Freire, R. Borojevic, Efficacy of autologous stem cell-based therapy for osteonecrosis of the femoral head in sickle cell disease: a five-year follow-up study, Stem Cell Res Ther 6 (2015) 110.

[272] F. Matsuoka, I. Takeuchi, H. Agata, H. Kagami, H. Shiono, Y. Kiyota, H. Honda, R. Kato, Morphology-based prediction of osteogenic differentiation potential of human mesenchymal stem cells, PLoS One 8(2) (2013) e55082.

[273] F. Matsuoka, I. Takeuchi, H. Agata, H. Kagami, H. Shiono, Y. Kiyota, H. Honda, R. Kato, Characterization of time-course morphological features for efficient prediction of osteogenic potential in human mesenchymal stem cells, Biotechnol Bioeng 111(7) (2014) 1430-9.

[274] J.A. Smith, Bone disorders in sickle cell disease, Hematol Oncol Clin North Am 10(6) (1996) 1345-56.